



UNIVERSITÄT
DES
SAARLANDES



Dynamic
Biomaterials

Printed Soft Optical Waveguides for Delivering Light into Deep Tissue

Dissertation

zur Erlangung des Grades

des Doktors der Naturwissenschaften

der Naturwissenschaftlich-Technischen Fakultät

der Universität des Saarlandes

von

Jun Feng

Saarbrücken

2020

Tag des Kolloquiums: 29.06.2020

Dekan: Prof. Dr. Guido Kickelbick

Berichterstatter: Prof. Dr. Aránzazu del Campo Bécares
Prof. Dr. Guido Kickelbick

Vorsitz: Prof. Dr.-Ing. Markus Gallei

Akad. Mitarbeiter: Dr. Lola Gonzalez-Garcia

Printed Soft Optical Waveguides for Delivering Light into Deep Tissue

Jun Feng

geb. In Sichuan, China

DISSERTATION

INM-Leibniz Institut für neue Materialien, Saarbrücken

…路漫漫其修远兮，吾将上下而求索…

屈原《离骚》

Abstract

To implement light-based diagnosis and therapies in the clinic, implantable patient-friendly devices that can deliver light inside the body while being compatible with soft tissues are needed. This Thesis presents the development of optical waveguides for guiding light into tissue, obtained by printing technologies from three different polymer combinations. Firstly, D,L-dithiothreitol (DTT) bridged PEG diacrylate were synthesized and printed into waveguides, which exhibited tunable mechanical properties and degradability, and low optical losses (as low as 0.1 dB cm^{-1} in visible range). Secondly, degradable waveguides from amorphous poly(D,L-lactide) and derived copolymers were developed by printing, which showed elasticity at body temperature and could guide VIS to NIR light in tissue for tens of centimeters. At last, soft and stretchable optical waveguides consisting of polydimethylsiloxane (PDMS) core and acrylated Pluronic F127 cladding were fabricated by coaxial extrusion printing, which could be stretched to 4 times of their length and showed optical loss values in tissue as low as $0.13 - 0.34 \text{ dB cm}^{-1}$ in the range of 405-520 nm. For proof-of-concept, above printed optical waveguides were used to deliver light across 5-8 cm tissue to remotely activate photochemical processes in in vitro cell cultures. The presented work exemplifies how rational study of medically approved biomaterials can lead to useful and cost-effective optical components for light applications.

Zusammenfassung

Neue optische Technologien verändern die Zukunft der Medizin und fördern die Entwicklung von Implantaten, die im Körper Licht abgeben. Diese Arbeit beschreibt drei gewebekompatible, optische Wellenleiter für medizinische Zwecke, die mit 3D-Extrusionsdruck gefertigt werden. Zum einen wurden Wellenleiter mit einstellbaren mechanischen Eigenschaften und kontrollierter Abbaubarkeit im Körper als Funktion des Dithiothreitol (DTT)-Anteils in DTT-modifizierten Polyethylenglykoldiacrylat-Hydrogelen entwickelt. Die bei der Extrusion in-situ-photopolymerisierten Wellenleiter haben nur 0,1 dB/cm optischen Verlust im VIS-Bereich und wurden verwendet, um photochemische Prozesse in In-vitro-Zellkulturen zu aktivieren. Zum anderen wurden im Körper abbaubare Wellenleiter aus amorphem Poly(D,L-Lactid) und dessen Copolymeren gedruckt. Diese Wellenleiter sind bei Körpertemperatur elastisch und leiten in mehreren zehn Zentimetern Gewebe Licht vom VIS- bis NIR-Bereich. Schließlich wurden mit koaxialem Extrusionsdruck weiche und dehnbare Wellenleiter hergestellt, die aus einem PDMS-Kern und einer acrylierten Pluronic F127 Hülle bestehen. Diese Wellenleiter sind aufs Vierfache dehnbar und haben in Gewebe nur 0,13 bis 0,34 dB/cm optische Verluste bei 405-520 nm. Die vorgestellte Arbeit zeigt, wie Materialauswahl mit Drucktechnologien kombiniert werden können, um optische Wellenleiter für medizinische Anwendungen mit bemerkenswerter Leistung bei angemessenem Aufwand zu entwickeln.

Acknowledgements

The experiments in this thesis were performed at INM-Leibniz Institute for New Materials, Saarbrücken. The work in this thesis would be impossible without the contribution from many individuals. I would like to thank all people who provided support and contributed to this thesis.

I would like to thank my supervisor Prof. Dr. Aránzazu del Campo for her support, guidance, motivation and encouragement to my work during my PhD. I am grateful to her for holding me in such interdisciplinary group where I was able to finish the work for my PhD thesis and I was allowed to learn a lot of knowledge beyond my background. And I am thankful to her for providing the opportunities for attending conferences and trainings.

I would like to thank Dr. Julieta Paez for her help and support during my PhD, especially at the beginning stage. I am very thankful to her for the discussions about the adhesive projects and other polymer related topics.

I am very thankful to Dr. Samuel Pearson for his kind support with the work for my PhD thesis, especially for his help with designing the materials for waveguides and his help with wording work.

I am very thankful to Dr. Malgorzata Katarzyna Wlodarczyk-Biegun for her kind guidance, discussions and suggestion about 3D printing.

I am thankful to Dr. Peter Rogin for his help with setting up the devices for measuring optical loss and thank him for the discussions about optical technologies. Marcus Koch is acknowledged for providing training SEM. Robert Drumm is acknowledged for measuring DSC. Dr. Claudia Fink-Straube and Ha Rimbach-Nguyen are acknowledged for their support in GPC measurement. Bruno Schäfer is acknowledged for his training on refractive index measurement. Karl-Peter Schmitt is acknowledged for his training on tensile test.

I would like to thank all group members for their kind cooperation. I am very thankful to Prof. Dr. Yijun Zheng (current affiliation: ShanghaiTech University) and Shardul Bhusari for their contribution to the application part of this thesis. I would like to thank Dr. Shifang Zhao and Maria Villiou for their help with cytocompatible experiments. Qiyang Jiang is acknowledged for providing caged RGD for 3D cell culture. I am thankful to Stefan Brück for his support in many experiments and his help with translating abstract for the thesis. Rocio Valbuena Mendoza is acknowledged for her help with 3D cell culture.

Special thanks to Martina Bonnard and Sabine Müller for their kind support during my stay in Germany.

I am really thankful to all my friends and family who supported and encouraged me during my PhD.

I would like to acknowledge China Scholarship Council (CSC) for providing funding for my PhD.

At last, my deepest gratitude to my wife and my parents for their support and encouragement, especially to my wife, Xi Zheng, for her accompanying in Germany. Without their support, I would not be able to make this come true.

Table of Contents

Motivation	1
1. Introduction	4
1.1 Light-tissue interactions and the applications of light in medicine.....	4
1.1.1 Light-tissue interactions.....	4
1.1.2 Application of light in medicine.....	12
1.2 Limited light penetration in tissue and methods to overcome it.....	16
1.2.1 Light penetration depth in tissue	16
1.2.2 Strategies to overcome limited light penetration in tissue.....	17
1.3 Biomaterial-based optical waveguides.....	18
1.3.1 Properties of biomaterials for optical waveguiding.....	18
1.3.2 State of the art in biomaterial-based optical waveguides	20
1.4 Approaches to fabricate optical waveguides.....	41
1.5 Printing technologies for biomaterials	43
1.5.1 Stimulus-triggered 3D printing	44
1.5.2 Deposition-based 3D printing	45
1.5.3 Emerging new 3D printing techniques	46
References.....	50
2. Printed hydrogel-based waveguides	58
2.1 Abstract	58
2.2 Introduction	58
2.3 Results and discussion	62
2.3.1 Synthesis of PEGDA-DTT prepolymers.....	62
2.3.2 Synthesis and physicochemical properties of PEGDA-DTT hydrogels	64
2.3.3 Optical properties of PEGDA-DTT based hydrogels	66
2.3.4 Printing optical waveguides	69
2.3.5 Optical properties of the printed PEGDA-DTT waveguides.....	73

2.3.6 Photoactivation of biological processes in vitro with printed PEGDA-DTT fibers	77
2.3.7 Core-cladding optical waveguides.....	80
2.4 Conclusive remarks.....	83
References.....	85
3. Printed waveguides from thermoplastic amorphous Poly(D,L-lactide) and derived copolymers	88
3.1 Abstract	88
3.2 Introduction.....	88
3.3 Results and Discussion	91
3.3.1 Printing optical waveguides from PLA and copolymers.....	93
3.3.2 Thermal, mechanical and optical properties of the printed waveguides	95
3.3.3 Photostimulation of biological processes across tissue with printed waveguides.....	100
3.4 Conclusive remarks.....	101
References.....	102
4. Printed waveguides from elastomeric materials	104
4.1 Abstract	104
4.2 Introduction.....	104
4.3 Results and discussion	107
4.3.1 Synthesis and physicochemical properties of Pluronic-DA	107
4.3.2 Optical properties of PDMS and Pluronic-DA.....	108
4.3.3 Printing optical waveguides	111
4.3.4 Optical and mechanical properties of the optical waveguides	114
4.3.5 Photoactivation of biological processes in vitro with printed waveguides	116
4.4 Conclusion	118
References.....	119
5. Conclusion and Outlook.....	122
6. Appendix.....	125

6.1 Appendix of Chapter 2	125
6.1.1 Materials and Methods.....	125
6.1.2 Supporting results.....	131
6.2 Appendix of Chapter 3	136
6.2.1 Materials and Methods.....	136
6.2.2 Supporting results.....	139
6.3 Appendix of Chapter 4	140
6.3.1 Experimental information	140
6.3.2 Supporting results.....	145
References.....	147
Publication list	148
Curriculum Vitae.....	149

Motivation

The fundamental interactions between light and tissue, mainly reflection, refraction, absorption and scattering, lead to photothermal, photomechanical, photochemical and photobiological effects, which have been widely exploited for light-based diagnosis, therapy and imaging tools. However, these fundamental interactions also hinder the application of light and optical techniques inside the body because they limit the penetration depth of light into the tissue. In order to apply the continuous progressing optical technologies including optogenetics to meet the daily demands in clinic, effective and implantable patient-friendly devices that can deliver light inside the body while offering tunable properties and compatibility with soft tissues are necessary. So far, wavefront shaping and implantable light sources (micro-LED) have been adopted to improve the penetrating property of light in tissue or to break this limitation. However, the penetrating depth of light in tissue after been corrected by wavefront shaping is still in millimeters range (≤ 2 mm), and the requirement of power supply and heat dissipation in tissue cause problems when applying micro-LED. As an interesting alternative, implantable optical waveguides provide a transparent route for light to propagate through tissue, which largely circumvents the losses caused by scattering and absorption in tissue. Conventional materials for optical waveguides include glass, plastics and crystals, which can effectively guide light in many kinds of environments. However, many of these optical materials are not appropriate for use inside the body, as they are hard and brittle.

Reported work has demonstrated that soft polymeric biomaterials can be used to fabricate optical waveguides for medical scenarios. Soft and biocompatible waveguides have been made from natural polymers such as silk, polysaccharide and gelatin. In order to facilitate controlled design and adjustable

physical/chemical/biological properties, degradable and non-degradable synthetic polymers, such as PEGDA and polyacrylamide hydrogels, PDMS have also been explored for this purpose. The waveguiding performance of these materials is far lower than optical waveguides from silica or polymers used in technical applications. Moreover, approaches to obtain these fibers so far, mainly by thermal drawing, soft lithography or molding, offer poor flexibility, controllability and upscaling possibilities. Printing technologies have shown potential for scalable manufacture and flexible designs for processing, and the possibility in integrating complicated and multifunctional components, such as optical, electronic and pharmacological components into small, flexible and biocompatible medical devices. So far, printing has rarely been used to fabricate optical waveguides. In this context, the objective of this PhD thesis was to select appropriate commercial polymers for optical waveguiding that could be processed by printing, and to develop optical waveguides with appropriate softness, degradability and optical performance to be used in medical applications. Along this general objective, this Thesis presents printed optical fibers from three polymer combinations and demonstrates their suitability for activating photochemical processes across tissue in in vitro experiments. The results of this work are structured as follows:

Chapter 1, Introduction, describes the fundamental interactions between light and tissue; the application of light in medicine for diagnosis and therapies; the limitation of light in penetrating tissue that hinder the application of light in clinic and current approaches to overcome this limitation. And it presents the state-of-the-art of biomaterials-based optical waveguides and a concise description of printing technologies for biomaterials.

Chapter 2 describes degradable hydrogel waveguides based on D,L-dithiothreitol (DTT) modified PEG diacrylate (PEGDA-DTT). It presents the synthesis and structural characterization of PEGDA-DTT precursors and their derived hydrogels,

the characterization of degradability and mechanical properties of the developed materials. The printing window to process PEGDA-DTT optical waveguides and the light guiding properties of printed fibers are also described. Finally, the application of the printed fibers to trigger cells migration in a photoactivatable hydrogel is presented. Improved waveguide designs by coaxial printing core/cladding waveguides are also shown.

Chapter 3 describes degradable optical fibers made of thermoplastic PLA and derived copolymers, with elastomeric properties at body temperature. The physicochemical characterization of the selected materials, the printability window for obtaining continuous fibers and the mechanical and optical properties of the obtained waveguides are described, together with in vitro demonstration of their optical performance.

Chapter 4 describes the design of printable and stretchable waveguides based on PDMS core and Pluronic-F127 cladding designs, their physicochemical and optical properties and performance.

Chapter 5 describes the most important conclusions in this PhD thesis and a brief outlook for the present work.

Chapter 6 contains the Appendix including all the materials and experimental methods, as well as supporting results.

1. Introduction

1.1 Light-tissue interactions and the applications of light in medicine

The early triumph in phototherapy by using ultraviolet (UV) to treat lupus vulgaris started medical application of light in modern time, with which Niels Finsen was awarded the Nobel Prize in 1903.^[1] Thereafter, this application was rapidly accelerated and extended with the continuous progress in comprehensive understanding of the physical properties of light and the interactions between light and tissues. Particularly the appearance of lasers in 1960s developed new paths for medical treatment. Nowadays, numerous medical devices based on laser have been developed, which are routinely used for therapy and diagnosis in the clinic.^[1a]

1.1.1 Light-tissue interactions

Light can interact with tissue in different modes: reflection, refraction, absorption and scattering (**Figure 1**).^[1a, 2] Reflection is commonly applied in medicine for diagnostics in endoscopy and otoscopy. Refraction is applied in refractive corneal surgery or the treatment of retinal detachment.^[2] When the energy of photons is strong enough to excite electronic transitions in molecules from the ground state to the excited state (in the UV to visible spectral range)^[3], or when the frequency of light matches the vibrational frequency of molecules^[4] (in the near-infrared (NIR) and infrared (IR) spectral range), light absorption will happen. The induced photo-excitation can cause photothermal, photochemical and photobiological

effects in the cells.^[5] These can be applied to diagnosis, therapy and imaging.^[1a] Finally, when light propagates in tissue, inhomogeneity or anisotropy of tissue properties can cause light scattering. The scattering leads to changes in the propagation path, polarization and spectrum of incident light. Based on light scattering in tissue, different diagnostic and imaging techniques have been developed.

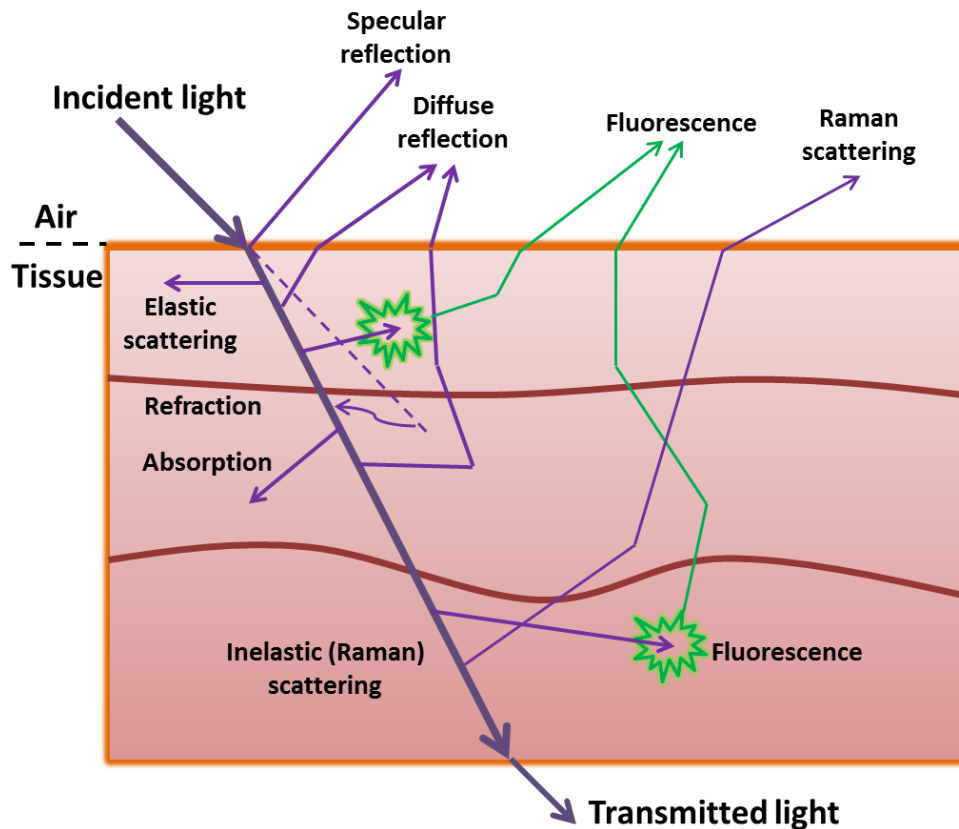


Figure 1. Scheme of light-tissue interactions. Reprinted after permission from ref^[6]. Copyright © 2004 Elsevier B.V.

1.1.1.1 Reflection and refraction

According to Fresnel's law, when light strikes the interface between two media with different RI, light can be reflected or/and refracted. These two behaviors of light are strongly related to each other.^[2] Reflection is the returning of incident light by the boundary between two media with different refractive index (RI),

such as air and tissue. There are two different types of reflection: specular reflection and diffuse reflection. Specular reflection happens when the reflecting surface is smooth that surface irregularities are smaller than the wavelength of incident light. The law of specular reflection states that the wave normals of the incident and reflected light are in the same plane to the normal of the reflecting surface, and that reflection and incident angles equal to each other. Different from specular reflection, diffuse reflection results from equal or larger irregularities on the reflecting surface comparing with the wavelength of light. In such condition, the incident and reflected light beams may not lie in one plane and the reflection angles may not equal incident angle. In real situation, diffuse reflection happens commonly when light strikes the surface of tissue because of the rather rough surface.

The speed of light wave depends on the media, which can be characterized by RI. Refraction happens when light propagates from one medium into another with different RI. In refraction, the relationship of incident angle (θ_1), refracted angle (θ_2), the speeds in media (v_1 and v_2) and RI of two media (n_1 and n_2) follows Snell's law, which can be given by:

$$\sin\theta_1/\sin\theta_2=v_1/v_2=n_1/n_2 \quad (1.1)$$

Ideally, the refraction can be followed by checking the difference of RI of two media. However, it is difficult to precisely measure RI of various tissues due to absorption and scattering. The RI of tissue can be approximately estimated through following equation: ^[7]

$$n=n_{\text{dry}}-(n_{\text{dry}}-n_{\text{water}})W \quad (1.2)$$

Where n stands for the estimated RI of tissue, n_{dry} is the RI of dry tissue; n_{water} is the RI of water and W is the water content. In medical applications, refraction

plays a more important role in irradiating transparent tissue like cornea than opaque tissue because of the difficulty of measuring the effect of refraction.^[2]

1.1.1.2 Absorption

Light absorption takes place when the energy of photons is strong enough to cause electrons transition^[3] or resonance of molecules^[4] in the media. A perfectly transparent matter allows light passing through without any absorption. For biological tissues, the transparency or opacity depends on the wavelength of light. For example, cornea and lens allow visible light passing through, but show strong absorptions in the range from NIR to IR because of water content. Several factors contribute to light absorption when propagating in tissue, mainly including the electronic structure of atoms and molecules in tissue, thickness of tissue layer, density of absorbing agents, the temperature of tissue, and the wavelength of light.^[2] The relationship between the thickness and absorption, concentration and absorption follows Lambert's law (equation 1.3) and Beer's law (equation 1.4) respectively:

$$I_z = I_0 \exp(-\alpha z) \quad (1.3)$$

and

$$I_z = I_0 \exp(-kcz) \quad (1.4)$$

Where z stands for the optical axis, I_0 is the intensity of incident light; I_z is the intensity of light after propagating a distance of z , α is the absorption coefficient of the medium, c is the concentration of absorbing agents and k is a parameter related to internal parameters.

When light propagates in biological tissues, water molecules or macromolecules including proteins and pigments are able to cause different kinds of light

absorption. In the wavelength range from UV to visible, proteins and pigments can absorb incident energy to excite the electronic transitions, which can cause discrete and intense (broad) absorption bands (**Figure 2**). There are several molecular components in tissue that can absorb light, including deoxyribonucleic acid (DNA)/ribonucleic acid (RNA), porphyrin, retinol, haemoglobin, nuclear acids, melanin, reduced nicotinamide adenine dinucleotide and flavin.^[8] Whereas in the infrared region, the absorption is primarily caused by water molecules, which can induce resonance when they absorb matchable frequency from incident light (**Figure 3**). However, in the near infrared (NIR) range, neither macromolecules nor water shows strong absorption, which allows light penetrating deeper in tissue. Thus the range of 600-1200 nm is recognized as a therapeutic window that enables light based treatment in deeper tissue.

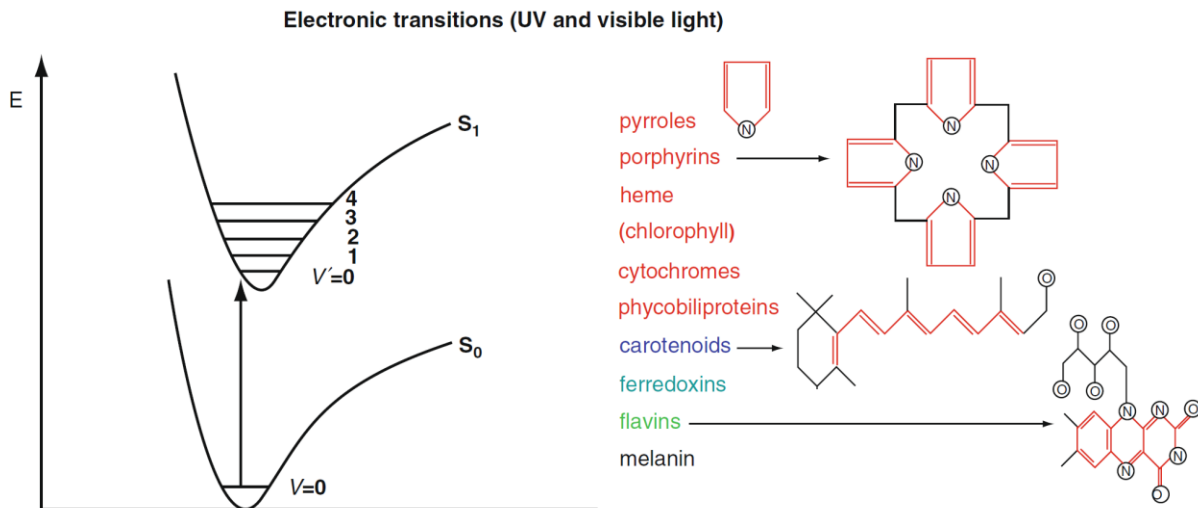


Figure 2. Electronic excitation from ground state to excited state after photon absorption and the chemical structures of possible chromophores existed in the tissue. Reprinted after permission from ref^[8]. Copyright © 2011, Springer-Verlag Berlin Heidelberg.

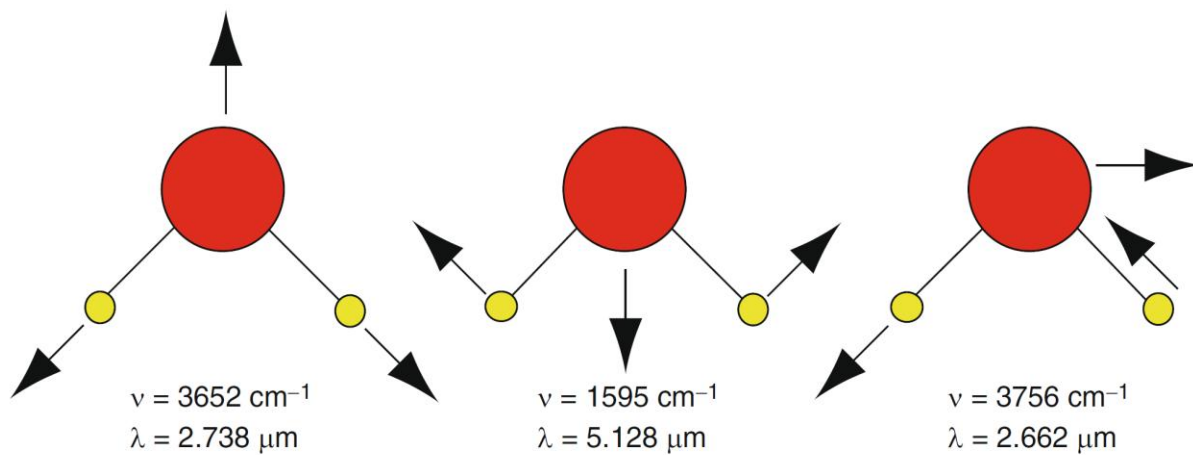


Figure 3. Different vibration modes of a water molecule with different absorption bands. Reprinted after permission from ref^[8]. Copyright © 2011, Springer-Verlag Berlin Heidelberg.

Photoexcitation of molecules as consequence of absorption can cause photothermal, photomechanical, photochemical and photobiological effects in tissues.^[1a] Photothermal effect occurs when the absorbed energy from light causing the increase of temperature in the local position of tissue. This photothermal effect has been used for medical applications, such as for incising tissue or coagulating blood. The required energy for increasing the temperature of tissue is determined by the expected temperature, light penetrating property in tissue, and the size of target tissue. Without heat dissipation, the temperature of 1 cm^3 tissue can be increased by $1 \text{ }^\circ\text{C}$ with 4 J heat.^[1a] In order to minimize the adjunctive damage of tissue in photothermal therapy, pulsed irradiation is adopted, which can avoid the heating diffusion during irradiation. However, the absorption of short laser pulses ($<1 \text{ }\mu\text{s}$) in tissue may cause pressure rise in local position (namely: photomechanical effect), which can form propagating stress waves with acoustic energy.^[1a] This effect has been adapted to fragment kidney stones with high optical intensity. The photothermal and photomechanical effects always accompany in the photoablation with intensive pulsed UV laser. For

example, molecular bond breakage and mechanical ejection of the tissue happen sequentially in photoablation.^[9] The interaction between excited molecule after absorbing a photon and the neighboring molecule can cause some chemical reactions, such as generating free radicals and singlet oxygen. When the neighboring molecule is biologically functional macromolecule like enzyme, photobiological effect can occur. The recently developed optogenetic therapies are based on photochemical and photobiological effects, which can be used to regulate cellular activity.^[10]

1.1.1.3 Scattering

Scattering is the primary light-tissue interaction determining the volumetric distribution of light intensity in the tissue.^[8] Two different light scattering modes can be differentiated depending on if there is energy change in the process: i) in elastic light scattering the direction of light propagation can be altered but without changes in the energy of the photons; ii) in inelastic light scattering the direction of propagation changes accompanying energy changes of the photon as result of inhomogeneity in the electric polarization in tissue.^[1a] The dimensions of the scattering structures of tissue determine the scattering type: i) sub-microscopic structures like macromolecules or nanoparticles; ii) microscopic structures including cells or intracellular structures; iii) macroscopic structures, such as muscle fibres, skin layers, or dentin tubules.^[8] When the size of scattering structure or the fluctuation of mass density is in the range much lower than optical wavelength, Rayleigh scattering could occur, while Mie-type light scattering could occur if the size scale of scattering structures is close to or much bigger than the optical wavelength.^[11] Therefore, the sub-microscopic structures of tissue can cause Rayleigh scattering, and the macroscopic and microscopic structures of tissue may cause Mie-type scattering (**Figure 4**). The Rayleigh scattering is rather isotropic and is determined by the polarization and the

wavelength, which is proportional to $1/\lambda^4$ (λ : light wavelength).^[8] Increasing the optical wavelength can rapidly decrease Rayleigh scattering. However, Mie-type scattering is nearly independent of λ , which normally is relatively stronger than Rayleigh scattering.^[11] In real situation, Rayleigh and Mie scattering always occur simultaneously when light propagates in tissue. The measured scattering coefficients as a function of wavelength can be expressed by $a \times \lambda^{-b}$, where a and b range from 19 to 79 cm^{-1} and 0.7 to 1.6 depending on tissue type, respectively.^[1a, 7]

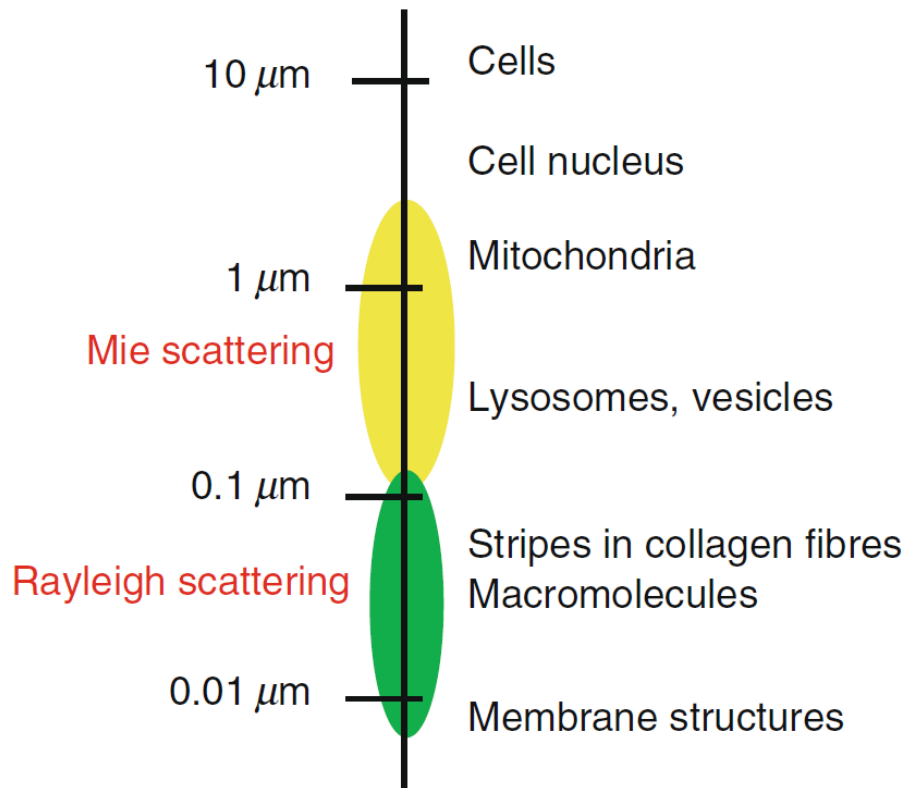


Figure 4. Different scattering from tissue structures with different dimensions. Reprinted after permission from ref^[8]. Copyright © 2011, Springer-Verlag Berlin Heidelberg.

In contrast to elastic scattering, an inelastic scattering process is always accompanied by some loss or increase of energy of the incident light, including dynamic light scattering resulting from moving scatterers, Brillouin scattering

arising from thermodynamically produced hypersonic waves and Raman scattering originating from molecular vibrations.^[1a] Among of these inelastic scatterings, Raman scattering is the most well studied and has been used in molecular vibrational studies. Normally, the scattering coefficients of elastic scattering are much higher than that of spontaneous inelastic scattering (several orders of magnitude higher).^[1a]

1.1.2 Application of light in medicine

The different interactions between light and tissue enable different applications of light in medicine (**Figure 5**). Based on the reflection and scattering, light can be employed for diagnosing and imaging in medicine. Absorption can cause different effects on tissues and cells, based on which optical therapy and laser surgery have been developed. Besides, part of the energy from absorbed light can be re-emitted through different forms, such as excited luminescence (like fluorescence), inelastic scattering, or acoustomechanical waves.^[1a] By collecting the signal carried by these re-emissions, information about the microstructure and molecular content of tissues can be obtained. Modern optical diagnostics and imaging techniques are developed based on such interactions.

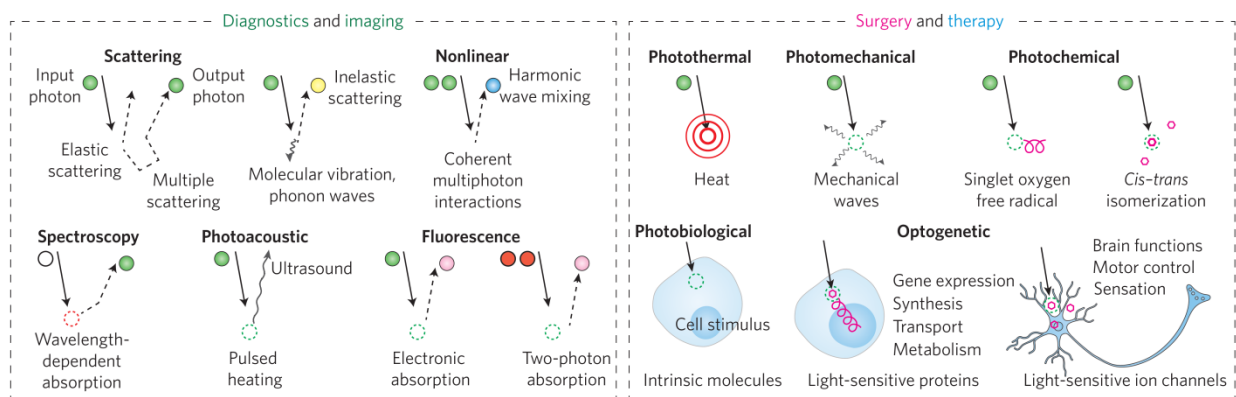


Figure 5. The commonly used optical mechanisms for diagnosis and imaging (left), and surgery and therapy (right). Circles represent incoming and outgoing photons,

and the arrows (solid and dotted) stand for their trajectories. Colors of the circles indicate the light spectrum; dotted circles indicate the absorption of input photons. For therapies, different effects caused by light on tissue and cells are pointed out. Reprinted after permission from ref^[1a]. Copyright © 2017, Springer Nature.

1.1.2.1 Applications of light in diagnosis

Optical technologies are widely used in medicine for diagnostics, such as laboratory testing, point-of-care testing, screening, monitoring and imaging.^[1a] As an alternative approach to laboratory-based analyses, point of care testing enables a wide range of diagnosis to be done quickly and simply in an outpatient setting without complicated infrastructure.^[12] For instance, optical imaging by a pulse oximeter has been used to estimate the patient's arterial oxygen saturation by examining the different light absorption between oxygenated and deoxygenated haemoglobin.^[13] Taking one step further from point-of-care testing, efforts have been made to develop personal healthcare devices, which are supposed to be portable and wearable. For example, smartphone can be converted into point-of-care settings, which can also be seen as portable personal healthcare devices.^[14] Another example, the epidermal electronics was fabricated to fulfill multi-functionalities simultaneously by configuring different functional components including electrodes, electronics, sensors, power supply and communication components into one soft, light weight, stretchable, elastomeric thin sheet.^[15] Imaging technologies play an important role in diagnosis. In routine diagnosis in clinic, numerous imaging techniques have been employed, i.e. laparoscopy, endoscopy, otoscopy, ophthalmoscopy or optical coherence tomography (OCT).^[1a] The technological innovations never stop pushing the development of optical based diagnosis. New technologies such as diffraction-unlimited super resolution imaging^[16] and rapid 3D imaging with light-sheet

microscopy at high spatiotemporal resolution^[17], etc. are in developing or on the way to clinic application. The high demand for preventive and accurate diagnostics of diseases will continuously drive the development of new diagnostic technologies.

1.1.2.2 Application in therapy

Based on endogenous or exogenous photoactive molecules, proteins and cells, different light-activated therapies have been developed, such as phototherapy, photochemical crosslinking, photodynamic therapy, photothermal therapy and optogenetic therapies. Light with different wavelengths carries different energy, which can cause different biological responses. UV light (100-400 nm) can cause cancer either by directly damage DNA (by UVB: 290-320 nm) or by generation of DNA-damaging free radicals (by UVA: 320-400 nm). Visible light (400-700 nm) is not strong enough to directly cause damage on DNA, but it can induce photobiological reactions of therapeutic relevance. For instance, blue light can isomerize bilirubin to facilitate its excretion, which has been employed to treat neonatal jaundice.^[18] Longer wavelengths (NIR: 700-1800 nm) are used for phototherapy. For example, 600-1000 nm exposure has been used for photobiomodulation (low-level laser-light therapy), which has shown the possibility for treating neck pain^[19] and chronic traumatic brain injury^[20], even though the mechanism behind is still not well understood. Photothermal effects of infrared light (1800-2200 nm) can be used for thermal neuromodulation, in which water absorption of infrared light can transiently increase the temperature that can cause the change of membrane capacitance and depolarize the target cell without any exogenous agents or genetic interventions.^[21] By employing exogenously delivered photosensitizer, nanoparticles or chemical crosslinkers, photodynamic therapy (PDT), photothermal therapy (PTT) and photochemical crosslinking (PCC) have been developed for photo-activation treatments.

The development of lasers further extended the applications of light in therapy. The high intensities, narrow wavelength spectrum and the possibility to use pulsed exposures have extended the applications of lasers in the fields such as ophthalmologic surgery, the treatment of cutaneous disorders, and tissue ablation in internal organs.^[1a] UV photons can break the peptide bonds of collagen fibers in cornea.^[22] The concept of selective photothermolysis was introduced in dermatological and aesthetic treatments, and has been widely used in cutaneous laser surgery to remove unwanted skin markings.^[23] With the assistance of fibre-optics, the laser can reach many inner or outer surfaces of organs and tissues, which allows lasers to be applied for surgeries in such as urology, gastroenterology, cardioangiology and otolaryngology. For example, through a flexible ureteroscope, a laser can be employed for lithotripsy to remove stones from the urinary tract (kidney, ureter, bladder or urethra).^[24]

Optogenetics is a new light-based technology that combines both of genetic and optical methods to achieve gain- or loss-of-function of precisely defined events in specific cells of living tissue and behaving animals.^[25] In a typical optogenetical protocol, target cells are genetically engineered with integration of microbial opsins that allow cells precisely respond to light (**Figure 6**).^[1a, 25a, 26] The key reagents used in optogenetics are light-sensitive proteins, including channelrhodopsin, bacteriorhodopsin and halorhodopsin for turning neurons on or off in response to light.^[26] The main applications of optogenetics are in neuromodulation.^[27] For instance, optogenetics provides insight into deep brain stimulation mechanisms in the treatment of Parkinson's disease.^[28] Besides, optogenetic tools can create synthetic gene circuits for other therapeutic application. For example, implanting optogenetically engineered cells into diabetic mice improved the blood-glucose homeostasis when irradiated by blue light.^[29]

Optogenetics is still in the early development stage and more efforts need to be done to facilitate it for clinical application.

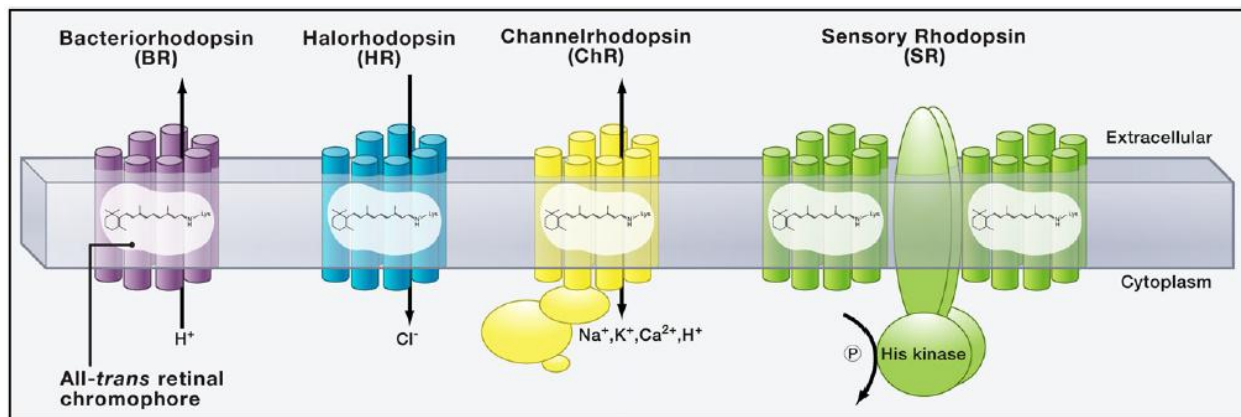


Figure 6. Type I Microbial Rhodopsins. Reprinted after permission from ref ^[26]. Copyright © 2011 Elsevier Inc.

Light plays a very important role in medical therapeutics and optical based techniques have become indispensable for routine treatments in clinic. However, the applications of light in medical therapy could never be restricted to above addressed examples. The continuous development of medical lasers and optical technologies is driving the emerging of optical based therapeutics. Optical based therapies in the clinic are expected to increase in number and modalities.

1.2 Limited light penetration in tissue and methods to overcome it

1.2.1 Light penetration depth in tissue

The penetration depth of light in tissue is wavelength and tissue dependent. In general, longer wavelengths can penetrate deeper in tissue (**Figure 7**).^[30] Due to the different RI between air and tissue, and the inhomogeneous RI within tissues, the incident light is partially reflected and scattered. This attenuates light when penetrating in tissue. Besides, absorption in UV and visible range, and resonance

in NIR and IR range further attenuate light in tissue. For example, blood hemoglobin is a major obstacle at wavelengths <600 nm and water at wavelengths >1000 nm.^[1b] According to the different types of tissue, the penetration depth of light is in the range of 0-1 mm at 400nm, 0.5-2 mm at 514 nm, 1-6 mm at 630 nm, and maximal at the spectrum of 700-900nm.^[1b, 30c] For the application of optical technologies in deep tissue and inner organs, the limited penetration depth must be overcome.

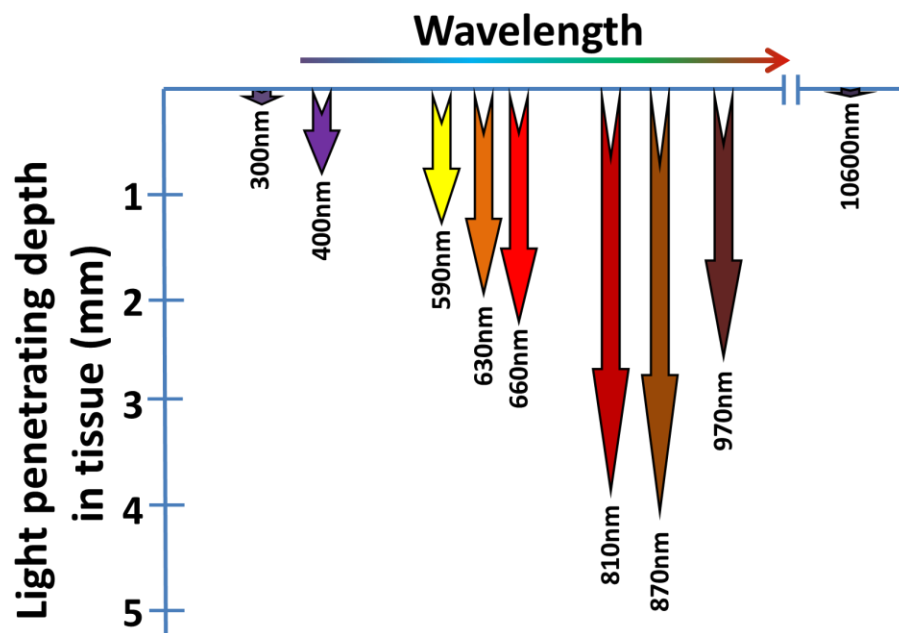


Figure 7. Light penetrating depth in skin tissue with different wavelengths. The image is adapted from ref^[1b].

1.2.2 Strategies to overcome limited light penetration in tissue

Approaches to overcome the limited light penetration in tissue can be classified into three categories: i) wavefront shaping; ii) implantable light sources; iii) implantable optical waveguides.^[31] Wavefront shaping is a recent approach which modulates an incident light beam across its input plane to match the scattering profile of a tissue and create a focus at a target plane well beyond the diffusion

limit of the tissue. This works by selectively directing more of the incident light intensity through areas which are found to navigate the scattering medium to arrive at the desired focal point, and avoiding irradiating areas which scatter outside the focal point.^[32] However, the focusing depth in tissue with this technology is still in millimeters range (≤ 2 mm).

Instead of obtaining light from an external light source, the light source can be directly implanted, for example, implantable micro-LED.^[33] This method successfully avoids the external light source and appropriate coupling system, but the requirement of power supply and heat dissipation in tissue cause some additional problems. Alternatively, implantable optical waveguides provide a more efficient way to deliver light to target location in deep tissue. The optical waveguides can provide a transparent route for light propagating through tissue, which largely circumvents the losses caused by scattering and absorption of tissue. Conventional materials for optical waveguides include glass, plastics and crystals, which can effectively guide light in many kinds of environments. However, many of these optical materials cannot meet the requirements for biomedical application considering their biocompatibility and/or mechanical properties.^[11] To address these problems, biomaterials with soft mechanical properties and high light transparency were introduced into this field. These will be described in the next sections.

1.3 Biomaterial-based optical waveguides

1.3.1 Properties of biomaterials for optical waveguiding

In order to apply biomaterials in optical waveguides, some materials properties related to optical function should be addressed. Optical loss (attenuation) is the most common used method to characterize the light guiding properties of

materials. There are several mechanisms determining the optical loss. For biomaterials, especially polymeric biomaterials, one of intrinsic loss originates from absorptions, including electronic and vibrational absorptions.^[34] Molecules can absorb energy in the range of ultraviolet and visible light to excite electrons transition from the ground state to the excited state.^[3] Organic compounds, especially those with a high degree of conjugation, have a strong light absorption in the UV-vis region.^[11] Based on molecular resonance, organic molecules can also absorb infrared light when the frequency of the absorbed radiation matches the vibrational frequency of molecules.^[4] The absorption of light, no matter from electrons transition or molecular resonance, could cause an intrinsic optical loss.

The second intrinsic optical loss is caused by scattering, which contains two types of intrinsic scattering from density fluctuations and compositional inhomogeneity (Mie scattering and Rayleigh scattering) and one extrinsic scattering from large inclusions.^[34] Based on the contributions to scattering from different sources, scattering coefficient is often fit with following equation^[34]:

$$\alpha_{scatter} = A + B/\lambda^2 + D/\lambda^4 \quad (1.5)$$

Where A is the contribution from large inclusions ($\gg \lambda$), B is the contribution from inhomogeneity with a dimension close to λ (Mie scattering), and D is the contribution from inhomogeneity at the atomic scale ($\ll \lambda$, Rayleigh scattering). The extrinsic scattering in polymeric biomaterials may result from impurities, such as particles, dust, bubbles and insoluble substance.^[34] Rayleigh scattering doesn't depend on the specific type of material but on the size of the particles relative to the wavelength of light. Since Rayleigh scattering has a magnitude proportional to $1/\lambda^4$, shorter wavelengths are scattered more than longer wavelengths, and it can be diminished rapidly as wavelength increases. For polymeric biomaterials, partially disordered network of long polymer chains and macromolecules can

cause Mie scattering, which can be several orders of magnitude stronger than Rayleigh scattering.^[11]

The third intrinsic factor determining the light guiding properties of materials is refractive index (RI). In order to obtain total internal reflection, an appropriate index difference is very important. For core/cladding structure waveguides, the core material must have a higher RI than that of cladding material.^[34] For single-material optical waveguides, the RI must be higher than that of the surrounding tissue (local RI of tissue: 1.33–1.51).^[7, 11] For single-material waveguide without a cladding, the microscopic inhomogeneity of RI in surrounding tissue are prone to cause optical loss. So for long distance delivery of light, core/cladding is the preferred structure for optical waveguides.

1.3.2 State of the art in biomaterial-based optical waveguides

1.3.2.1 Waveguides from natural source biomaterials

Silk proteins represent one special member of biopolymers, normally produced by silkworms and spiders. Owing to its excellent mechanical properties, biocompatibility, biodegradability, silk has been widely applied in tissue engineering, drug delivery, Electronics, sensors and filtration.^[35] Besides, the favorable clarity of silk proteins makes it a promising candidate for the application of biocompatible optics or photonic components.^[11] Based on its high transparency and refractive index, silk has also been used to fabricate optical waveguides. Parker et al.^[36] fabricated optical waveguides from biocompatible silk through direct ink writing (**Figure 8 A**). An aqueous silk fibroin solution was extruded into a methanol-rich coagulation reservoir, in which the printed waveguides can maintain their rod-like morphology. The printed waveguides showed 0.25 dB/cm and 0.81 dB/cm propagating loss at 633 nm for the straight and curved waveguides, respectively (**Figure 8 B**), which is consistent to that of

silk fibroin films (0.25 to 0.75 dB/cm). In order to further improve the light guiding property in silk-based optical waveguides, step-index optical waveguides were made by encapsulating silk film (RI=1.54) within a silk hydrogel (RI=1.34) to form a core/cladding structure. The core/cladding waveguides demonstrate capability of guiding light through biological tissue.^[37] In order to simplify the process of regeneration of silk protein, Kujala et al.^[38] fabricated optical waveguides from non-regenerated silkworm silk and studied their linear and nonlinear optical properties. Loss coefficient of the natural silk fiber was assessed to be around 2.8 dB/mm. The high optical loss was mainly caused by the scattering from debris and torsional twisting of the fiber.

Besides silkworm silk, spider silk proteins have also been fabricated into optical waveguides. Huby et al.^[39] studied the efficiency of pristine dragline silk made optical fiber. The optical loss coefficient of the spider fiber was estimated around 10.5 dB/cm. Tow et al.^[40] designed a proof-of-concept experiment proving the possibility to use pristine spider silk to sense ambient relative humidity (RH) level. In order to overcome the limitation of the low yield of natural spider silk and to improve the light guiding property, Qiao et al.^[41] fabricated a recombinant spider silk optical waveguide by using genetically engineered spider silk protein (**Figure 8 C**). The attenuation coefficient of recombinant spider silk optical waveguide was 0.8 ± 0.1 dB/cm in air and 1.9 ± 0.3 dB/cm in mouse tissue.

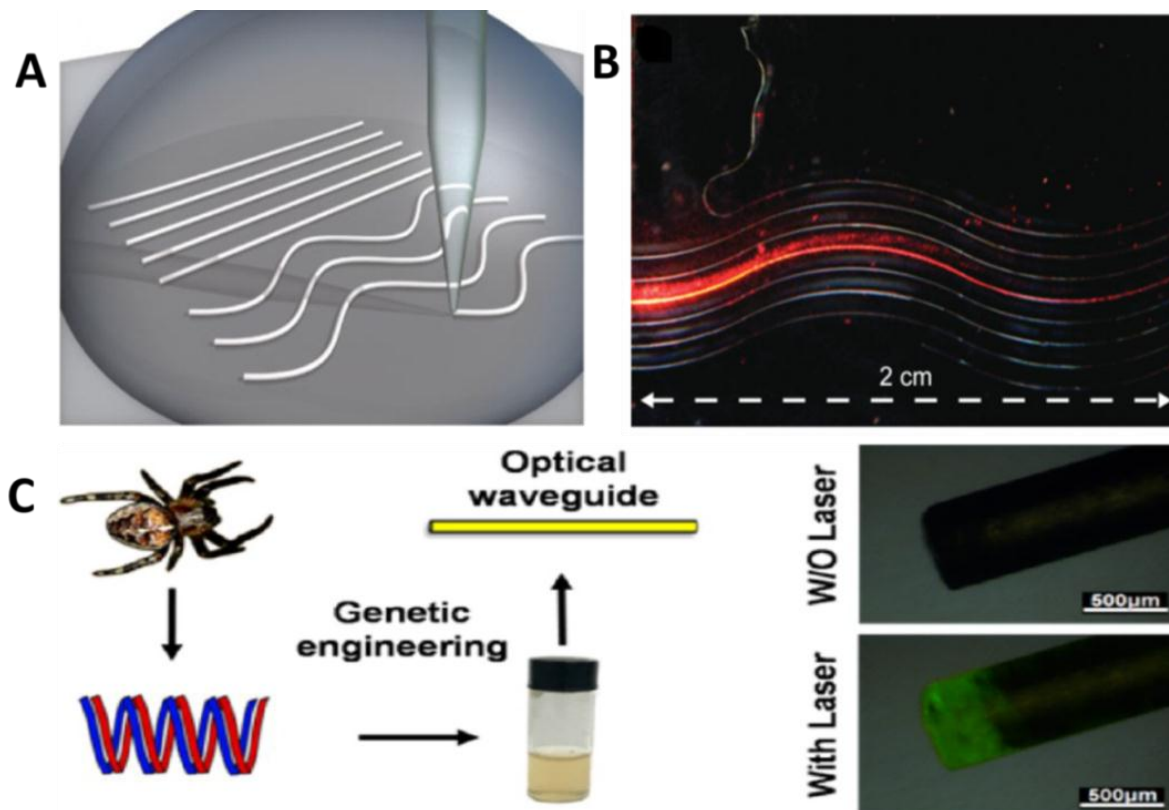


Figure 8. (A) Scheme of direct-writing silk fibroin solution in a methanol-rich coagulation reservoir with straight and curvy structures. (B) Red light from a He:Ne laser propagates in printed curvy silk waveguides. (C) The process of fabricating spider silk optical waveguides from genetically engineered spider (right) and images of optical waveguides fabricated from spider silk without and with laser (left). (A and B) Reprinted after permission from ref^[36]. Copyright © 2009 WILEY-VCH Verlag GmbH & Co. KGaA, Weinheim. (C) Reprinted after permission from ref^[41]. Copyright © 2017, American Chemical Society.

Chitosan is the second most abundant polysaccharides in nature, which is one of the major cationic linear polymers. It has been widely applied in biomedical and industrial fields.^[42] The primary amino groups allow chitosan exhibiting good sorption characteristics to both the cationic and anionic forms of noble metals by adjusting the pH.^[43] Mironenko et al.^[44] demonstrated chitosan/Ag nanoparticles thin film composites by in situ reduction of pre-adsorbed Ag⁺ ions in chitosan film. The refractive index of the composite film can be tuned by adjusting the silver

volume fraction in the film. With a similar method, hydrogen sulfide sensors were fabricated based on chitosan optical planar waveguides coating with Ag and Au nanoparticles. The composite sensors with Ag and Au nanoparticles can detect H₂S gas at concentration ranging from 0.1 to 100 ppm and from 5 to 300 ppm, respectively.^[45]

Cellulose is another natural polysaccharide. Its high transparency of visible light enables it applicable for optical fibers. Dupuis et al.^[46] presented a porous double-core optical fiber fabricated by thermal drawing two coaxial cellulose butyrate tubes that were separated by hydroxypropyl cellulose powder. Transmission loss of this biodegradable fiber reached between 1 and 2 dB/cm. It's potential to apply this double-core optical fiber for laser delivery by collapsing the hole of inner core, or for drug delivery by leaving the hole open.

Agarose is an agar derived polysaccharide. Based on the tunable refractive index of agarose hydrogel by simply changing the concentration, it is also possible to apply it to prepare waveguides. Jain et al.^[47] fabricated biocompatible optofluidic waveguides from agarose through a soft lithography process. The waveguides showed an average loss of 13 dB/cm, which in principle can be improved by increasing the concentration of agarose. They also demonstrated the possibility of encapsulating cells and biomolecules inside the waveguide.

Gelatin is derived from collagen through acid and alkaline processing.^[48] Chen et al.^[49] fabricated waveguides by spin-coating gelatin on rigid substrates, such as GaAs, LiNbO₃, glass, and aluminum. Doping with ammonium dichromate in gelatin waveguide makes it possible to integrate single and multiplexed gratings in one substrate, which can be used to carry out different functions for optical interconnects and signal processing. Manocchi et al.^[50] made planar core/cladding waveguides through layer-by-layer spin-coating technique. Gelatin (RI: 1.536) was

used as the core and agarose (RI: 1.4969) as cladding layers. Total internal reflection was observed when light propagating in this waveguide.

Besides above mentioned biomaterials, bio-derived peptide and microorganisms are also good examples for using natural source materials to fabricate optical waveguides. The wide optical transparency of bio-derived peptide nanostructures^[51] made them promising materials for optical waveguides. The dimensions and shapes of native peptide nanostructures enable them passive guiding light and/or guiding excited fluorescence along the axis of peptide in near UV–visible–NIR region,^[52] and their asymmetric structures endow peptides the possibility to possess nonlinear optical effects.^[53] Living organisms can be directly used as sources of materials for photonic and optoelectronic devices.^[54] Xin et al.^[55] demonstrated an optical strategy to directly form biophotonic waveguides (bio-WGs) by trapping *Escherichia coli* (*E. coli*) cells with an abrupt tapered optical fiber (ATF) (**Figure 9**). The results showed multiple *E. coli* were trapped and connected together with highly ordered organizations, forming bio-WGs with lengths from 4.6 to 54.5 μm .

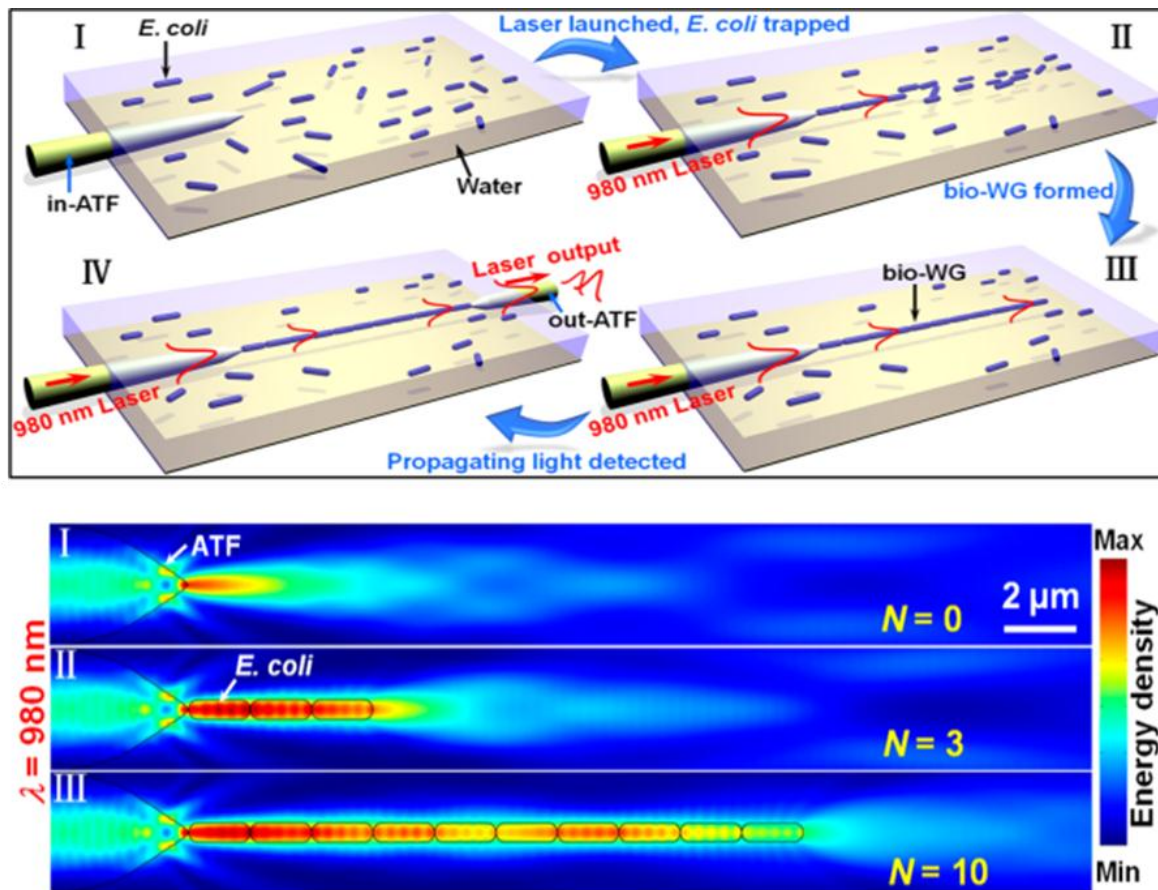


Figure 9. Up: Scheme of trapping *E. coli* and its light guiding. I, placing the in-ATF in a *E. coli* suspension; II, launching 980 nm laser into the in-ATF, *E. coli* starts to be trapped; III, The trapped and connected *E. coli* forming a bio-WG; IV, guided light is received by an out-ATF. Below: Energy density distribution in the ATF with different number (0, 3 and 10) of trapped *E. coli*. Reprinted after permission from ref^[55]. Copyright © 2013, American Chemical Society.

1.3.2.2 Waveguides from synthetic biomaterials

Thermoplastic biomaterials

It has been a long history since synthetic polymers like poly(methylmethacrylate), polystyrene, polyacrylate, polyurethane or epoxy resins have been applied as optical materials for waveguides.^[34, 56] These materials, however, are not ideal for medical applications because of limited biocompatibility or high rigidity. Polylactic

acid (PLA) is a well-studied biodegradable synthetic polymer for optical waveguides. PLA has three enantiomeric forms: PLLA, PDLA and PDLA, in which D and L refer to dextroisomer and leveisomer. By changing the ratio of D to L enantiomers, PLA polymers can range from amorphous form to semi-crystalline and highly crystalline form. PLA is commonly copolymerized with polyglycolic acid (PGA) to adjust the degradability and crystallinity. There are several reports about the application PLA and PLGA for implantable photonic devices. Nizamoglu et al.^[57] showed a series of implantable light-delivery devices made of biodegradable polymers (PLA, PLGA), and validated their effectiveness for inducing photochemical processes in deep tissue. They designed a comb-shaped slab waveguide for light delivery (**Figure 10 A**), which demonstrated successful photochemical tissue bonding treatment of a full-thickness skin incision (>1 cm deep), which is not possible by conventional surface illumination. Kim et al. fabricated a lens-assisted optical microneedle array (**Figure 10 B**) from PLA for percutaneous light delivery.^[58] With this array, a 9-fold enhancement of light delivery at the treatment depth in bovine tissue was achieved compared to without it. Gierej et al.^[59] presented the fabrication of biodegradable and biocompatible optical fiber from commercially available poly(D,L-lactic acid) (PDLLA) by a thermal drawing process. The fabricated optical fiber showed excellent transmittance with optical loss 0.11 dB/cm at 772 nm. With the same method, Fu et al.^[60] presented implantable and biodegradable optical waveguides from poly(L-lactic acid) (PLLA) (**Figure 10 C**). They found the thermal drawing process caused crystalline-to-amorphous transition of PLLA and the prepared optical fibers showed good mechanical flexibility and optical guiding properties. By employing the PLLA fibers, they achieved deep brain fluorescence sensing and optogenetic interrogation in vivo.

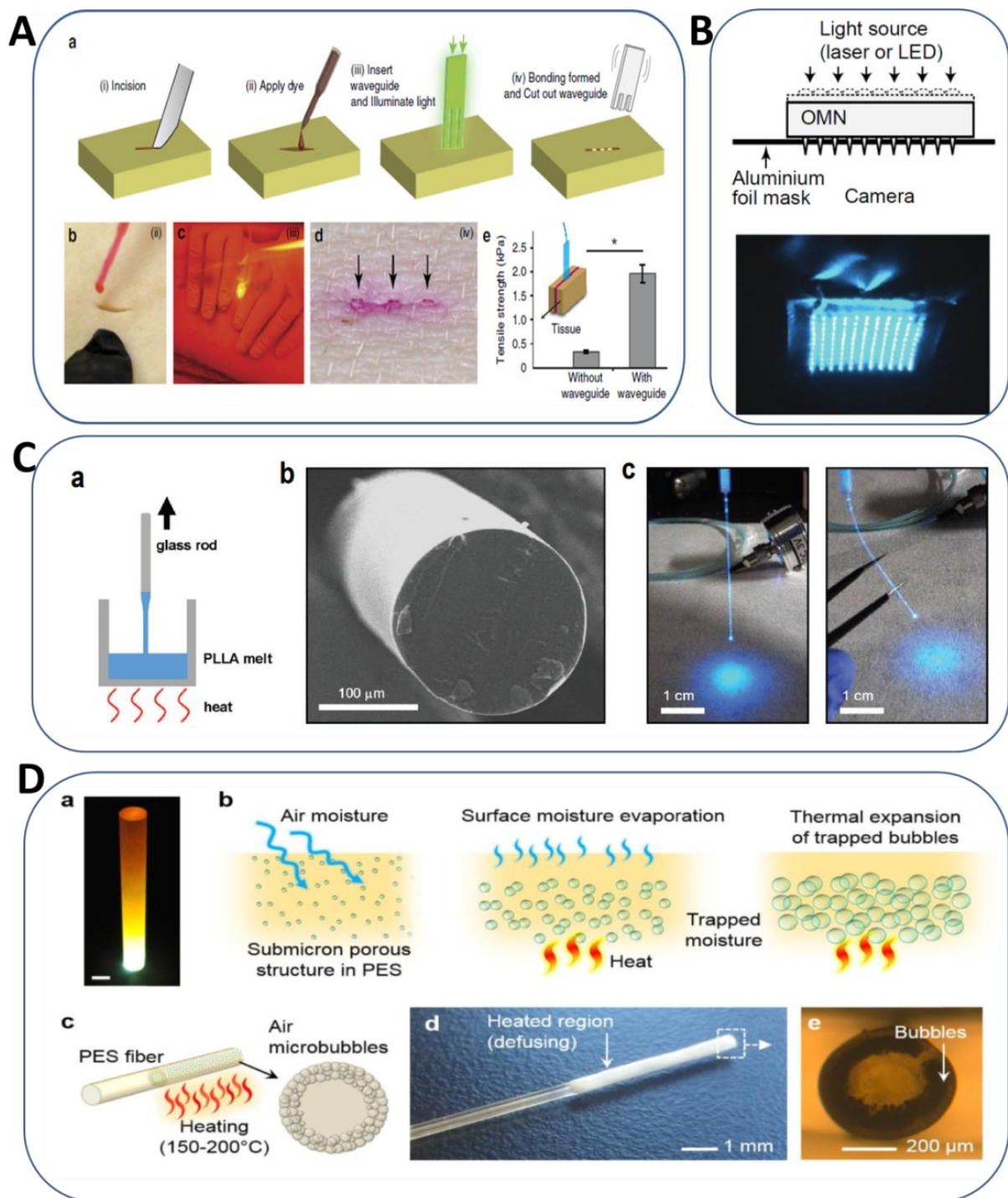


Figure 10. (A) a: Scheme of applying waveguides to deliver light into deep tissue to activate tissue glue. (i) Cutting skin incision; (ii) Applying Rose Bengal dye to the wound and removing extra solution; (iii) A delivering light through a prepared optical waveguide into the wound; (iv) Trimming the waveguide part out of skin surface. b–d: Experimental operations of steps (ii), (iii) and (iv). (e) Shear tensile strength of PTB bonds with and without waveguide in porcine skin. The improved

strength of PTB bonds with optical waveguide was obtained. (B) Light transmission through an optical microneedles array--up: Scheme of the setup; below: 491 nm blue light transmitting through an optimally aligned optical microneedles array. (C) a: Scheme of fabricating PLLA fibers through thermal drawing process; b: cross-section of the PLLA fiber characterized by SEM; c: Blue light (473 nm) is propagating in 5 cm long straight and bending PLLA fibers. (D) a: Rayleigh scattering from nanoscale pores shown in a 20 cm-long PES rod illuminated with white light from the bottom (scale bar = 1 cm); b: Scheme of forming diffusing air bubbles inside PES fiber; c: Illustration of heat treated fiber with a scattering layer underneath the surface; d: Picture of heat treated PES fiber; e: Cross section of heat treated PES fiber. (A) Reprinted from ref^[57a] under a Creative Commons Attribution 4.0 International License. Copyright © 2016, Springer Nature. (B) Reprinted (adapted) with permission from ref^[58]. Copyright © 2016 Optical Society of America. (C) Reprinted after permission from ref^[60]. Copyright © 2017 WILEY-VCH Verlag GmbH & Co. KGaA, Weinheim. (D) Reprinted after permission from ref^[61]. Copyright © 2019 Optical Society of America.

Besides PLA and PLGA, various other thermoplastic biomaterials have been used to prepare photonic devices. Choi et al.^[62] presented using a surgical suture made of polydioxanone (PDA) as optical fiber to deliver light into tissue. With this optical suture, the coupled light (632.8 nm) can be delivered through a chicken breast tissue down to 35mm. Shabahang et al.^[61] demonstrated optical fibers made of Polyethersulfone (PES) through thermal drawing process, which exhibited optical loss from 0.2 to 0.8 dB/cm in the red and near infrared spectral ranges. Through post-processing techniques, fibers with custom-tunable scattering profiles were fabricated (**Figure 10 D**), which may be useful for phototherapy. Reddy et al.^[63] developed a low-loss (<5 dB/cm) core/cladding-

based photonic waveguide platform with parylene C as core and PDMS as cladding. The compact, flexible, biocompatible waveguides may have the potential to apply in wearable or implantable devices. However, the optical guiding properties may be able to be improved if the rough surface on the sidewall of waveguides caused by the reactive ion etching of Parylene C can be solved.

Hydrogel based biomaterials

Hydrogels are cross-linked macromolecular networks, which can swell and retain a large fraction of water in their structure, but will not dissolve in water.^[64] Due to the biocompatibility, retention of water and the ability to respond to external stimuli under physiological conditions, hydrogels have been used for extensive application, such as sanitary products, bioseparation, biomedical engineering, etc.^[64b] Besides, the transparency and adjustable mechanical properties achieved by changing polymer content, molecular weights, and crosslinking density enable hydrogels to apply in fabrication of optical waveguides.

Polyethylene glycol (PEG) based hydrogels have been well studied for the development of optical waveguides. The excellent biological properties, like biocompatibility, nonimmunogenicity, resistance to protein adsorption and high water retention^[11] make PEG based hydrogels suitable for drug delivery, tissue engineering and cosmetics, as well as optical waveguides for light delivery in tissue or even in the body. Choi et al.^[29b] fabricated PEG diacrylate (PEGDA) based hydrogel waveguides (**Figure 11 A**), in which optogenetically engineered cells were encapsulated that can generate and secrete glucagon-like peptide-1 helping the body respond to insulin. By implanting the waveguide in the subcutaneous space in a diabetic mouse model, they realized light-controlled therapy. The blue light was delivered uniformly onto the cells and activated them to produce

glucagon-like peptide-1. The results showed improved glucose homeostasis in mouse. They further demonstrated the real-time monitoring systemic cellular toxicity of quantum dot by implanting optical waveguides that encapsulate heat-shock-protein-coupled fluorescent reporter cells. Francone et al.^[65] fabricated a sensor based on a waveguide with a grating readout section from poly(ethylene glycol dimethacrylate), N-isopropylacrylamide, and acrylic acid by thermal nanoimprint lithography. The fabricated sensor can be used to detect pH and water through characterizing the topography changes by AFM, SEM, or a specific optical set-up. Heo et al.^[66] developed continuous glucose monitors by polymerizing a precursor solution containing glucose-responsive monomers, acrylamide and acryl-PEG in microcapillaries coated with Pluronic® surfactant. The glucose responsiveness of fluorescent hydrogel fibers have been tested both in vitro and in vivo conditions.

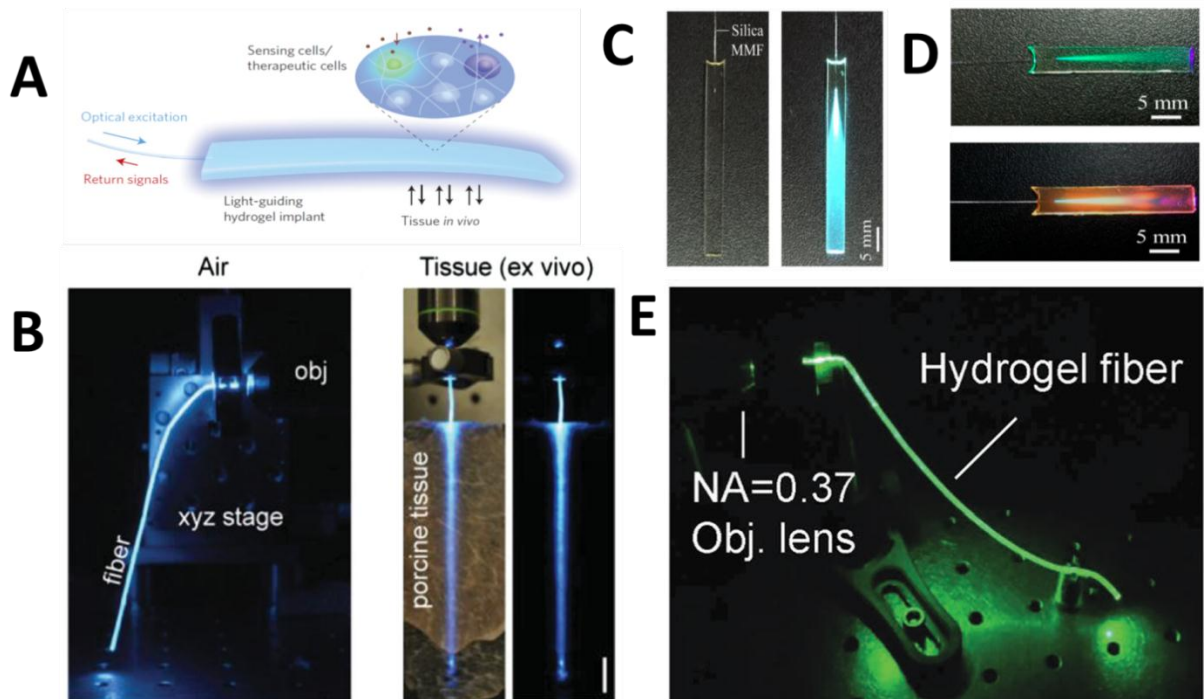


Figure 11. (A) Scheme of a hydrogel based waveguide with engineered cells for in vivo sensing and therapy encapsulated inside. Environmental stimuli can trigger cells in the waveguide to generate luminescence (achieve sensing) and external

light can activate them to secrete cytokines and hormones (achieve therapy). Simultaneously real-time monitoring and controlling biological system in vivo can be achieved by bidirectional optical communication with the cells. (B) Blue light (492 nm) propagates along the fibers in air and in tissue. Scale bar: 1 cm. (C) Light coupled in the carbon dots (CDs) doped PEGDA hydrogel based waveguides. (D) Up: 405 nm light coupled into a QDs_(TGA)-doped hydrogel waveguide; Below: Waveguide after coating. (E) 532 nm laser light propagates along the stretchable fiber. (A) Reprinted after permission from ref^[29b]. Copyright © 2013, Springer Nature. (B) Reprinted after permission from ref^[31b]. Copyright © 2015 WILEY-VCH Verlag GmbH & Co. KGaA, Weinheim. (C) Reprinted from ref^[67] under a Creative Commons Attribution 4.0 International License. Copyright © 2017, Springer Nature. (D) Reprinted after permission from ref^[68]. Copyright © 2018, American Chemical Society. (E) Reprinted after permission from ref^[69]. copyright © 2016 WILEY-VCH Verlag GmbH & Co. KGaA, Weinheim.

However, the photobleaching of the fluorophore, different light scattering and thickness of tissues may cause over/underestimating readouts.^[11, 70] To address this issue, core/cladding structure waveguides were fabricated. Choi et al.^[31b] developed a core/clad hydrogel fiber with photo-crosslinked PEGDA hydrogel as core and calcium coordinated alginate as cladding (**Figure 11 B**). They adopted two steps to prepare the fiber. Firstly, they made the core by UV-crosslinking PEGDA precursor solution in a platinum-cured silicone tubular mold, which can be removed by swelling in dichloromethane. Secondly, a layer of clad was formed by successively dipping the core in a sodium alginate and calcium chloride solution. The fabricated core/clad fibers showed better light-guiding properties than that of a single-index core-only PEG fiber. They explored the possibility of applying fabricated fibers in optical sensing of blood oxygenation levels in live mice.

Yetisen et al.^[70a] created hydrogel-based core/cladding optical fibers by utilizing a copolymer of acrylamide and PEG diacrylate for core and a Calcium gelled alginate for cladding. The optical fiber was employed to sense glucose, which was realized by covalently incorporating 3-(acrylamido)phenylboronic acid molecules in the fiber that can induce the change of swelling property and volume of hydrogel when binding with glucose. The effect of core diameter, cladding thickness and refractive index on light propagation in this fiber was characterized by both computation and experimental evaluation.^[71] Johannsmeier et al.^[72] reported mechanical properties tunable hydrogel waveguides from PEGDA and poly(ethylene glycol) dimethacrylate monomers (PEGDMA) for light delivery. Total reflection was achieved by forming a fiber-shaped structure inside a block gel.

To extend the application, the optical fibers can be functionalized by doping with fluorescent dye, nanoparticles, quantum dots (QDs), metal–organic framework (MOF), or by integrating microlens array. Jiang et al.^[71] fabricate a step-index core/cladding optical fiber from poly(acrylamide-co-poly(ethylene glycol) diacrylate) as core and Ca-alginate as cladding. The fibers were doped with fluorescent dye and gold nanoparticles and demonstrated yellow-red and red illumination. But further experiment in the application of doped optical fiber needs to be done. Guo et al.^[67] fabricated fluorescent hydrogel waveguides from carbon dots (CDs) doped PEGDA hydrogel for on-site detection of heavy metal ions (**Figure 11 C**). The presented CDs-doped waveguide exhibited efficient light confinement and showed high sensitivity of sensing mercury ions. They further demonstrated optical waveguides (**Figure 11 D**) incorporated with thioglycolic acid capped quantum dots (QDs_(TGA)), which were coated with a thin porous film containing glutathione capped QDs (QDs_(GSH)).^[68] The waveguides were designed into tapered structure that enables more light extraction to excite the coating film. With the waveguide sensor, rapid and selective detection of Pb²⁺ can be

achieved and a linear response to Pb^{2+} ions in the range of 0–5 μM was obtained. Zhou et al.^[73] developed core/cladding optical fiber sensors made from PEGDA as core and alginate-calcium as cladding. The core was doped with two different CdTe quantum dots (QDs) in discrete section: red emissive N-Acetyl-L-cysteine capped QDs (rQDs) and green emissive thioglycolic acid capped quantum dots (gQDs). The QDs doped optical fibers can be used to selectively detect Fe^{3+} in a range of 0-3.5 μM based on that rQDs can be quenched by Fe^{3+} and gQDs can immune to Fe^{3+} as built-in reference. By integrating metal–organic framework (MOF) in a step-index hydrogel fiber, a sensing platform was fabricated, which can be used to detect fluorescence.^[74] For example, with EuNDC (H₂NDC = 1,4-naphthalenedicarboxylic acid) micro powders in the core of fiber, it can be used to selectively detect explosive picric acid (PA) spectrally and visually. Elsherif et al.^[75] fabricated optical fiber probes from polyethylene glycol diacrylate (PEGDA) for continuous glucose, alcohol and pH monitoring. The detection was achieved by functionalizing the tips of optical fibers with a glucose-responsive-hydrogel-based, or alcohol- and pH-responsive-hydrogel-based asymmetric microlens array (**Figure 12**). The fabricated biocompatible optical fiber proved to be easy readout and showed comparable response to the functionalized silica fiber.

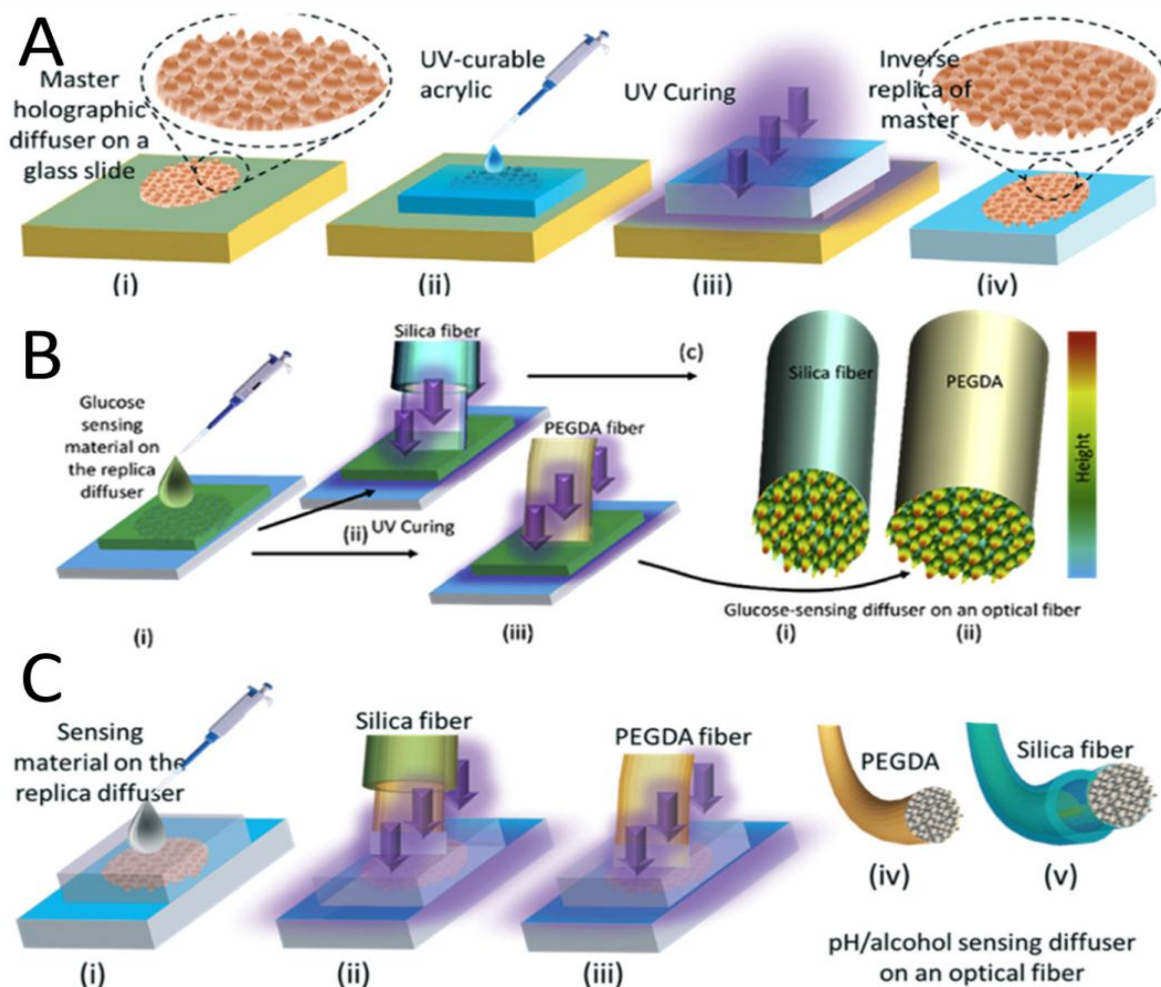


Figure 12. Processes of fabricating sensors based on hydrogel microlens array. (A) Scheme of fabricating the asymmetric microlens arrays (diffusing microstructures). (B-C) The processes of functionalizing optical fiber's tip. (A and C) from ref^[75b] reproduced by permission of The Royal Society of Chemistry. (B) Reprinted after permission from ref^[75a]. Copyright © 2019 Elsevier B.V.

Besides PEG based hydrogel, polyacrylamide (PAM) hydrogel has also been used for the development of optical waveguides. Guo et al.^[69] designed a series of highly stretchable and tough optical fibers made of alginate-polyacrylamide hydrogel. A core/clad step-index structure was prepared to achieve total internal reflection by using different polymer concentration for core and cladding (**Figure 11 E**). Based on the high scalability of hydrogel fiber along the axis, they

demonstrated a possible application in strain sensing. Wang et al.^[76] presented ultrasoft and highly stretchable optical fibers made from alginate-polyacrylamide hydrogel, which properly fit the mechanical properties of neural tissues. By implanting the optical fibers in free-moving animals, they realized modulating the animals' behavior through optogenetic stimulation.

Elastomeric biomaterials

The soft and stretchable properties of elastomeric materials are interesting for their use of optical waveguides in medicine. Poly(dimethylsiloxane) (PDMS) finds wide applications in microfluidics^[77], cell culture scaffolds^[78], flexible electronics^[79], and medical devices^[80] based on its biocompatibility, low autofluorescence, moldability with submicron resolution and high oxygen permeability. Besides, the optical transparency of PDMS allows a range of application in optics including optofluidic channels^[77c, 81], optical interconnects^[82], blazed gratings^[83], adaptive lenses^[84], solid immersion lenses^[85]. Further researches on light guiding properties of PDMS have also been done. Missinne et al.^[86] introduced stretchable optical waveguides by using PDMS as optical links and researched the effect of stretching and bending on the light guiding properties of the links. By meriting the stretchability and transparency of PDMS, Ramuz et al.^[87] demonstrated the fabrication of a pressure-sensitive artificial skin, in which PDMS served as the waveguide and substrate. The presented pressure sensors showed good cycling stability, tolerance to bending and low hysteresis with varying applied pressure. To et al.^[88] proposed highly stretchable optical sensors for pressure, strain, and curvature measurement. The sensors are made of PDMS elastomer coated with a thin gold reflective layer. The sensors are working by forming micro-cracks within the reflective layer that results in escaping of part of light and higher optical power losses in light transmission when the sensors are stretched, compressed, or bent. Kwok et al.^[89] fabricated a

waveguide of PDMS elastomer to deliver light for Scleral cross-linking (SXL) (**Figure 13 A**). They performed SXL on fresh porcine eyes with this waveguide and found the sclera cross-linked with the waveguides had two times higher Young's modulus compared to that with no irradiation (**Figure 13 A**). In order to improve the light guiding property and prevent light leakage to nontarget, periorbital tissue, they further designed a core/cladding waveguide with polyurethane as core and PDMS as cladding, which was further coated with reflective silver coating on the top and side surfaces of the waveguide^[90]. With the new design, a 200% increase in the Young's modulus at 5% strain was achieved for ex vivo crosslinked eyes (**Figure 13 B**). By doping dye in PDMS fiber, Guo et al.^[91] made a highly flexible and stretchable optical strain sensor for human motion detection. The quantification of tensile strains was achieved by detecting the absorption changes of the light passing through the dye-doped fiber. Guo et al.^[92] fabricated stretchable core/cladding optical fiber with different mixing ratio of the base to curing agent for core and cladding (5:1 for core, 20:1 for cladding). By incorporating upconversion nanoparticles (UCNPs) in the cladding, the fibers can be used to sense the temperature ranging from 25°C to 70 °C with high linearity and sensitivity. Kolle et al.^[93] fabricated tunable band-gap optical multilayer fibers by first forming a bilayer of PDMS and polystyrene-polyisoprene-polystyrene triblock copolymer (PSPI), which was subsequently rolled up onto a thin glass fiber to form the multilayer cladding (**Figure 13 D**). The band-gap can be tuned by adjusting the thickness of initial materials or stretching the fabricated multilayer fiber after removal of the glass core. Missinne et al.^[94] presented an artificial optical skin with a novel type of optical force sensing elements, which can achieve sensing by detecting the change in coupling between two arrays of crossing polymer waveguides sealed in a PDMS matrix. Zhao et al.^[95] fabricated stretchable core/cladding optical waveguides, with a transparent polyurethane rubber as core

and a highly absorptive silicone composite as cladding (**Figure 13 E**). The waveguides were introduced into a robotic hand for strain sensing (**Figure 13 E**).

Besides above elastomers, citrate-based elastomers and some commercial elastomers have also been employed for optical fibers. Shan et al.^[96] developed a step-index optical fiber made of two citrate-based elastomers, with poly(octamethylene citrate) (POC) as cladding and poly(octamethylene maleate citrate) (POMC) as core. The fabricated optical fibers showed very soft and flexible mechanical properties and low optical propagating loss (0.4 dB/cm), which showed the potential application of delivering and collecting light in deep tissue (**Figure 13 C**). Leber et al.^[97] fabricated stretchable step-index optical fibers by co-extrusion of two commercial elastomers. The core/cladding fibers (**Figure 13 F**) exhibited low optical loss of 0.8 dB/cm and extreme stretchability up to 545% at break. Three applications were reported in this work: a knee brace to monitor knee movement during walking and running; a glove for tracking finger movement and an impact sensor in a tennis racket, which confirmed the stable and reliable optomechanical property under repeated exposure to large strains and high-speed impacts.

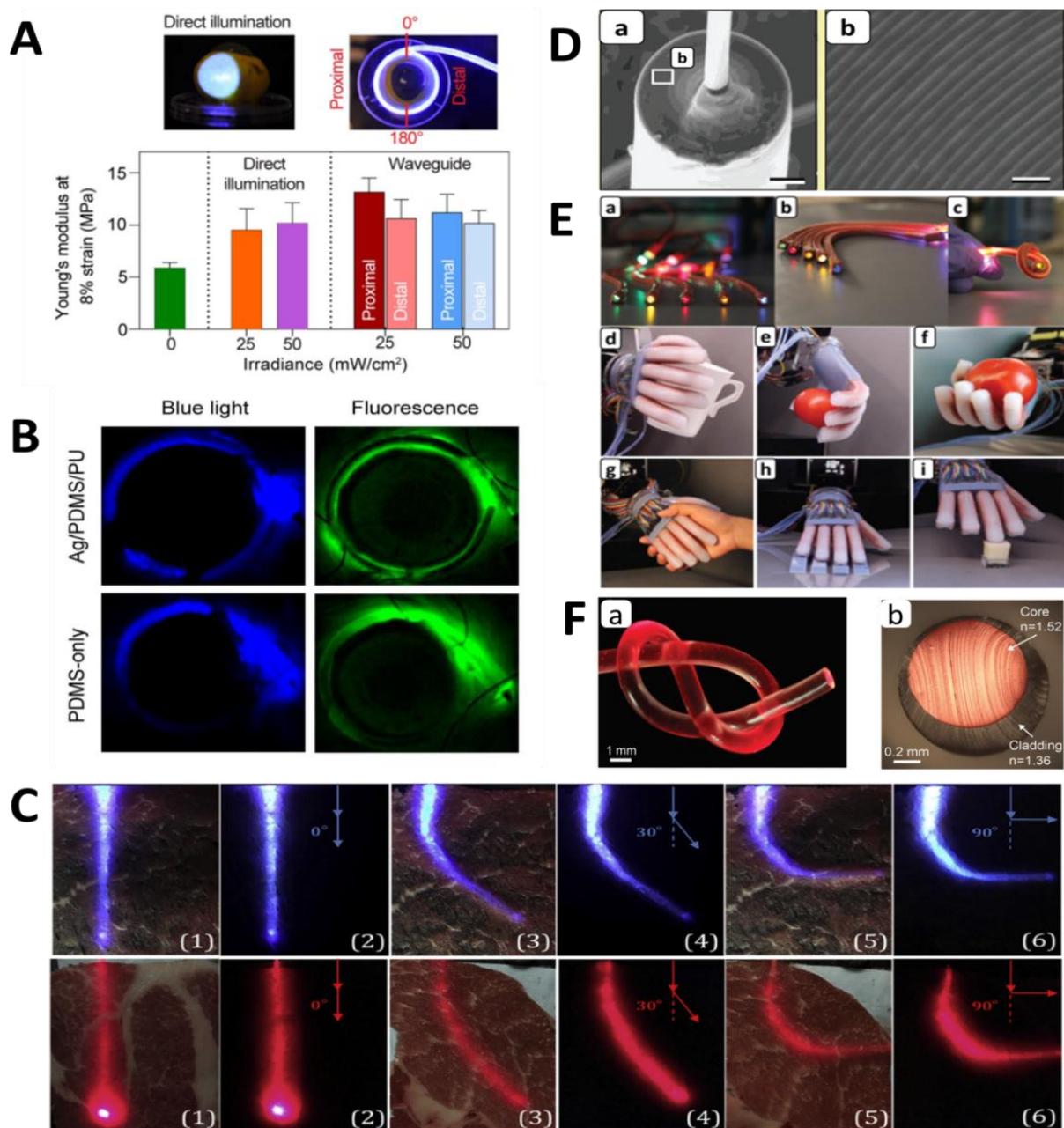


Figure 13. (A) Illumination without and with PDMS waveguides for Scleral cross-linking and the Young's modulus at 8% strain. With waveguide, the stiffness of scleral tissues at the proximally and distally treated halves of the eye is not significantly different from each other and is similar to the positive control irradiated with direct illumination. (B) Images of light delivery through Ag/PDMS/PU and PDMS-only waveguides. (C) Blue light (473 nm) (up) and red light (633 nm) (below) propagates along the citrate-based optical fibers through porcine muscle at different bending angles of (1, 2) 0, (3, 4) 30 and (5, 6) 90

degree recorded with environmental light on (1, 3, 5) and off (2, 4, 6), respectively. (D) a: Scanning electron micrograph of the cross-section of multilayer wrapped fiber; b: Scanning electron micrograph of the cross-section of cladding layers. Scale bars: 20 μ m (D-a) and 1 μ m (D-b). (E) a-c: flexible waveguides with LEDs inserted in one end; d-i: artificial hand holding a coffee mug (d), grasping a tomato (e and f), shaking a human hand (g), lateral scanning over surfaces to detect roughness and shape (h), probing the softness of a soft sponge using the middle finger (i). (F) a: A fiber is tied into a knot with light propagating inside; b: cross-section of core/cladding fiber. (A) Reprinted from ref^[89]. Copyright 2017 The Authors. (B) Reprinted from ref^[90]. Copyright 2019 The Authors. (C) Reprinted after permission from ref^[96]. Copyright © 2017 Elsevier Ltd. (D) Reprinted after permission from ref^[93]. Copyright © 2013 WILEY-VCH Verlag GmbH & Co. KGaA, Weinheim. (E) Reprinted after permission from ref^[95]. Copyright © 2016, American Association for the Advancement of Science. (F) Reprinted after permission from ref^[97]. Copyright © 2018 WILEY-VCH Verlag GmbH & Co. KGaA, Weinheim.

Bioresorbable inorganic glass

Despite inorganic optical waveguides cannot properly match the mechanical properties of tissue, the overwhelming superiority of light guiding property still drive researchers to develop novel inorganic optical waveguides. Phosphate-based glasses have proved to be bioresorbable biomaterials and have been widely used in biomedical applications since early 80's.^[98] For example, phosphate glass hollow fibers were fabricated as release systems for biomedical applications.^[99] Based on the excellent optical properties, phosphate glasses have been applied for biomedical optics. A series of bioresorbable calcium-phosphate based glasses

were fabricated^[98b, 100], which present a wide transparent window from UV to near near-infrared region. Podrazky et al.^[101] reported a biodegradable phosphate-based optical fiber from high purity biocompatible chemicals (P_2O_5 – CaO – Na_2O – SiO_2 – MgO). The fabricated optical fiber showed very low attenuation less than 30 dB/m in the range 400-1600 nm and proved to be biodegradable in physiological solutions. A pH sensor was prepared based on the inorganic fiber and showed promising performance in the range of pH from 5.0 to 7.0.

1.3.2.3 Multifunctional fibers

Besides guiding light, optical waveguides can incorporate additional functions. Lu et al.^[102] developed highly flexible fiber probes from polycarbonate (PC, for core), cyclic olefin copolymer (COC, for cladding) and conductive polyethylene (CPE, for electrodes) by thermal drawing technique (**Figure 14 A**). The fabricated fiber showed low optical loss even under high bending deformation angles (270°) and small curvature (0.5mm). By harnessing the probes, they realized simultaneous recording and optogenetically stimulating neural activity in the spinal cord of transgenic mice. Instead of integrating conductive polyethylene in the fiber, they prepared another multifunctional fiber by dip coating of silver nanowires (AgNWs) and PDMS layers following thermally drawing cyclic olefin copolymer (COC) wrapped polycarbonate (PC) cylinders. With this fiber, they also achieved simultaneous stimulation and recording in transgenic mice.^[103] Andres et al.^[104] and Seongjun et al.^[105] fabricated multifunctional fibers from a series of polymers and metal, which compose of optical waveguides, electrodes and microfluidic channels (**Figure 14 B**). With the multifunctional fibers, simultaneously optical stimulation, electrode recording and drug delivery in behaving mice with high resolution can be achieved.

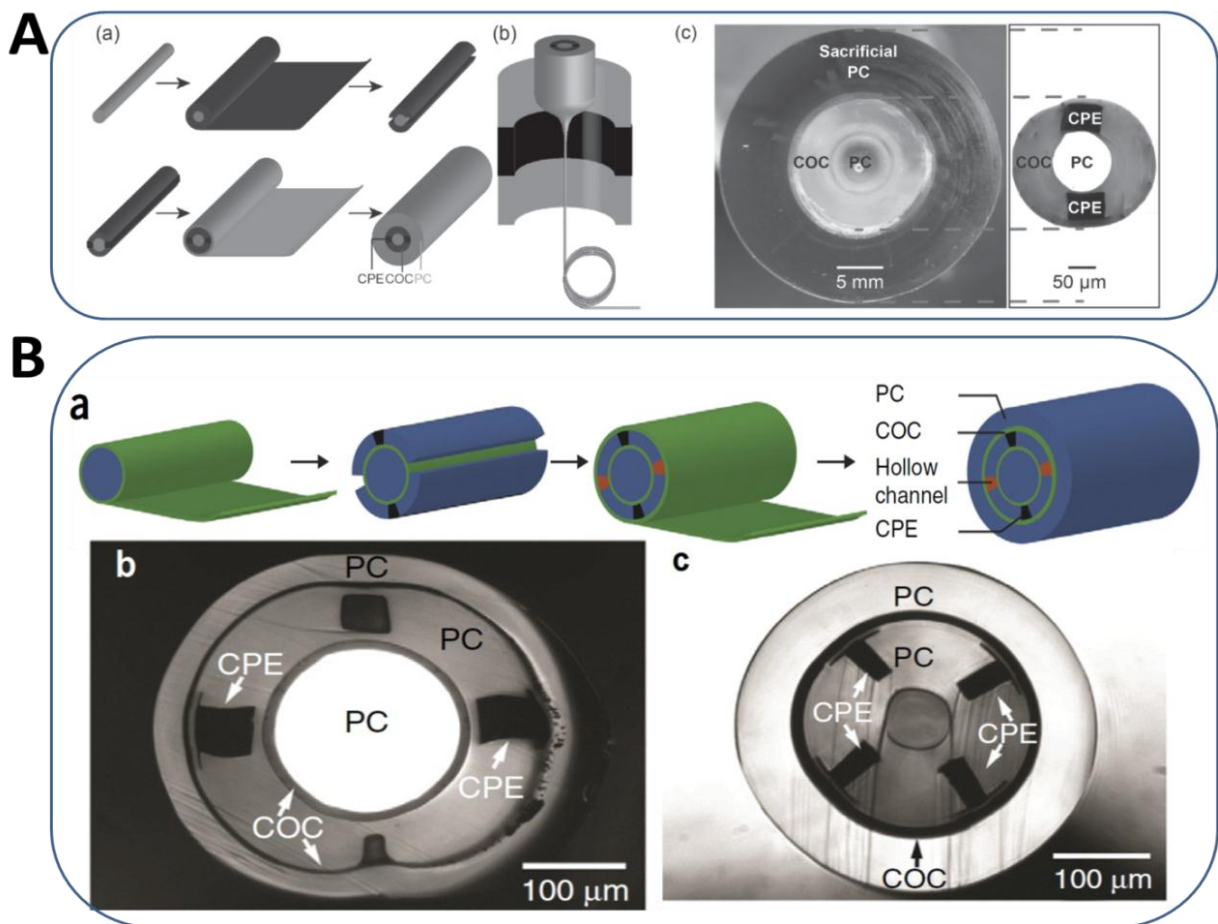


Figure 14. (A) Scheme of fabricating all-polymer neural fiber probes--a: fabrication of the preform; b: thermo-drawing the preform into a fiber; c: Left: the cross section of the preform; Right: cross-section of the polymer fiber after thermo-drawing the preform and etching the sacrificial PC layer. (B) The fabrication of multimodality fiber probe—a: A scheme of preparing the preform for multimodality fiber probes; b-c: Cross-sectional of multimodality fiber. (A) Reprinted (adapted) with permission from ref^[102]. Copyright © 2014 WILEY-VCH Verlag GmbH & Co. KGaA, Weinheim. (B) Reprinted after permission from ref^[104]. Copyright © 2015, Springer Nature.

1.4 Approaches to fabricate optical waveguides

Three different approaches have been mainly used to fabricate implantable optical waveguides: i) thermal drawing; ii) soft lithography; and iii) molding.

Thermal drawing is performed by heating a macrostructured preform and drawing it into extended lengths of microstructured form.^[106] This method has been commonly employed for fabricating conventional inorganic optical waveguides. Besides, thermal drawing has been used to fabricate biomaterial-based optical waveguides. For example, poly(L-lactic acid) (PLLA)-based optical fibers with diameter of 220 μm were fabricated through thermal drawing approach.^[60] Thermal drawing has been applied to fabricate multifunctional polymer fibers with delicate structures.^[31a, 102-105, 107] With these fibers, multifunction including stimulating, recording and drug delivery can be simultaneously achieved. However, the application of this method in biomaterials based optical waveguides is only limited to thermoplastic polymers.

Soft lithography represents a non-photolithographic method by employing elastomeric stamps, molds and conformable photomasks for fabricating or replicating two- and three-dimensional micro- and nanostructures.^[108] Soft lithography has been widely used to fabricate functional components and devices in different areas, such as optics, microelectronics, biology, biochemistry as well optical waveguides.^[108c, 109] An agarose hydrogel based optical waveguide has been successfully fabricated by soft lithography.^[47] So far, this approach is commonly used to fabricate or replicate complicated micro- and/or nanostructures.

Molding is the process to manufacture products by shaping flowable raw materials, such as plastic, glass, metal and ceramic, with a rigid mold. Molding processes are also the most commonly used approach to fabricate biomaterials based optical waveguides, especially for hydrogel based waveguides. For example, several polyacrylamide^[69, 76], PEG diacrylate^[29b, 31b, 75] and PDMS^[89-90] based optical waveguides have been fabricated by molding. However, this method is not suitable to prepare complicated structures. For example, to

fabricate a core/cladding structured fibers, multi-steps must be taken: step 1—forming the core in a mold; step 2—removing core from mold; step 3—dip-coating to form cladding layer. ^[31b, 69]

More recently, printing technologies have shown potential for scalable manufacture and flexible designs for processing. So far, printing has not been widely used to fabricate optical waveguides. Only few simple samples can be found in literatures, such as a direct ink writing technique was employed to fabricate silk hydrogel based waveguides^[36] and photocurable optical fibers with fugitive cladding.^[110] However, the possibility in fabricating complicated and multifunctional devices makes printing technologies promising processing techniques in integrating optical, electronic, mechanical and eventually pharmacological components into small, flexible and biocompatible medical devices. Thus printing technologies should be further exploited to prepare optical waveguides. In next section, printing technologies for biomaterials will be discussed in detail.

1.5 Printing technologies for biomaterials

For the fabrication of biomaterials in biomedical industry, a variety of printing technologies have been developed in the last years. These can be roughly classified into two main categories (**Figure 15**): i) stimulus-triggered printing; ii) deposition-based printing.^[111] Additional printing techniques in development are surface tension-assisted 3D printing^[112] or tomographic reconstruction 3D printing^[113]. In this section, several standard and emerging printing techniques will be briefly discussed.

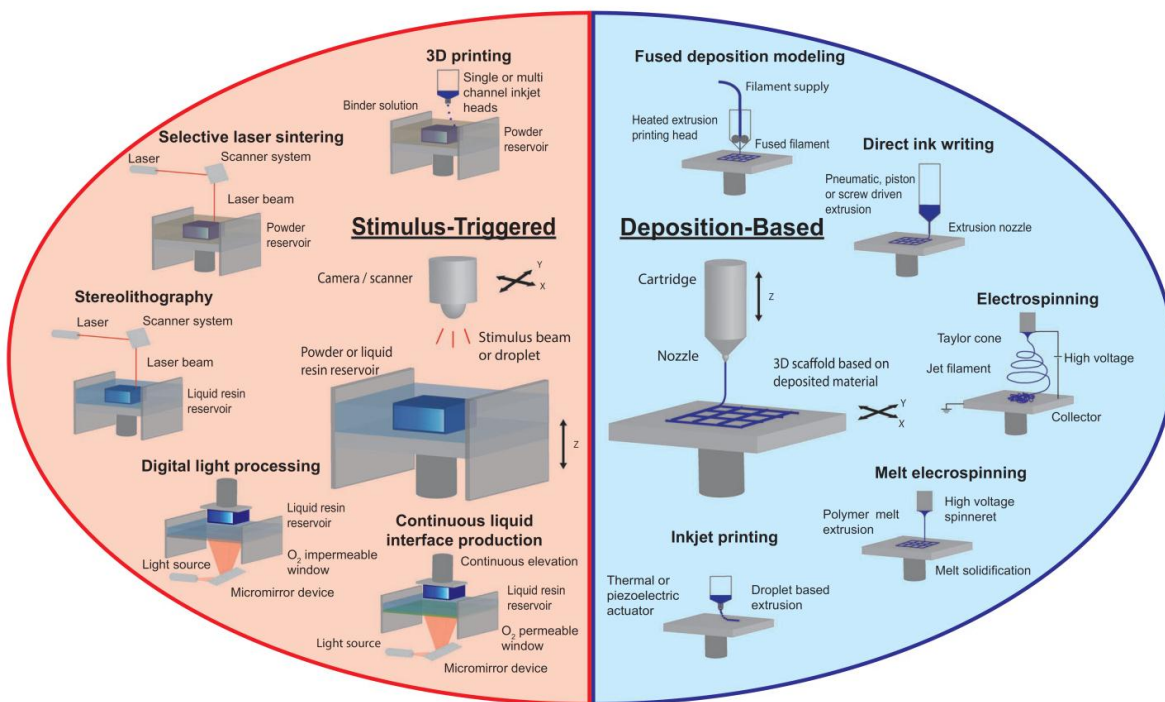


Figure 15. Classification of established 3D printing technologies available for the fabrication biomaterials. Left: Stimulus-triggered 3D printing technologies; Right: Deposition-based 3D printing technologies. Reprinted after permission from ref^[111]. Copyright © 2019 WILEY-VCH Verlag GmbH & Co. KGaA, Weinheim.

1.5.1 Stimulus-triggered 3D printing

For stimulus-triggered 3D printing, the desired 3D object is formed by solidifying components with a trigger, such as a binder solution or laser beam, at specific spatial locations (**Figure 15-left**).^[111] There are around five commonly used techniques to realize stimulus-triggered 3D printing, including stereolithography, binder jetting, selective laser sintering, digital light processing and continuous liquid interface production. Stereolithography (SLA) is considered to be the first commercially available solid freeform fabrication technique, which was developed in 1986.^[114] SLA employs light to cure photosensitive resin in regions of light exposure.^[111] Combining with medical imaging techniques, such as MRI or CT scan, SLA has been widely used in biomedical applications, including patient-

specific models, implants and tissue engineering.^[114-115] The binder jetting is performed by depositing a binder material on top a confined layer of fluent porous material like a powder to form a layer of bonded powder material at the region where the binder is printed.^[116] This technique can be applied to fabricate complex geometries with various materials, such as metal, ceramics and polymers, which can be employed for drug delivery devices^[117], tissue engineering scaffold^[118] and complex bone substitutes^[119]. For selective laser sintering (SLS), a laser is employed to heat the defined regions of a powder bed to fuse the powder into a solidified structure. Basically, SLS can be used to print any kind of powder-based biomaterials including metal, ceramics and polymers, which can be adapted for the application in tissue engineering and medical implants.^[111, 115] Digital light processing (DLP) is based on photolithography, which employs a digital micromirror or liquid-crystal display to project a 2D pattern into photosensitive resin to cure the entire layer. Then the cured layer is raised vertically to allow fresh resin to flow in and being cured by the second pattern to form the second layer. The same manner is repeated to obtain a 3D object.^[111, 115] This technique has been commercialized and applied in several biomedical applications, like dental crowns, shells for hearing aid components and molds for tissue engineering.^[115, 120] Continuous liquid interface production (CLIP) is an improved version of DLP by replacing oxygen impermeable window with oxygen permeable window, which enables the formed part to be withdrawn easily and continuously from the resin reservoir.^[121] So far, this efficient technique has been commercialized and been used for the design of custom biomaterials.^[111]

1.5.2 Deposition-based 3D printing

Deposition-based 3D printing is realized by depositing material in a defined manner to obtain the designed 3D objects without stimulus to trigger the solidification (**Figure 15-right**). Here five commonly used deposition-based 3D

printing techniques will be introduced including fused deposition modeling, inkjet printing, electrospinning, melt electrospinning and direct ink writing. Fused deposition modeling (FDM) is normally used to print thermoplastic polymers, which is performed by extruding melted materials as filaments that get solidified upon cooling.^[111] The material is deposited at the defined regions and forming 3D objects layer-by-layer. Even though this technique is the second most widely used printing technique, its disadvantages including low Z-axis resolution, slow building speed, low surface quality, and inappropriate extruding conditions make it inappropriate for biomedical applications.^[115, 122] Inkjet printing is based on droplet dispensing that is driven by thermal or piezoelectric actuators, with which the hydrogel precursor is directly dispensed through a nozzle and deposited onto the collecting platform.^[111] Due to the high spatial resolution of droplets, this technique is widely applied to print cells.^[123] Both electrospinning and melt electrospinning writing (MEW) are based on high voltage electric field, which is applied to charge the ejected polymer and guide it to the collector.^[111] However, the alignment of printed fibers is significantly improved by adopting MEW, which is beneficial to enhancing the mechanical properties of printed structures.^[124] Direct ink writing (DIW) employs piston, pneumatic or screw-driven robotic dispensing to extrude materials, which is commonly used to print hydrogel based inks and bioinks. However, it's very difficult to keep the fidelity of extruded hydrogel precursors without stimulus to trigger solidification. In such case, a shear-thinning support bath is very practical, which allow the liquid precursor to maintain the form after being dispensed.^[125]

1.5.3 Emerging new 3D printing techniques

Even though plenty of 3D printing techniques have been established, new 3D printing technologies continue to emerge enabling the on-demand fabrication of new biomaterials and complex structures. For instance, an acoustophoretic

printing platform was developed for droplet generation and patterning of disparate materials with unprecedented range of physical properties.^[126] This technique employs the acoustic properties of a single subwavelength ultrasonic cavity to generate a highly controllable and localized acoustic pressure that allows the formation of monodisperse drops. Recently, surface tension-assisted additive manufacturing was developed to fabricate mechanically supported multicomponent (bio)materials.^[112] In the process, a fenestrated support structure was first printed with SLA or SLS and then was coated and biofunctionalized by exploiting surface tension to integrate polymer networks across the windows of the support structure. In order to print soft matter voxel by voxel with multi-materials, Skylar-Scott et al.^[127] designed multimaterial multinozzle 3D printing (MM3D) method. To realize MM3D printing, they designed multinozzles with different dimensions: 0D nozzle—single nozzle with multichannels, 1D nozzle—multinozzles in one array, 2D nozzle—multinozzles in multiarrays (**Figure 16 a-c**). Each nozzle of the printheads can be connected up to eight different materials. During printing, the materials can be switched rapidly by a bank of fast-cycling pneumatic solenoids (**Figure 16 d**). With this method, complex architectures with designed composition and structures from multimaterials have been printed in voxel level resolution (**Figure 16 e**).

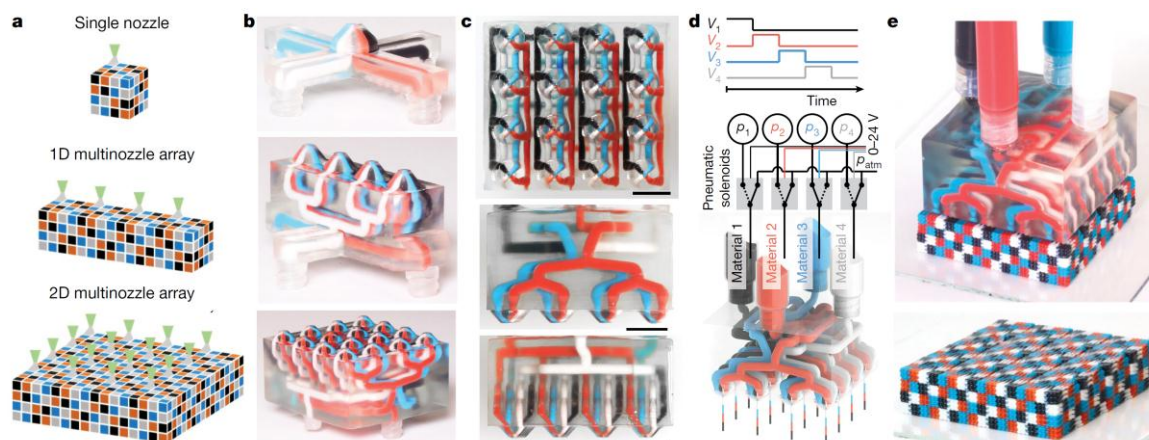


Figure 16. Design of multimaterial multinozzle 3D (MM3D) printheads. a, Scheme of voxelated architectures printed by using a single nozzle, 1D nozzle array and 2D nozzle array. b, pictures of single nozzle, 1D nozzle array and 2D nozzle array printheads. c, Photographs of the top (top) and side (middle and bottom) sections of a 4 × 4-nozzle, four-material, 2D nozzle array printhead. Scale bars, 10 mm. d, Illustration of MM3D printhead operation, where V1–V4 represent the voltage waveforms controlling the extrusion pressures p1–p4 for materials 1–4, and p_{atm} represents the atmospheric pressure. e, Voxelated architecture printed using a 4 × 4-nozzle, four-material, 2D nozzle array printhead. Reprinted after permission from ref^[127]. Copyright © 2019, Springer Nature.

In stimulus-triggered 3D printing, research on advancing utilization of light has been constantly reported. For example, multiphoton lithography was adopted to fabricate high spatial resolution of objects based on the outstanding feature resolution and the possibility to arbitrarily position the active focus volume within a 3D construct.^[128] The combination of food dye additives as photoabsorbers and projection stereolithography were employed to fabricate highly complex vascular networks and topologies for studies of fluid mixers, valves, intervascular transport, nutrient delivery, and host engraftment.^[129] By employing a mobile liquid interface (a fluorinated oil), a stereolithographic 3D printing approach was adopted to rapidly and large-volume fabricate polymeric components.^[130] Taking one step further from stereolithography, volumetric printing technologies were developed, which are based on the projection of a series of 2D optical patterns within a volume of a photosensitive polymeric precursor.^[113, 131] Instead of by layer-by-layer building blocks, volumetric printing enables the fabrication of entire objects at once.^[131c] In the evolution from the first conceptualization based on superposition of multiple beams^[131a] to the latest generation inspired by computed tomography (**Figure 17**)^[113], volumetric printing techniques have been

applied to fabricate technical photopolymers including acrylates^[113, 131a] and elastomeric resins^[131b], as well as generate cell-laden tissue constructs^[131c].

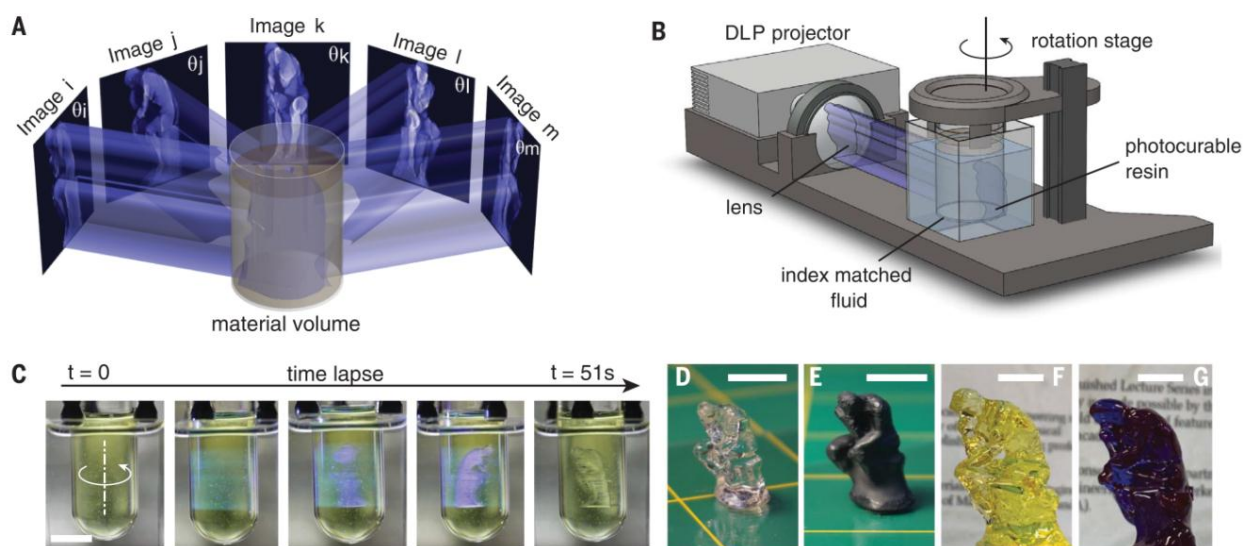


Figure 17. Volumetric 3D fabrication. (A) Fundamental concept: Patterned irradiation from different directions carrying a computed 3D exposure dose to a photoactive material. (B) Scheme of the computed axial lithography (CAL) system with a digital light processor–based projector. (C) Sequential state of the built architecture during a volumetric print, which was done in 1 min. (D) The completed 3D matter from (C). (E) Painted object from (D). (F-G) Larger (40-mm-tall) objects with the same geometry to (C) containing different dyes. Scale bars: 10 mm. Reprinted after permission from ref^[113].

In summary, 3D printing techniques have been exploited to fabricate a broad range of structures. The emerging 3D printing approaches will continue to optimize the functions of printing technologies from the perspectives of speed and resolution of printed objects. Furthermore, the available and developing printing technologies that can be used to fabricate biomaterials will further facilitate the development of biomedicine.

References

- [1] a) S. H. Yun, S. J. Kwok, *Nature biomedical engineering* 2017, 1, 0008; b) D. Barolet, presented at Seminars in cutaneous medicine and surgery 2008.
- [2] M. H. Niemz, *Laser-tissue interactions*, Springer, 2007.
- [3] a) A. Mehta, *Pharma XChange* 2011, 13, 12; b) D. A. Skoog, F. J. Holler, S. R. Crouch, *Principles of instrumental analysis*, Cengage learning, 2017.
- [4] B. Stuart, *Kirk-Othmer Encyclopedia of Chemical Technology* 2000, 1.
- [5] L. Fodor, R. Sobec, in *Aesthetic Applications of Intense Pulsed Light*, Springer 2020, p. 13.
- [6] H. Zeng, A. McWilliams, S. Lam, *Photodiagnosis and Photodynamic Therapy* 2004, 1, 111.
- [7] S. L. Jacques, *Physics in Medicine & Biology* 2013, 58, R37.
- [8] R. Steiner, in *Laser and IPL technology in dermatology and aesthetic medicine*, Springer 2011, p. 23.
- [9] R. Srinivasan, *Science* 1986, 234, 559.
- [10] E. S. Boyden, F. Zhang, E. Bamberg, G. Nagel, K. Deisseroth, *Nature neuroscience* 2005, 8, 1263.
- [11] S. Shabahang, S. Kim, S. H. Yun, *Advanced Functional Materials* 2018, 28, 1706635.
- [12] a) S. A. Boppart, R. Richards-Kortum, *Science translational medicine* 2014, 6, 253rv2; b) P. K. Drain, E. P. Hyle, F. Noubary, K. A. Freedberg, D. Wilson, W. R. Bishai, W. Rodriguez, I. V. Bassett, *The Lancet infectious diseases* 2014, 14, 239.
- [13] S. Thangaratinam, K. Brown, J. Zamora, K. S. Khan, A. K. Ewer, *The Lancet* 2012, 379, 2459.
- [14] L. Shen, J. A. Hagen, I. Papautsky, *Lab on a Chip* 2012, 12, 4240.
- [15] D.-H. Kim, N. Lu, R. Ma, Y.-S. Kim, R.-H. Kim, S. Wang, J. Wu, S. M. Won, H. Tao, A. Islam, *Science* 2011, 333, 838.
- [16] T. Grotjohann, I. Testa, M. Leutenegger, H. Bock, N. T. Urban, F. Lavoie-Cardinal, K. I. Willig, C. Eggeling, S. Jakobs, S. W. Hell, *Nature* 2011, 478, 204.
- [17] B.-C. Chen, W. R. Legant, K. Wang, L. Shao, D. E. Milkie, M. W. Davidson, C. Janetopoulos, X. S. Wu, J. A. Hammer, Z. Liu, *Science* 2014, 346, 1257998.
- [18] M. J. Maisels, A. F. McDonagh, *New England Journal of Medicine* 2008, 358, 920.
- [19] R. T. Chow, M. I. Johnson, R. A. Lopes-Martins, J. M. Bjordal, *The Lancet* 2009, 374, 1897.
- [20] M. A. Naeser, R. Zafonte, M. H. Krengel, P. I. Martin, J. Frazier, M. R. Hamblin, J. A. Knight, W. P. Meehan III, E. H. Baker, *Journal of neurotrauma* 2014, 31, 1008.

- [21] M. G. Shapiro, K. Homma, S. Villarreal, C.-P. Richter, F. Bezanilla, *Nature communications* **2012**, *3*, 736.
- [22] a) T. Sakimoto, M. I. Rosenblatt, D. T. Azar, *The Lancet* **2006**, *367*, 1432; b) J. Marshall, S. L. Trokel, S. Rothery, R. R. Krueger, *Ophthalmology* **1988**, *95*, 1411.
- [23] a) R. R. Anderson, J. A. Parrish, *Science* **1983**, *220*, 524; b) E. L. Tanzi, J. R. Lupton, T. S. Alster, *Journal of the American Academy of Dermatology* **2003**, *49*, 1; c) M. C. Grossman, C. Dierickx, W. Farinelli, T. Flotte, R. R. Anderson, *Journal of the American Academy of Dermatology* **1996**, *35*, 889.
- [24] a) M. Sofer, J. D. Watterson, T. A. Wollin, L. Nott, H. Razvi, J. D. Denstedt, *The Journal of urology* **2002**, *167*, 31; b) C. Ell, G. Lux, J. Hochberger, D. Müller, L. Demling, *Gut* **1988**, *29*, 746.
- [25] a) K. Deisseroth, *Nature methods* **2011**, *8*, 26; b) O. Yizhar, L. E. Fenno, T. J. Davidson, M. Mogri, K. Deisseroth, *Neuron* **2011**, *71*, 9; c) K. Deisseroth, *Nature neuroscience* **2015**, *18*, 1213.
- [26] F. Zhang, J. Vierock, O. Yizhar, L. E. Fenno, S. Tsunoda, A. Kianianmomeni, M. Prigge, A. Berndt, J. Cushman, J. Polle, *Cell* **2011**, *147*, 1446.
- [27] P. Mahmoudi, H. Veladi, F. G. Pakdel, *Journal of medical signals and sensors* **2017**, *7*, 71.
- [28] V. Gradinaru, M. Mogri, K. R. Thompson, J. M. Henderson, K. Deisseroth, *Science* **2009**, *324*, 354.
- [29] a) H. Ye, M. Daoud-El Baba, R.-W. Peng, M. Fussenegger, *Science* **2011**, *332*, 1565; b) M. Choi, J. W. Choi, S. Kim, S. Nizamoglu, S. K. Hahn, S. H. Yun, *Nature photonics* **2013**, *7*, 987.
- [30] a) K. Kalka, H. Merk, H. Mukhtar, *Journal of the American Academy of Dermatology* **2000**, *42*, 389; b) B. Wilson, M. Patterson, *Physics in Medicine & Biology* **1986**, *31*, 327; c) C. R. Simpson, M. Kohl, M. Essenpreis, M. Cope, *Physics in Medicine & Biology* **1998**, *43*, 2465.
- [31] a) R. Nazempour, Q. Zhang, R. Fu, X. Sheng, *Materials* **2018**, *11*, 1283; b) M. Choi, M. Humar, S. Kim, S. H. Yun, *Advanced Materials* **2015**, *27*, 4081.
- [32] a) H. Yu, J. Park, K. Lee, J. Yoon, K. Kim, S. Lee, Y. Park, *Current Applied Physics* **2015**, *15*, 632; b) R. Horstmeyer, H. Ruan, C. Yang, *Nature photonics* **2015**, *9*, 563; c) H. Ruan, J. Brake, J. E. Robinson, Y. Liu, M. Jang, C. Xiao, C. Zhou, V. Gradinaru, C. Yang, *Science advances* **2017**, *3*, eaao5520.
- [33] T.-i. Kim, J. G. McCall, Y. H. Jung, X. Huang, E. R. Siuda, Y. Li, J. Song, Y. M. Song, H. A. Pao, R.-H. Kim, *Science* **2013**, *340*, 211.
- [34] H. Ma, A. Y. Jen, L. R. Dalton, *Advanced Materials* **2002**, *14*, 1339.
- [35] W. Huang, S. Ling, C. Li, F. G. Omenetto, D. L. Kaplan, *Chemical Society Reviews* **2018**, *47*, 6486.
- [36] S. T. Parker, P. Domachuk, J. Amsden, J. Bressner, J. A. Lewis, D. L. Kaplan, F. G. Omenetto, *Advanced Materials* **2009**, *21*, 2411.

- [37] M. B. Applegate, G. Perotto, D. L. Kaplan, F. G. Omenetto, *Biomedical optics express* **2015**, *6*, 4221.
- [38] S. Kujala, A. Mannila, L. Karvonen, K. Kieu, Z. Sun, *Scientific reports* **2016**, *6*, 22358.
- [39] N. Huby, V. Vié, A. Renault, S. Beaufils, T. Lefèvre, F. Paquet-Mercier, M. Pézolet, B. Bêche, *Applied Physics Letters* **2013**, *102*, 123702.
- [40] a) K. H. Tow, D. M. Chow, F. Vollrath, I. Dicaire, T. Gheysens, L. Thévenaz, presented at 2017 25th Optical Fiber Sensors Conference (OFS) **2017**; b) K. H. Tow, D. M. Chow, F. Vollrath, I. Dicaire, T. Gheysens, L. Thévenaz, *Journal of Lightwave Technology* **2017**, *36*, 1138.
- [41] X. Qiao, Z. Qian, J. Li, H. Sun, Y. Han, X. Xia, J. Zhou, C. Wang, Y. Wang, C. Wang, *ACS Applied Materials & Interfaces* **2017**, *9*, 14665.
- [42] C. Choi, J.-P. Nam, J.-W. Nah, *Journal of Industrial and Engineering Chemistry* **2016**, *33*, 1.
- [43] S. Y. Bratskaya, Y. A. Azarova, E. Matochkina, M. Kodess, Y. G. Yatluk, A. Pestov, *Carbohydrate polymers* **2012**, *87*, 869.
- [44] A. Mironenko, E. Modin, A. Sergeev, S. Voznesenskiy, S. Bratskaya, *Chemical Engineering Journal* **2014**, *244*, 457.
- [45] A. Y. Mironenko, A. Sergeev, A. Nazirov, E. Modin, S. Voznesenskiy, S. Y. Bratskaya, *Sensors and Actuators B: Chemical* **2016**, *225*, 348.
- [46] A. Dupuis, N. Guo, Y. Gao, N. Godbout, S. Lacroix, C. Dubois, M. Skorobogatiy, *Optics letters* **2007**, *32*, 109.
- [47] A. Jain, A. H. Yang, D. Erickson, *Optics letters* **2012**, *37*, 1472.
- [48] Y. Tabata, Y. Ikada, *Advanced drug delivery reviews* **1998**, *31*, 287.
- [49] R. T. Chen, W. Phillips, T. Jansson, D. Pelka, *Optics letters* **1989**, *14*, 892.
- [50] A. K. Manocchi, P. Domachuk, F. G. Omenetto, H. Yi, *Biotechnology and bioengineering* **2009**, *103*, 725.
- [51] a) N. Amdursky, M. Molotskii, E. Gazit, G. Rosenman, *Applied Physics Letters* **2009**, *94*, 261907; b) J. Ryu, S. Y. Lim, C. B. Park, *Advanced Materials* **2009**, *21*, 1577.
- [52] a) A. Handelman, B. Apter, T. Shostak, G. Rosenman, *Journal of Peptide Science* **2017**, *23*, 95; b) A. Handelman, N. Lapshina, B. Apter, G. Rosenman, *Advanced Materials* **2018**, *30*, 1705776.
- [53] a) A. Handelman, S. Lavrov, A. Kudryavtsev, A. Khatchatourians, Y. Rosenberg, E. Mishina, G. Rosenman, *Advanced Optical Materials* **2013**, *1*, 875; b) R. W. Boyd, *Nonlinear optics*, Elsevier, **2003**.
- [54] F. Milano, A. Punzi, R. Ragni, M. Trotta, G. M. Farinola, *Advanced Functional Materials* **2019**, *29*, 1805521.
- [55] H. Xin, Y. Li, X. Liu, B. Li, *Nano letters* **2013**, *13*, 3408.
- [56] J. Harris, R. Shubert, J. Polky, *JOSA* **1970**, *60*, 1007.

- [57] a) S. Nizamoglu, M. C. Gather, M. Humar, M. Choi, S. Kim, K. S. Kim, S. K. Hahn, G. Scarcelli, M. Randolph, R. W. Redmond, *Nature communications* **2016**, *7*, 10374; b) S. Nizamoglu, M. C. Gather, M. Humar, M. Choi, S. Kim, K. S. Kim, S. K. Hahn, G. Scarcelli, M. Randolph, R. W. Redmond, presented at Novel Optical Materials and Applications **2017**.
- [58] M. Kim, J. An, K. S. Kim, M. Choi, M. Humar, S. J. Kwok, T. Dai, S. H. Yun, *Biomedical optics express* **2016**, *7*, 4220.
- [59] A. Gierej, M. Vagenende, A. Filipkowski, B. Siwicki, R. Buczynski, H. Thienpont, S. Van Vlierberghe, T. Geernaert, P. Dubruel, F. Berghmans, *Journal of Lightwave Technology* **2019**, *37*, 1916.
- [60] R. Fu, W. Luo, R. Nazempour, D. Tan, H. Ding, K. Zhang, L. Yin, J. Guan, X. Sheng, *Advanced Optical Materials* **2018**, *6*, 1700941.
- [61] S. Shabahang, S. Forward, S.-H. Yun, *Optics express* **2019**, *27*, 7560.
- [62] W. J. Choi, K. S. Park, B. H. Lee, *Journal of biomedical optics* **2014**, *19*, 090503.
- [63] J. W. Reddy, M. Chamanzar, *Optics letters* **2018**, *43*, 4112.
- [64] a) E. M. Ahmed, *Journal of advanced research* **2015**, *6*, 105; b) F. Ganji, F. S. Vasheghani, F. E. VASHEGHANI, **2010**.
- [65] A. Francone, T. Kehoe, I. Obieta, V. Saez-Martinez, L. Bilbao, A. Khokhar, N. Gadegaard, C. Simao, N. Kehagias, C. Sotomayor Torres, *Sensors* **2018**, *18*, 3240.
- [66] Y. J. Heo, H. Shibata, T. Okitsu, T. Kawanishi, S. Takeuchi, *Proceedings of the National Academy of Sciences* **2011**, *108*, 13399.
- [67] J. Guo, M. Zhou, C. Yang, *Scientific reports* **2017**, *7*, 7902.
- [68] J. Guo, H. Huang, M. Zhou, C. Yang, L. Kong, *Analytical chemistry* **2018**, *90*, 12292.
- [69] J. Guo, X. Liu, N. Jiang, A. K. Yetisen, H. Yuk, C. Yang, A. Khademhosseini, X. Zhao, S. H. Yun, *Advanced Materials* **2016**, *28*, 10244.
- [70] a) A. K. Yetisen, N. Jiang, A. Fallahi, Y. Montelongo, G. U. Ruiz-Esparza, A. Tamayol, Y. S. Zhang, I. Mahmood, S. A. Yang, K. S. Kim, *Advanced Materials* **2017**, *29*, 1606380; b) T. Saxl, F. Khan, M. Ferla, D. Birch, J. Pickup, *Analyst* **2011**, *136*, 968; c) E. A. Moschou, B. V. Sharma, S. K. Deo, S. Daunert, *Journal of fluorescence* **2004**, *14*, 535.
- [71] N. Jiang, R. Ahmed, A. A. Rifat, J. Guo, Y. Yin, Y. Montelongo, H. Butt, A. K. Yetisen, *Advanced Optical Materials* **2018**, *6*, 1701118.
- [72] S. Johannsmeier, M. Torres, T. Ripken, D. Heinemann, A. Heisterkamp, presented at Optogenetics and Optical Manipulation **2018** **2018**.
- [73] M. Zhou, J. Guo, C. Yang, *Sensors and Actuators B: Chemical* **2018**, *264*, 52.
- [74] L. Zhao, J. Gan, T. Xia, L. Jiang, J. Zhang, Y. Cui, G. Qian, Z. Yang, *Journal of Materials Chemistry C* **2019**, *7*, 897.

- [75] a) M. Elsherif, M. U. Hassan, A. K. Yetisen, H. Butt, *Biosensors and Bioelectronics* 2019, 137, 25; b) M. Elsherif, R. Moreddu, M. U. Hassan, A. K. Yetisen, H. Butt, *Lab on a Chip* 2019, 19, 2060.
- [76] L. Wang, C. Zhong, D. Ke, F. Ye, J. Tu, L. Wang, Y. Lu, *Advanced Optical Materials* 2018, 6, 1800427.
- [77] a) J. C. McDonald, G. M. Whitesides, *Accounts of chemical research* 2002, 35, 491; b) G. Comina, A. Suska, D. Filippini, *Lab on a Chip* 2014, 14, 424; c) D. Psaltis, S. R. Quake, C. Yang, *Nature* 2006, 442, 381.
- [78] a) R. N. Palchesko, L. Zhang, Y. Sun, A. W. Feinberg, *PloS one* 2012, 7, e51499; b) Y. Sun, Q. Jallerat, J. M. Szymanski, A. W. Feinberg, *Nature methods* 2015, 12, 134.
- [79] D.-H. Kim, R. Ghaffari, N. Lu, J. A. Rogers, *Annual review of biomedical engineering* 2012, 14, 113.
- [80] B. D. Ratner, A. S. Hoffman, F. J. Schoen, J. E. Lemons, *Biomaterials science: an introduction to materials in medicine*, Elsevier, 2004.
- [81] V. Lien, Y. Berdichevsky, Y.-H. Lo, *IEEE Photonics Technology Letters* 2004, 16, 1525.
- [82] S. Kopetz, D. Cai, E. Rabe, A. Neyer, *AEU-International Journal of Electronics and Communications* 2007, 61, 163.
- [83] Y. Xia, E. Kim, X.-M. Zhao, J. A. Rogers, M. Prentiss, G. M. Whitesides, *Science* 1996, 273, 347.
- [84] a) L. Pang, U. Levy, K. Campbell, A. Groisman, Y. Fainman, *Optics express* 2005, 13, 9003; b) D.-Y. Zhang, N. Justis, Y.-H. Lo, *Applied Physics Letters* 2004, 84, 4194.
- [85] Y. Gambin, O. Legrand, S. R. Quake, *Applied Physics Letters* 2006, 88, 174102.
- [86] J. Missinne, S. Kalathimekkad, B. Van Hoe, E. Bosman, J. Vanfleteren, G. Van Steenberge, *Optics express* 2014, 22, 4168.
- [87] M. Ramuz, B. C. K. Tee, J. B. H. Tok, Z. Bao, *Advanced Materials* 2012, 24, 3223.
- [88] C. To, T. L. Hellebrekers, Y.-L. Park, presented at 2015 IEEE/RSJ International Conference on Intelligent Robots and Systems (IROS) 2015.
- [89] S. J. Kwok, M. Kim, H. H. Lin, T. G. Seiler, E. Beck, P. Shao, I. E. Kochevar, T. Seiler, S.-H. Yun, *Investigative ophthalmology & visual science* 2017, 58, 2596.
- [90] S. J. Kwok, S. Forward, C. M. Wertheimer, A. C. Liapis, H. H. Lin, M. Kim, T. G. Seiler, R. Birngruber, I. E. Kochevar, T. Seiler, *Investigative ophthalmology & visual science* 2019, 60, 2563.
- [91] J. Guo, M. Niu, C. Yang, *Optica* 2017, 4, 1285.
- [92] J. Guo, B. Zhou, C. Yang, Q. Dai, L. Kong, *Advanced Functional Materials* 2019, 1902898.

- [93] M. Kolle, A. Lethbridge, M. Kreysing, J. J. Baumberg, J. Aizenberg, P. Vukusic, *Advanced Materials* **2013**, *25*, 2239.
- [94] J. Missinne, G. Van Steenberge, B. Van Hoe, K. Van Coillie, T. Van Gijsegheem, P. Dubruel, J. Vanfleteren, P. Van Daele, presented at Photonics Packaging, Integration, and Interconnects IX **2009**.
- [95] H. Zhao, K. O'Brien, S. Li, R. F. Shepherd, *Science Robotics* **2016**, *1*, eaai7529.
- [96] D. Shan, C. Zhang, S. Kalaba, N. Mehta, G. B. Kim, Z. Liu, J. Yang, *Biomaterials* **2017**, *143*, 142.
- [97] A. Leber, B. Cholst, J. Sandt, N. Vogel, M. Kolle, *Advanced Functional Materials* **2019**, *29*, 1802629.
- [98] a) J. Burnie, T. Gilchrist, S. Duff, C. Drake, N. Harding, A. Malcolm, *Biomaterials* **1981**, *2*, 244; b) E. Ceci-Ginistrelli, D. Pugliese, N. G. Boetti, G. Novajra, A. Ambrosone, J. Lousteau, C. Vitale-Brovarone, S. Abrate, D. Milanese, *Optical Materials Express* **2016**, *6*, 2040.
- [99] G. Novajra, J. Lousteau, D. Milanese, C. Vitale-Brovarone, *Materials Letters* **2013**, *99*, 125.
- [100] D. Pugliese, E. Ceci-Ginistrelli, N. G. Boetti, A. Ambrosone, J. Lousteau, D. Milanese, presented at 2016 18th International Conference on Transparent Optical Networks (ICTON) **2016**.
- [101] O. Podrazky, P. Peterka, S. Vytykáčová, J. Proboštová, M. Kuneš, O. Lyutakov, E. Ceci-Ginistrelli, D. Pugliese, N. G. Boetti, D. Janner, presented at Optical Fibers and Sensors for Medical Diagnostics and Treatment Applications XVIII **2018**.
- [102] C. Lu, U. P. Froriep, R. A. Koppes, A. Canales, V. Caggiano, J. Selvidge, E. Bizzi, P. Anikeeva, *Advanced Functional Materials* **2014**, *24*, 6594.
- [103] C. Lu, S. Park, T. J. Richner, A. Derry, I. Brown, C. Hou, S. Rao, J. Kang, C. T. Moritz, Y. Fink, *Science advances* **2017**, *3*, e1600955.
- [104] A. Canales, X. Jia, U. P. Froriep, R. A. Koppes, C. M. Tringides, J. Selvidge, C. Lu, C. Hou, L. Wei, Y. Fink, *Nature biotechnology* **2015**, *33*, 277.
- [105] S. Park, Y. Guo, X. Jia, H. K. Choe, B. Grena, J. Kang, J. Park, C. Lu, A. Canales, R. Chen, *Nature neuroscience* **2017**, *20*, 612.
- [106] N. D. Orf, O. Shapira, F. Sorin, S. Danto, M. A. Baldo, J. D. Joannopoulos, Y. Fink, *Proceedings of the National Academy of Sciences* **2011**, *108*, 4743.
- [107] A. Abouraddy, M. Bayindir, G. Benoit, S. Hart, K. Kuriki, N. Orf, O. Shapira, F. Sorin, B. Temelkuran, Y. Fink, *Nature materials* **2007**, *6*, 336.
- [108] a) Y. Zheng, *Bioinspired Design of Materials Surfaces*, Materials Today, **2019**; b) J. A. Rogers, R. G. Nuzzo, *Materials today* **2005**, *8*, 50; c) Y. Xia, G. M. Whitesides, *Annual Review of Materials Science* **1998**, *28*, 153.
- [109] G. M. Whitesides, E. Ostuni, S. Takayama, X. Jiang, D. E. Ingber, *Annual review of biomedical engineering* **2001**, *3*, 335.

- [110] D. J. Lorang, D. Tanaka, C. M. Spadaccini, K. A. Rose, N. J. Cherepy, J. A. Lewis, *Advanced Materials* **2011**, *23*, 5055.
- [111] E. A. Guzzi, M. W. Tibbitt, *Advanced Materials* **2019**, 1901994.
- [112] H. Ragelle, M. W. Tibbitt, S.-Y. Wu, M. A. Castillo, G. Z. Cheng, S. P. Gangadharan, D. G. Anderson, M. J. Cima, R. Langer, *Nature communications* **2018**, *9*, 1184.
- [113] B. E. Kelly, I. Bhattacharya, H. Heidari, M. Shusteff, C. M. Spadaccini, H. K. Taylor, *Science* **2019**, *363*, 1075.
- [114] F. P. Melchels, J. Feijen, D. W. Grijpma, *Biomaterials* **2010**, *31*, 6121.
- [115] M. Touri, F. Kabirian, M. Saadati, S. Ramakrishna, M. Mozafari, *Advanced Engineering Materials* **2019**, *21*, 1800511.
- [116] E. M. Sachs, J. S. Haggerty, M. J. Cima, P. A. Williams, Google Patents, 1993.
- [117] W. Katstra, R. Palazzolo, C. Rowe, B. Giritlioglu, P. Teung, M. Cima, *Journal of Controlled Release* **2000**, *66*, 1.
- [118] C. X. F. Lam, X. Mo, S.-H. Teoh, D. Hutmacher, *Materials Science and Engineering: C* **2002**, *20*, 49.
- [119] M. Castilho, C. Moseke, A. Ewald, U. Gbureck, J. Groll, I. Pires, J. Teßmar, E. Vorndran, *Biofabrication* **2014**, *6*, 015006.
- [120] J. J. Beaman, C. Atwood, T. L. Bergman, D. Bourell, S. Hollister, D. Rosen, WORLD TECHNOLOGY EVALUATION CENTER INC BALTIMORE MD, 2004.
- [121] J. R. Tumbleston, D. Shirvanyants, N. Ermoshkin, R. Januszewicz, A. R. Johnson, D. Kelly, K. Chen, R. Pinschmidt, J. P. Rolland, A. Ermoshkin, *Science* **2015**, *347*, 1349.
- [122] S.-S. D. Carter, P. F. Costa, C. Vaquette, S. Ivanovski, D. W. Hutmacher, J. Malda, *Annals of biomedical engineering* **2017**, *45*, 12.
- [123] T. Boland, X. Tao, B. J. Damon, B. Manley, P. Kesari, S. Jalota, S. Bhaduri, *Materials Science and Engineering: C* **2007**, *27*, 372.
- [124] M. Castilho, A. van Mil, M. Maher, C. H. Metz, G. Hochleitner, J. Groll, P. A. Doevendans, K. Ito, J. P. Sluijter, J. Malda, *Advanced Functional Materials* **2018**, *28*, 1803151.
- [125] a) T. J. Hinton, Q. Jallerat, R. N. Palchesko, J. H. Park, M. S. Grodzicki, H.-J. Shue, M. H. Ramadan, A. R. Hudson, A. W. Feinberg, *Science advances* **2015**, *1*, e1500758; b) C. B. Highley, C. B. Rodell, J. A. Burdick, *Advanced Materials* **2015**, *27*, 5075; c) A. Lee, A. Hudson, D. Shiwerski, J. Tashman, T. Hinton, S. Yerneni, J. Bliley, P. Campbell, A. Feinberg, *Science* **2019**, *365*, 482; d) G. Luo, Y. Yu, Y. Yuan, X. Chen, Z. Liu, T. Kong, *Advanced Materials* **2019**, 1904631.
- [126] D. Foresti, K. T. Kroll, R. Amissah, F. Sillani, K. A. Homan, D. Poulidakos, J. A. Lewis, *Science advances* **2018**, *4*, eaat1659.
- [127] M. A. Skylar-Scott, J. Mueller, C. W. Visser, J. A. Lewis, *Nature* **2019**, *575*, 330.

- [128] a) J. Stampfl, R. Liska, A. Ovsianikov, *Multiphoton lithography: Techniques, materials, and applications*, John Wiley & Sons, 2016; b) J.-F. Xing, M.-L. Zheng, X.-M. Duan, *Chemical Society Reviews* 2015, 44, 5031.
- [129] B. Grigoryan, S. J. Paulsen, D. C. Corbett, D. W. Sazer, C. L. Fortin, A. J. Zaita, P. T. Greenfield, N. J. Calafat, J. P. Gounley, A. H. Ta, *Science* 2019, 364, 458.
- [130] D. A. Walker, J. L. Hedrick, C. A. Mirkin, *Science* 2019, 366, 360.
- [131] a) M. Shusteff, A. E. Browar, B. E. Kelly, J. Henriksson, T. H. Weisgraber, R. M. Panas, N. X. Fang, C. M. Spadaccini, *Science advances* 2017, 3, eaao5496; b) D. Loterie, P. Delrot, C. Moser, 2018; c) P. N. Bernal, P. Delrot, D. Loterie, Y. Li, J. Malda, C. Moser, R. Levato, *Advanced Materials* 2019, 31, 1904209.

2. Printed hydrogel-based waveguides

2.1 Abstract

This chapter describes the extrusion printing of degradable optical waveguides based on poly(ethyleneglycol), PEG, hydrogels. The obtained waveguides are flexible and soft. Their degradation kinetics is tunable by adjusting the molar mass of the gel precursor, which was synthesized by linking polyethylene glycol diacrylate (PEGDA) with varying proportions of D,L-dithiothreitol (DTT). The printed waveguides have very good optical properties and were used to activate photochemical processes in in vitro cell cultures. Core/cladding designs to improve the optical performance combining PEGDA-DTT with acrylated Pluronic hydrogel are also presented.

2.2 Introduction

Polyethylene glycol (PEG) is an important non-ionic type of synthetic polymer, which has been widely used for biomedical applications, such as drug delivery, tissue engineering and surface modification. PEG presents suitable properties for biological application, including excellent biocompatibility, nonimmunogenicity, enhanced permeability and retention effect, and resistance to protein adsorptions.^[1] PEG is obtained by cationic or anionic polymerization of ethylene oxide. The polymerization reaction can lead to linear or branched structures depending on the form of initiator. The terminal groups of the backbone are terminated by hydroxyl groups, which provide the possibility to modify PEG with

different functionalities.^[2] The introduced functional group at each terminal can be the same or different, which provides versatile possibility for fabricating PEG hydrogels or for conjugating with biological molecules.^[1a] PEG can be dissolved in several organic solvents, which makes end-group modifications even more easily. At the same time, the PEG diol backbone endows PEG high water solubility that provides a prerequisite for applying PEG in biological applications. As a synthetic polymer, PEG also demonstrates highly controllable design and adjustable physical/chemical/biological properties. For example, with anionic polymerization of ethylene oxide, low polydispersity index (PDI) of PEG can be easily obtained, which endow PEG high homogeneity, structure controllability and reproducibility.^[1d]

There are several crosslinking approaches have been employed to fabricate end-functionalized PEG hydrogels, such as photopolymerization of acrylated PEG,^[3] radiation of PEG polymer solutions,^[2, 4] click chemistry between azide and alkyne groups^[5], enzyme catalyzed reaction between conjugated peptides (Glutaminyl and Lysine residues)^[6], Michael-type addition between acrylate and thiol groups^[7] etc.^[1a] Among them, photopolymerization of acrylated PEG is the most common used approach. Using light-initiated polymerization, PEGDA allows in-situ formation of hydrogel with spatial-temporal control. This has been used to encapsulate living cells in 3D structures.^[1a, 8] Normally, PEG hydrogels are considered as non-degradable materials. However, PEG can be modified with degradable segments, such as polyester^[9] and disulfide^[10], to enhance its degradability.

Besides above mentioned advantages, PEG hydrogels possess a good balance between transparency and biocompatibility, which allow PEG hydrogels being applied in optical waveguides.^[11] As described in section 1.3.2.2, PEG diacrylate (PEGDA) hydrogels have been fabricated as optical waveguides for many different applications. The transparency of hydrogel basically is determined by the

solubility of polymeric precursor and the crystallinity, which are related to the water content and molecular mass of polymers.^[11] To obtain transparent PEGDA hydrogels, proper concentrations must be selected according to different molecular mass. For waveguiding, a large refractive index (RI) difference between the waveguide and the surrounding tissue (or cladding material) is necessary. For a hydrogel, the RI increases linearly with the polymer content. Low molar mass PEGDA (e.g. 500 or 700 Da) forms transparent hydrogels only when the concentration is above 50 wt%^[12], causing very stiff hydrogels (42.9 MPa with 40 v/v% of 508 Da PEGDA^[13]). High molar mass PEGDA (e.g. > 2 kDa) forms transparent (and less stiff) hydrogels at all concentrations^[11-12], but the solutions are highly viscous and difficult to process. Obtaining high concentration PEG solutions which can be processed and lead to soft hydrogels requires modification of the PEG backbone to render it less prone to crystallization. One possible strategy is to react low molecular weight PEGDA with DL-dithiothreitol, to get chains with higher molecular weight but less regularity^[10b]. The thioether linkages distributed in the backbone of these precursors provide OH side groups which inhibit crystallinity and render all the precursors liquid and rapidly soluble in water. Furthermore, the linkages make the ester bonds less hydrolytically stable than those in PEGDA, meaning that faster degradability can be achieved as shown by Hudalla.^[10b]

In order to further strengthen the light guiding property of optical waveguides, core/cladding structures have been fabricated to achieve total internal reflection. For example, alginate hydrogel has been employed as a cladding material for PEGDA or polyacrylamide cores, and the fabricated core/cladding waveguides exhibited 20%-60% less optical loss than single fibers.^[12b, 14] To achieve total internal reflection, the materials in core should hold higher RI than that of cladding materials because total internal reflection only happens when light propagates from one media with higher RI to another media with lower RI.

Pluronic F127 is an amphiphilic triblock copolymer consisting of ethylene oxide (EO) and propylene oxide (PO) blocks approved by FDA (U.S. Food and Drug Administration) for pharmaceutical applications.^[15] Its aqueous solutions (when concentration is higher than CMC) demonstrate thermo-reversibility, they are fluid below the transition temperature and form physical gels above the transition temperature,^[16] which makes them perfect sacrificial materials. The formed physical gels exhibit strong shear-thinning property that makes them interesting materials for processing, in particular for printing.^[17] For example, 40 wt% of Pluronic F127 was employed as sacrificial material to print vascular channels.^[18] The gel was printed into a network imbedded in a methacrylated gelatin (GelMA) hydrogel. The evacuated channels can be obtained by removing cooled Pluronic solution. Pluronic F127 gel also has been used as sacrificial supporting material for co-extrusion printing of slow polymerization inks.^[19] The liquid inks can be confined in the core for long term curing. Afterwards, the pure core can be obtained by removing the supporting Pluronic layer by simply cooling down. Pluronic physical gels can also be stabilized by introducing covalent crosslinking groups, i.e. acrylates, as terminal groups of Pluronic chains which can be activated after physical gel formation. This allows the synthesis of tough and stretchable gels from easily processing precursors.^[20] Being self-assembled systems, Pluronic gels absorb and scatter light and, therefore, they are not appropriate materials for guiding light, in particular in the UV and Vis ranges. However, the printability and relative low refractive indices of Pluronic solutions makes them very useful as supportive and cladding material for waveguide fabrication.

In this chapter a printable DL-dithiothreitol (DTT)-bridged PEGDA (PEGDA-DTT)^[10b] is presented as a suitable PEG-based hydrogel precursor for printing optical waveguides. The possibility to print fibers with tunable mechanical properties and degradation rates is tested, as well as their performance for light guiding in air and in tissue. Printed PEG fibers with improved optical performance by coaxial

printing of PEG with medically-approved Pluronic F127 in core/cladding design are also attempted.

2.3 Results and discussion

2.3.1 Synthesis of PEGDA-DTT prepolymers

PEGDA chains were reacted with DTT units to afford PEGDA-DTT precursors by reaction of the acrylate and thiol groups in water in the presence of triethylamine by Michael-type addition reaction (**Figure 1A**).^[10b] An excess of PEGDA was used in order to obtain acrylate-terminated PEGDA-DTT chains for later crosslinking and hydrogel formation. The kinetics of the reaction was followed by monitoring the free thiol groups in the mixture using a fluorometric thiol assay. The thiol concentration decreases by more than 5 orders of magnitudes within the first minute (**Figure 1B**), and decreases a further 3-fold in 10 minutes. The reaction is almost quantitative, with the final thiol concentration below 1 μM . The consumption of acrylate groups originating from PEGDA was quantified by ^1H NMR spectroscopy for each DTT/PEGDA ratio (**Figure A1** in Appendix). The measured concentration of remaining acrylate groups, which reside at the termini of the resulting PEGDA-DTT chains, decreased with increasing feed ratio of DTT to PEGDA and was consistent with the expected theoretical estimation (**Table 1**). PEGDA-DTT products were named according to the feed ratio of DTT to PEGDA used for synthesis, i.e. PEGDA-DTT-50, PEGDA-DTT-75, PEGDA-DTT-87.5 and PEGDA-DTT-93.75 for ratios 0.5, 0.75, 0.875 and 0.9375 between DTT and PEGDA. The freeze dried PEGDA-DTT products were viscous liquids at room temperature, which dissolve rapidly in water (unlike comparable molar mass PEGDA). Their viscosity increased with the feed ratio of DTT to PEGDA (**Figure 1C** and **Table 1**) as consequence of the increasing chain length. The higher molar masses of the

PEGDA-DTT products with increasing content of DTT bridges was confirmed by size exclusion chromatography (SEC) analysis (**Table 1**). The dispersities are in the range of 1.8 - 2.8, and increased with increasing DTT/PEGDA ratios (**Table 1**).

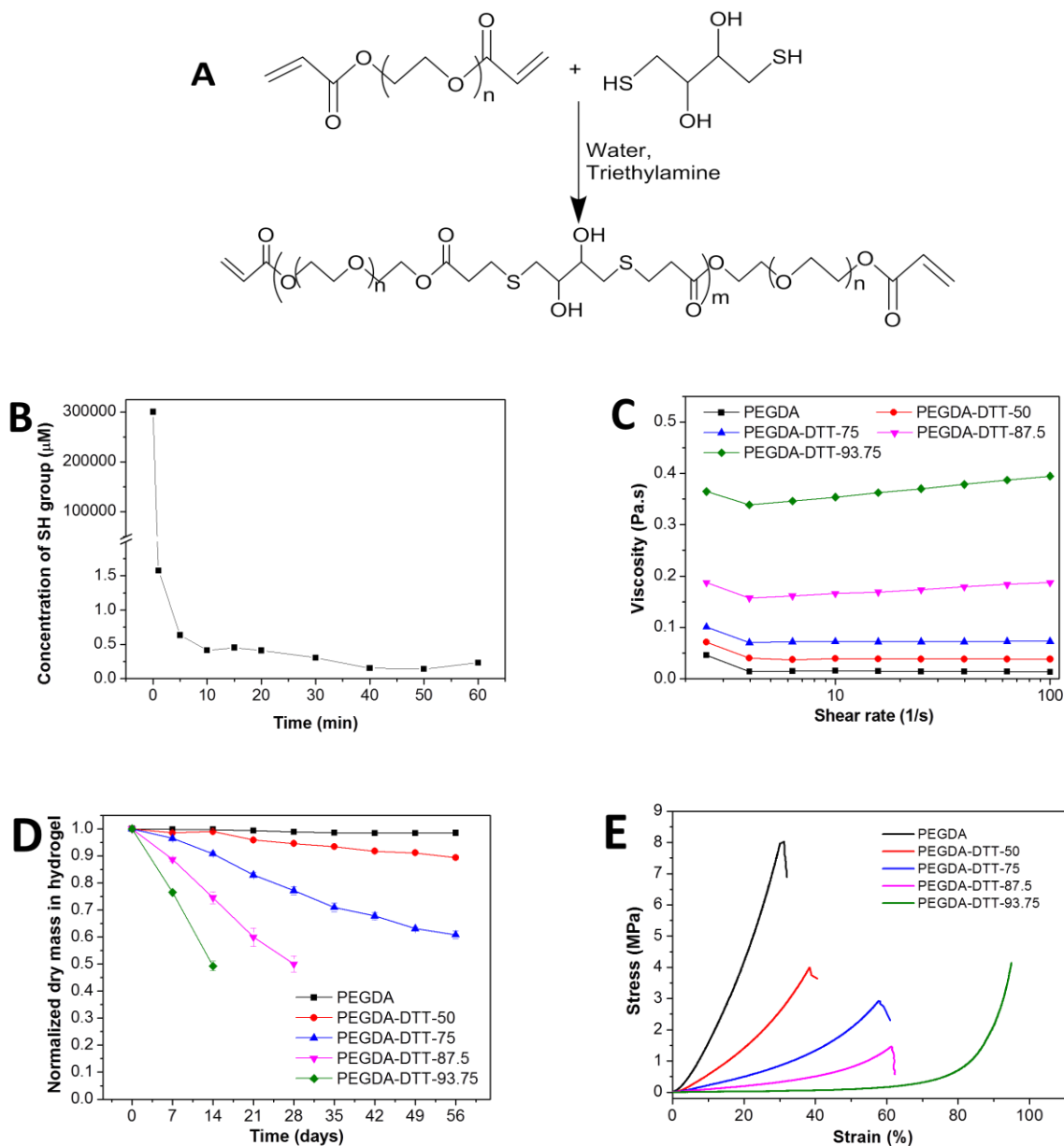


Figure 1. Chemical design and physical properties of PEGDA-DTT prepolymers and hydrogels (A) Synthesis of PEGDA-DTT polymer from PEGDA and DTT precursors. (B) Kinetics of the Michael addition reaction between acrylate groups of PEGDA and thiol groups of DTT as followed by a Fluorometric Thiol Assay Kit. (C) The viscosity of PEGDA-DTT solutions (50 wt%) measured at different shear rate at

room temperature; (D) Degradation kinetic curves of 70 wt% PEGDA-DTT hydrogels. The graph shows the normalized dry mass of the gel as function of incubation time in PBS at 37 °C. (E) Stress-strain curve of compressive tests of 70 wt% PEGDA-DTT based hydrogels.

2.3.2 Synthesis and physicochemical properties of PEGDA-DTT hydrogels

PEGDA-DTT hydrogels were prepared by photocrosslinking water solutions of PEGDA-DTT precursors at different concentrations using Irgacure 2959 as initiator and a 365 nm light source. The polymer solution was polymerized within a Teflon ring of diameter 5 mm and thickness 3 mm that was sandwiched between two glass slides. Gels were homogeneous and transparent, and became less stiff and pale yellow with increasing DTT/PEGDA ratio. The swelling ratio, degradation rate, and Young's modulus of the PEG-DTT hydrogels were characterized as function of DTT/PEGDA ratio. The swelling ratio increased from 73% to 539% with increasing DTT/PEGDA ratio (**Table 1**). This is in agreement with a lower crosslinking degree expected from the lower number of acrylate groups per unit mass, which generates a larger mesh size and therefore a higher water uptake. The degradation kinetics of the hydrogels was measured in PBS at 37°C over 56 days. Across the four compositions, the degradation rate increased with increasing pre-polymer chain length (**Figure 1D**), i.e. with increasing number of DTT units per pre-polymer chain. The proximal thioether bond provides a more positive partial charge to the carbonyl carbon of the acrylate ester, forming the expected degradation sites of the hydrogels by facilitating reaction with nucleophilic hydroxyl anions as the primary step of base-catalyzed ester hydrolysis.^[10b, 21] Over the same time scale, PEGDA 700 Da hydrogel did not degrade (**Figure 1D**). These experiments demonstrate that PEGDA-DTT gels allow modulation of the degradation kinetics by simply varying the feed ratio of DTT to PEGDA.

The mechanical properties of PEGDA-DTT hydrogels were analyzed with compression tests. **Figure 1E** shows the corresponding stress-strain curves. The Young's modulus of 70 wt% hydrogels decreased from 22 MPa to 140 kPa with increasing DTT/PEGDA ratio from 0 to 0.9375 (**Table 1**). The decreasing stiffnesses are attributed to the decreasing crosslinking degrees as the length of the PEGDA-DTT precursors increase. The stress at break decreased from 7.7 MPa to less than 1.8 MPa and the strain at break increased from 32% to more than 65% with increasing DTT/PEGDA ratio (**Table 1**). These results indicate that the mechanical properties of PEGDA-DTT hydrogels can be tuned by two orders of magnitude by simply changing the ratio of DTT to PEGDA. This is a relevant feature for the fabrication of optical waveguides to be used for clinical applications as it allows adaptation of the waveguide mechanics to the mechanics of the specific tissue in the application.

Table 1. Physicochemical properties of PEGDA-DTT prepolymers and hydrogels.

	PEGDA-700	PEGDA-DTT- 50	PEGDA-DTT- 75	PEGDA-DTT- 87.5	PEGDA-DTT- 93.75
Relative content of acrylate groups (calculated)	100%	50%	25%	12.5%	6.25%
Relative content of acrylate groups (measured) ^{a)}	100%	49.4±0.6%	24.4±1.6%	12.2±1.0%	6.4±0.1%
Viscosity [Pa*s] ^{b)}	0.046	0.071	0.101	0.187	0.365
M _n , number averaged molecular weight ^{c)}	700	4272	6134	9052	11879
Polydispersity index ^{c)}	-	1.81	2.06	2.56	2.83
Swelling ratio in water [%] ^{d)}	73±2	108±2	186±2	291±1	539±23
Swelling ratio in tissue ^{d)}	16±2%	17±1%	44±1%	87±2%	/
Young's modulus [MPa] ^{e)}	22.8±1.5	7.9±0.2	2.7±0.3	0.9±0.1	0.14±0.02
Stress at break [MPa] ^{e)}	7.6±0.9	3.9±0.5	2.9±0.8	1.8±0.6	no break
Strain at break [%] ^{e)}	32±3	38±3	54±4	65±3	no break

a) The percentage of acrylate groups in PEGDA-DTT products was measured by ¹HNMR; b) The viscosity of the precursor solutions were measured by flow sweep on a rheometer at polymer concentration of 50 wt% in water; c) The number-averaged molecular weight, M_n, and the polydispersity of PEGDA-DTT products were measured by GPC (M_n of PEGDA-700 was obtained from manufacture); d)

Swelling ratios correspond to 70 wt% PEGDA-DTT hydrogels or fibers after immersion in water for 24h or after being sandwiched between two pieces of muscle tissue for 1h; e) Young's Modulus correspond to 70 wt% PEGDA-DTT hydrogels and were measured in compression tests. Stress-strain curve, stress and strain at break were obtained from compression test with 70 wt% PEGDA-DTT.

2.3.3 Optical properties of PEGDA-DTT based hydrogels

Absorption and scattering are the most important factors affecting the light guiding properties of materials. For biomaterials, especially polymeric biomaterials, intrinsic optical loss originates from absorption, including electronic and vibrational absorption.^[22] Scattering typically arises from density fluctuations, compositional inhomogeneity, and large inclusions.^[22] The most important extrinsic factor for effective lightguiding is the refractive index (RI) of the surrounding medium, which needs to be lower than that of the waveguide in order to achieve total internal reflection. Since the RI of human tissues ranges from 1.38 to 1.51,^[23] achieving total internal reflection can be a challenge for hydrogel waveguides with high water contents (RI water = 1.33).

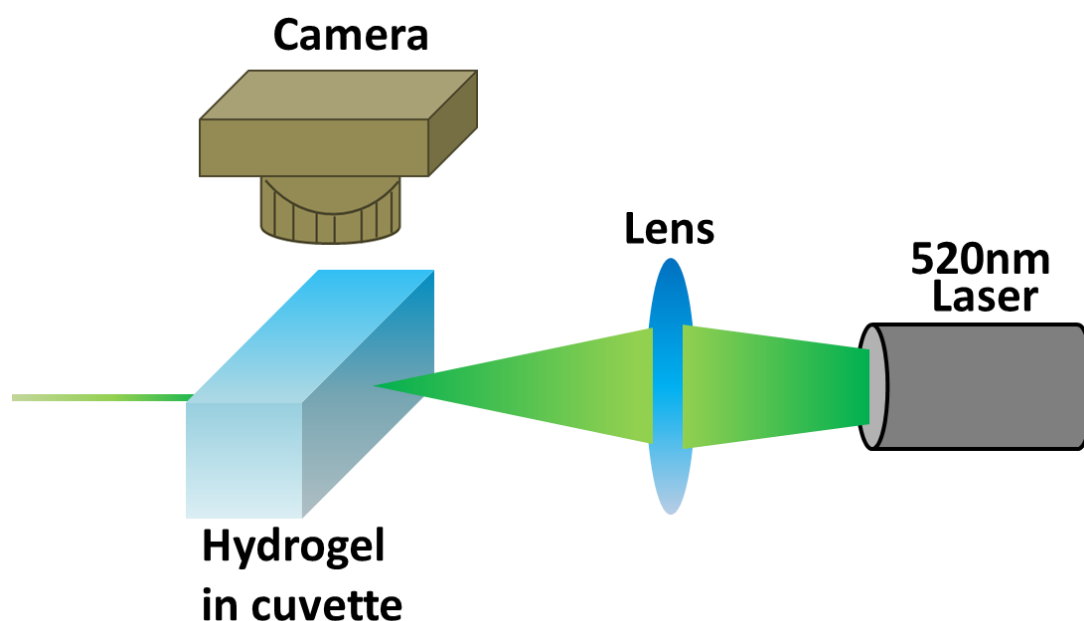
The absorption of PEGDA-DTT based hydrogels within the spectral range from 350 nm to 800 nm was measured by UV-Vis spectrophotometry (**Figure 2A** and **A2A** in Appendix). Each PEGDA/DTT composition was analyzed at different polymer concentrations ranging from 10 wt% up to 70 wt% (in 10 wt% increments). Below 400 nm absorbance was high in all systems due to electronic transitions of the organic groups.^[24] Above 400 nm the introduction of DTT significantly lowered the absorbance versus the PEGDA 700 Da reference hydrogel, in particular at polymer concentrations below 50 wt% (**Figure A2A** in Appendix). At low concentrations, the transparency of PEGDA hydrogels increases with increasing molar mass since

phase segregation is avoided.^[11] The same effect is observed here. PEGDA-DTT also displays pendant OH groups along the polymer chain (contributed by the DTT units, **Figure 1A**) which could further enhance hydration of the formed polymer networks. Precursor solutions and derived hydrogels with 75 mol% of DTT were transparent at all polymer concentrations (**Figure A2A** and **A2B** in Appendix).

The scattering properties of PEGDA-DTT hydrogels were compared using a home-made setup (**Scheme 1**). A 520 nm laser passed through a cuvette containing the hydrogel. The scattered light, which arises from structural inhomogeneity in the hydrogels,^[11] was captured with a camera situated perpendicular to the incident light beam. All four PEGDA-DTT hydrogels showed ~50% less scattering than PEGDA hydrogel at a polymer concentration of 70 wt% (**Figure 2B**). For a particular PEGDA-DTT composition, gel scattering ratio decreased with polymer concentration; the 80 wt% gel made from PEGDA-DTT-87.5 for example shows less than half the scattering intensity of the 40 wt% gel (**Figure A2C** in Appendix). These data are in agreement with the formation of more homogeneous polymer networks, which reduces scattering, and with the less favored phase separation in PEGDA chains at higher polymer concentrations as reported by other authors.^[11-12] The scattering observed at polymer concentrations >50% is mainly associated with Mie-type light scattering of partially disordered networks and is unavoidable.^[11]

The RI of 70 wt% PEGDA-DTT based hydrogels increased with DTT content from 1.435 to 1.46 (**Figure 2C**), and indicates that the introduction of DTT bridges could improve the light confinement ability of PEGDA-DTT waveguides in tissues and lead to optical waveguides with higher optical performance. The RI of PEGDA-DTT also increased with polymer content. **Figure A2D** in Appendix shows that the RI of PEGDA-DTT-93.75 gels increased linearly from 1.36 to 1.46 when the polymer concentration changed from 20 wt% to 70 wt%.

In summary, the introduction of DTT bridges in PEGDA precursor leads to a comprehensive improvement in hydrogel optical properties versus PEGDA alone: PEGDA-DTT-X hydrogels with $X \geq 75$ are highly transparent in the visible wavelength range for all the tested concentrations (5 wt% to 70 wt%), with higher concentrations showing additional benefits of higher RI and lower light scattering. These are all relevant properties for the application of PEGDA-DTT hydrogels as optical waveguides, and suggest that higher concentrations of PEGDA-DTT could be most suitable for producing efficient printed waveguides.



Scheme 1. Home-made setup to characterize the relative scattering of PEGDA-DTT hydrogels.

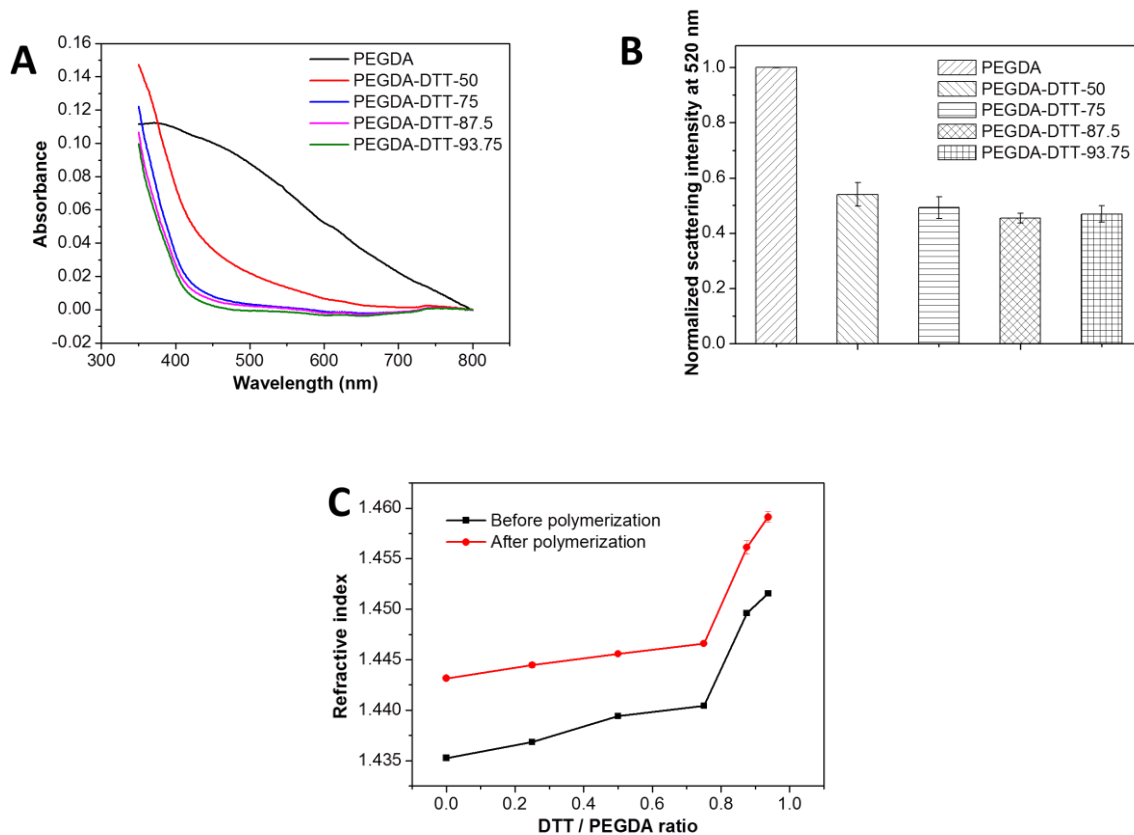


Figure 2. Optical properties of PEGDA-DTT hydrogels. (A) UV-Vis spectrum of 10 wt% PEGDA-DTT hydrogels. (B) The relative scattering of 70 wt% PEGDA-DTT hydrogels with different DTT/PEGDA ratio; (C) The refractive index of 70 wt% PEGDA-DTT based hydrogels before and after polymerization.

2.3.4 Printing optical waveguides

Optimization of printing conditions and printability windows

PEGDA-DTT solutions were tested as inks for printing using an extrusion-based printer coupled to an illumination source for in-situ photo-polymerization (**Figure 3A**: left and middle). In order to facilitate printing and achieve high shape fidelity of the printed fibers, a transparent silicone tubing was inserted at the end of the needle tip (**Figure 3A**: right).^[25] The light beam for initiating the radical polymerization of the acrylate groups, leading to crosslinking of the ink, was illuminating on the silicone tube. Printing conditions and polymer compositions to

obtain homogeneous and continuous fibers were tested. Printing pressure was varied between 5 and 50 kPa, illumination intensity between 10-100% and silicone tubes with diameters 310 and 510 μm were used. The printing parameters for obtaining continuous threads with good fidelity were identified and are represented in **Figure 4**.

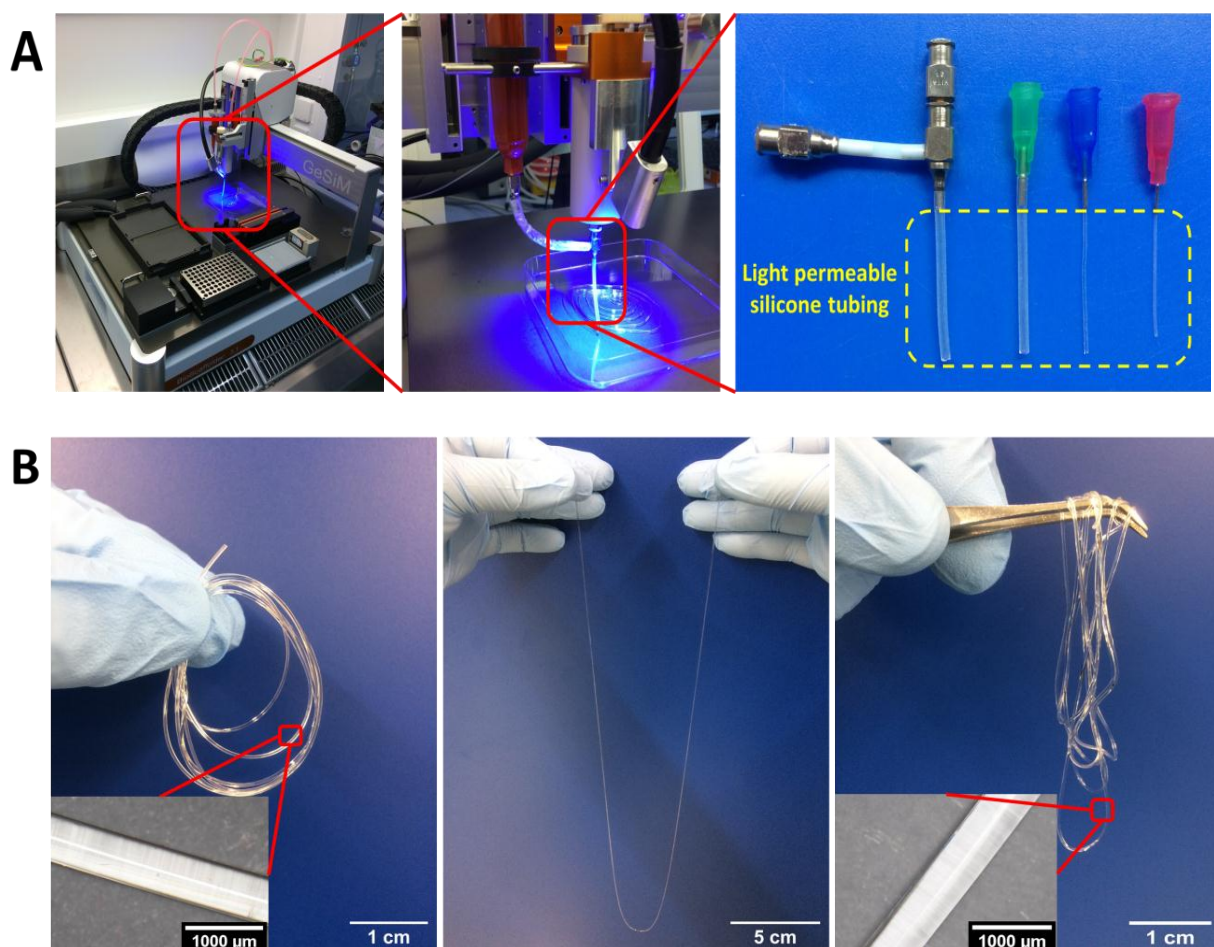


Figure 3. (A) Printing setup: left—printing stage of 3D-Bioscaffolder from GESIM, middle—printing head mounted with coaxial needle, right—printing needles extended with silicone tubes. (B) Images of printed 70 wt% PEGDA-DTT fibers with 510 μm silicone tube. Left PEGDA-DTT-50; middle PEGDA-DTT-87.5; right PEGDA-DTT-93.75 fiber. Scale bar of insets corresponds to 1000 μm .

Initially, a 70wt% PEGDA solution was used. Increasing printing pressure leads to faster printing and required higher illumination intensity to accelerate photopolymerization while the printed material passes through the silicone tube in order to obtain good quality fibers. The printing window for the 310 μm silicone tube was wider than for the 510 μm tube (**Figure 4A**). Two reasons contribute to this difference. (i) The thicker wall of the 510 μm tube (200 vs 120 μm , data from manufacture) that allows less light to penetrate. (ii) The shorter residence time of the materials within the illumination spot. Extending the length of the illuminated area or the tube (**Figure 4B**) or increasing the concentration of initiator in the ink (**Figure 4C**) extended the printability window by prolonging the polymerization time or accelerating the polymerization rate respectively. The printability window was dependent on polymer concentration (**Figure 4D**). Within 50 to 70 wt% polymer concentration, the printability window was wider at higher concentration of polymer precursor in the solution. The higher concentration provides a higher viscosity of the printed thread and solidifies faster upon light exposure, enhancing printing fidelity. Increasing the polymer concentration also moved the printing window to higher pressures and lower exposure doses (**Figure 4D**). This may be attributed to the higher viscosity and faster solidification of the ink in the tube, which negatively affect printability. This viscosity-induced shifting of the printing window also happened when printing PEGDA-DTT inks with increasing ratio of DTT bridges (**Figure 4E**), which also showed higher viscosity. Especially, for PEGDA-DTT-93.75, the shifting and narrowing of printing window happened simultaneously due to the very high viscosity of PEGDA-DTT-93.75 solution.

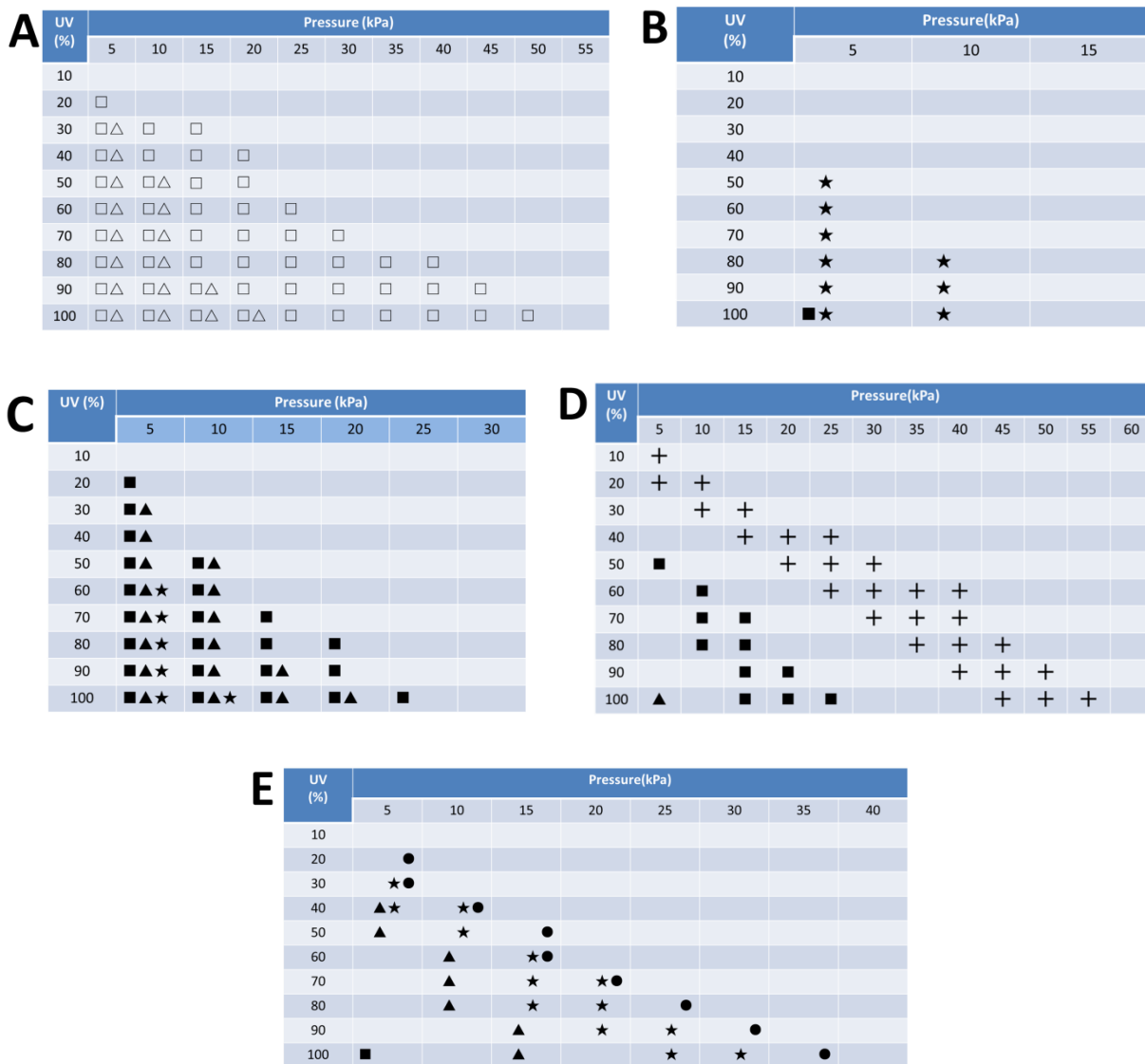


Figure 4. Printing parameter windows at different printing conditions and for different polymer compositions (A) 70wt% PEGDA with 0.1wt% initiator printed using silicone tubing of different diameters and constant length (4cm). Hollow squares correspond to silicone tube of 310 μm diameter and hollow triangles to 510 μm . (B) 50wt% PEGDA-DTT-50 with 0.2wt% initiator printed with different silicone tubing lengths and constant tubing diameter (510 μm). Solid squares correspond to 2cm long tubes, solid stars to 4 cm tubes. (C) 70wt% PEGDA printed using a 4 cm long and 510 μm diameter silicone tube and different initiator concentrations. Solid squares correspond to 0.2 wt% initiator, solid triangles to 0.1 wt% initiator, solid stars to 0.05 wt% initiator. (D) PEGDA-DTT-50 at 0.2wt%

initiator concentration printed using 2 cm long and 510 μm diameter silicone tube and different polymer concentrations. Cross correspond to for 70 wt%, solid square to 60 wt% and solid triangle to 50 wt% PEGDA-DTT-50 concentration. (E) 50 wt% PEGDA-DTT printed at different DTT concentrations containing 0.2 wt% initiator and using a 2 cm long and 510 μm diameter silicone tube. Solid circles correspond to PEGDA-DTT-93.75, solid stars to PEGDA-DTT-87.5, solid triangles to PEGDA-DTT-75, solid squares to PEGDA-DTT-50, solid crosses to PEGDA.

Within the printability windows, continuous fibers (we tested up to 50 cm length) can be easily printed (**Figure 3B**). The obtained fibers exhibit high transparency, shape fidelity, and homogeneity, and are flexible (**Figure 3B**). The surface of the printed fibers was smooth as viewed by optical microscopy (**Figure 3B**: insets), which is inherited directly from the inner wall of the silicone tube extension used for curing. The printed fibers become less stiff with increasing concentration of DTT content in the ink. **Figure 3B** shows the higher flexibility of printed PEGDA-DTT-93.75 vs. PEGDA-DTT-50 fibers. These results are consistent with the mechanical properties measured on the bulk hydrogels (**Table 1**), and demonstrate the possibility to adapt the mechanical properties of the printed fibers to the mechanics of target tissues. However, low stiffness also brings some disadvantages. For example, the more flexible fibers get stuck to themselves more easily and become more difficult to handle (**Figure 3B**: right).

2.3.5 Optical properties of the printed PEGDA-DTT waveguides

In order to quantify the light guiding properties of the printed fibers, we evaluated the optical loss in air and in tissue by using a home-made setup (**Scheme 2**). A laser beam (with wavelength 405, 450, 520 nm) was focused at one end of the printed waveguide and the intensity of the light propagated along the waveguide was indirectly measured at given distances. For this purpose, the

intensity of auto-fluorescence emitted perpendicular to the fiber direction was imaged with a camera, and quantified as a proxy for the intensity of the guided light. In order to exclude scattered light from the signal, a 550 nm long pass filter was used for imaging. The captured images were analyzed by ImageJ software to obtain the auto-fluorescence intensity at different positions (distance: Z , intensity: I_0 and I_z). The optical loss $\alpha(\lambda)$ (in dB per length unit) was calculated by equation (1):^[26]

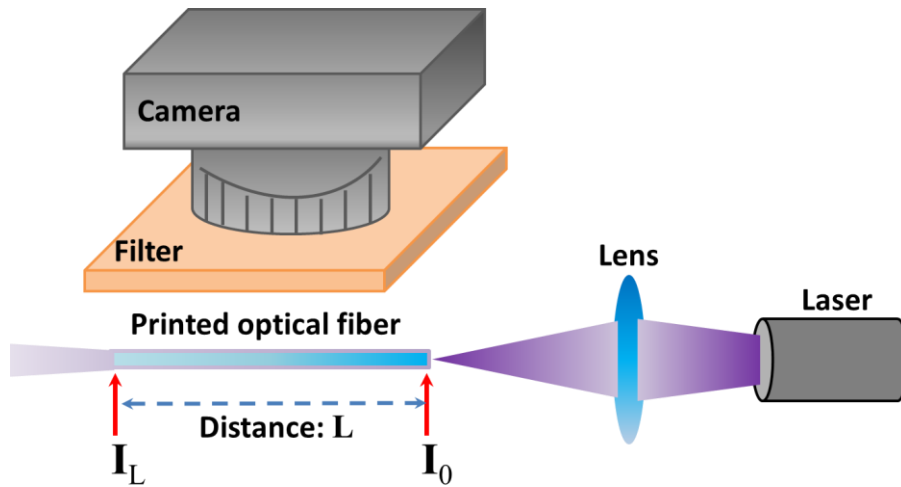
$$\alpha(\lambda) = \frac{10}{Z} \log \frac{I_0}{I_z} \quad (1)$$

Light at wavelengths ≥ 670 nm did not excite the auto-fluorescence of the waveguides and, therefore, the optical loss could only be quantified for 405, 450 and 520nm laser beams. Printed 70 wt% PEGDA-DTTs waveguides showed optical losses in air between 0.1 dB cm^{-1} (at 520 nm) and 0.4 dB cm^{-1} (at 405 nm) (**Figure 5A** and **Figure A3A** in Appendix), with higher optical loss at shorter wavelengths mostly a consequence of higher absorbance (**Figure 2A** and **Figure A2A** in Appendix). The optical loss decreased with increasing polymer concentration (**Figure 5B** and **Figure A3B** in Appendix). Two main factors contribute to this trend: (i) the higher refractive index of hydrogels with higher polymer concentration (**Figure A2D** in Appendix), which facilitates total internal reflection and allows better confinement of light in the waveguide, and (ii) hydrogels with higher polymer concentration presented lower scattering (**Figure A2C** in Appendix). The optical loss was not significantly influenced by the DTT/PEGDA ratio (**Figure 5A**). The propagation of wavelengths ≥ 670 nm was checked visually (**Figure A3** in Appendix). All printed waveguides guided light with wavelength ≥ 670 nm to distances greater than 20 cm.

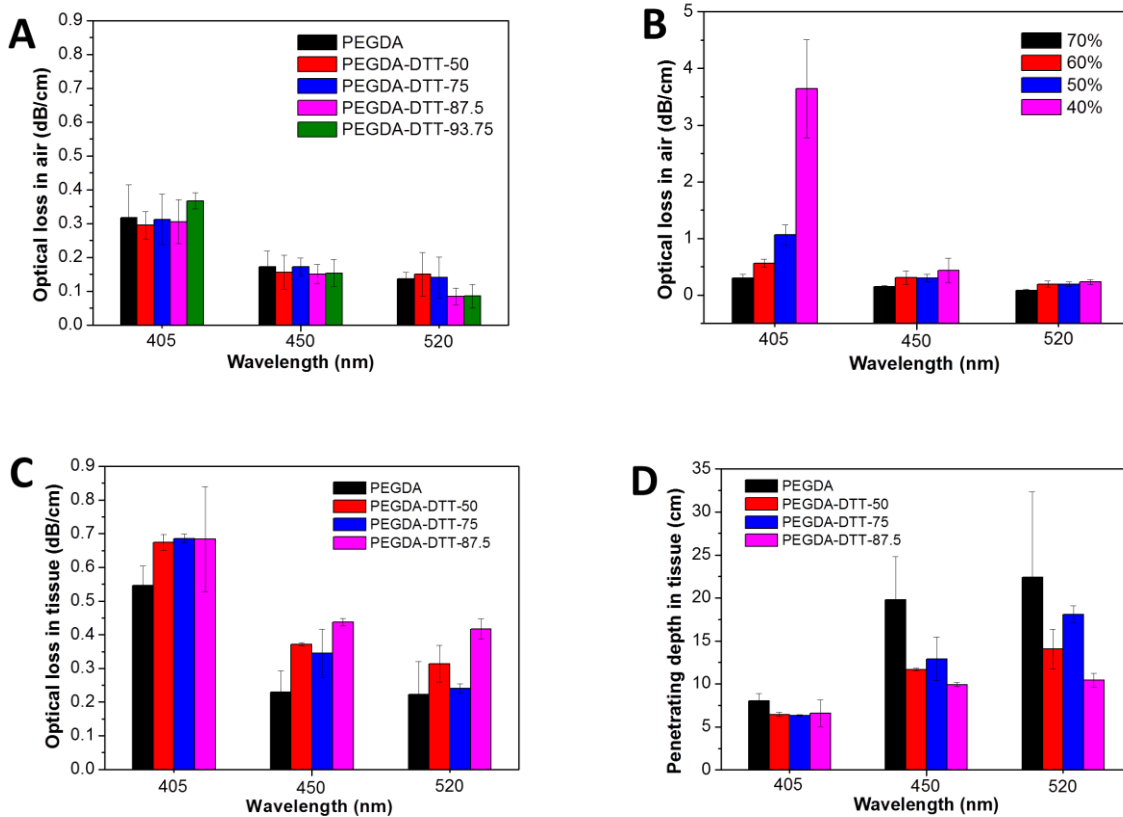
We also characterized the light guiding properties of the printed waveguides through tissue, in order to mimic the real application conditions in a medical scenario. For this purpose the printed waveguide was sandwiched between two

pieces of porcine muscle tissue. The auto-fluorescence intensity of the waveguide before and after passing through tissue was quantified. The optical loss in tissue was higher than in air (**Figure 5C**). This can be attributed to (i) the higher refractive index of tissue, which narrows the critical incident angle for total internal reflection, and (ii) the rough surface of porcine tissue that can cause more scattering than air. Besides these factors, waveguides within tissue uptake moisture and swell, which decreases the polymer concentration (**Table 1**) and the refractive index to the detriment of light guidance. When sandwiched between porcine muscles, printed fibers with higher DTT contents exhibited a slightly higher optical loss, which can be attributed to the decreasing stiffness (**Table 1**). The lower stiffness of the fiber favors macro or micro bending when in contact with the tissue, which decreases the light guiding properties of fiber. It is interesting to note that most reported biomaterials-based optical waveguides exhibit optical losses in the range of 0.1 - 28 dB cm⁻¹.^[11] The presented optical waveguides in this report, with the additional benefits of tunable mechanics and degradability, are excellent competitors and show optical attenuation values at the low end of this range.

In order to describe the light guiding properties of the waveguides more intuitively, the optical loss values were converted to tissue penetration depths – defined as the distance at which the intensity of auto-fluorescence decreases to 1/e. The penetration depth increased at longer wavelengths and was 6, 10 and 10 cm for wavelengths of 405, 450 and 520nm respectively (**Figure 5D and 5E**). The penetration depth decreased slightly with higher content of DTT bridges due to the lower stiffness as explained above.



Scheme 2. Home-made setup to characterize the light guiding properties of printed optical waveguides.



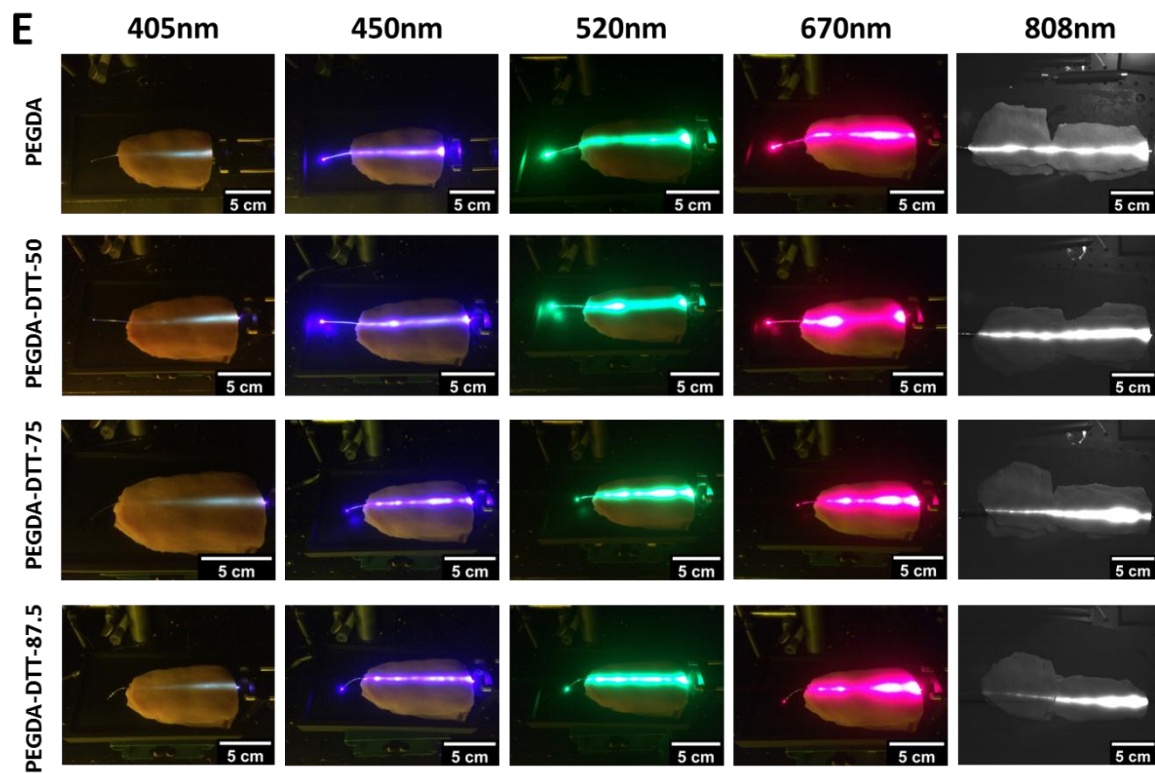
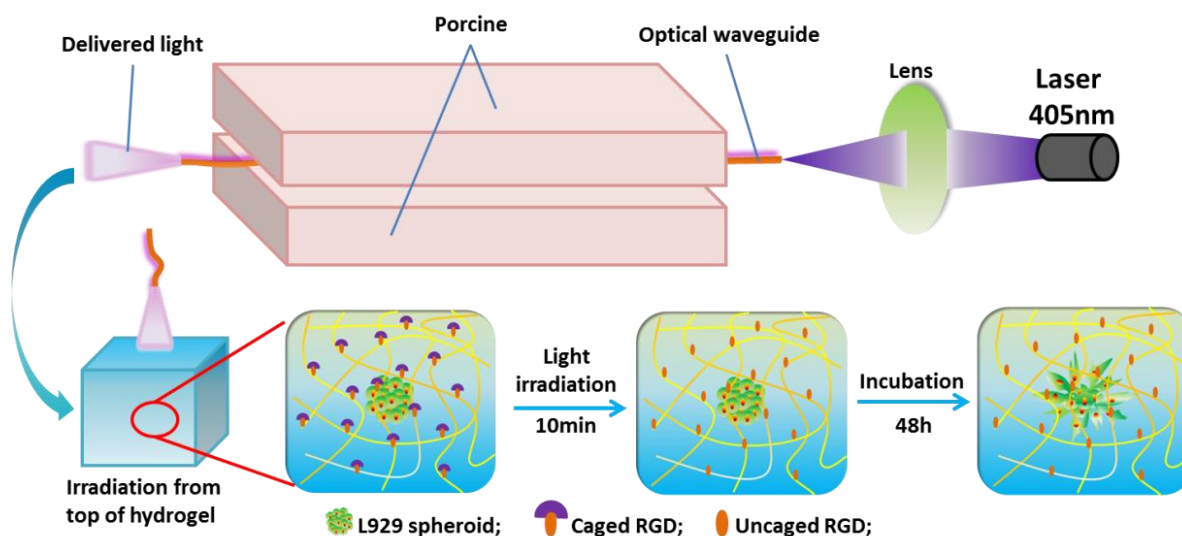


Figure 5. Waveguiding properties of PEGDA-DTT printed fibers. (A) Optical loss in air measured at different wavelengths in printed 70 wt% PEGDA-DTTs waveguides with increasing DTT concentration. (B) Optical loss in air measured at different wavelengths in printed PEGDA-DTT-87.5 waveguides with increasing polymer concentration (40-70 wt%). (C) Optical loss in tissue measured at different wavelengths in printed 70 wt% PEGDA-DTTs waveguides with increasing DTT concentration. (D) Tissue penetrating depth of guided light by printed 70 wt% PEGDA-DTT waveguides with increasing DTT concentration. (E) Images of waveguides sandwiched in tissue and coupled to lasers of different waveguides. Scale bar corresponds to 5cm. All experiments were repeated for at least three times.

2.3.6 Photoactivation of biological processes in vitro with printed PEGDA-DTT fibers

The capability of PEGDA-DTTs waveguides to guide light and photoactivate biological processes was tested in vitro. These experiments were performed in

collaboration with Dr. Yijun Zheng. A waveguide was used to deliver 405 nm light through porcine tissue to test (**Scheme 3**), from a tissue regeneration perspective, the possibility to trigger migration of cells from spheroids to colonize a surrounding photoactivatable hydrogel.^[27]

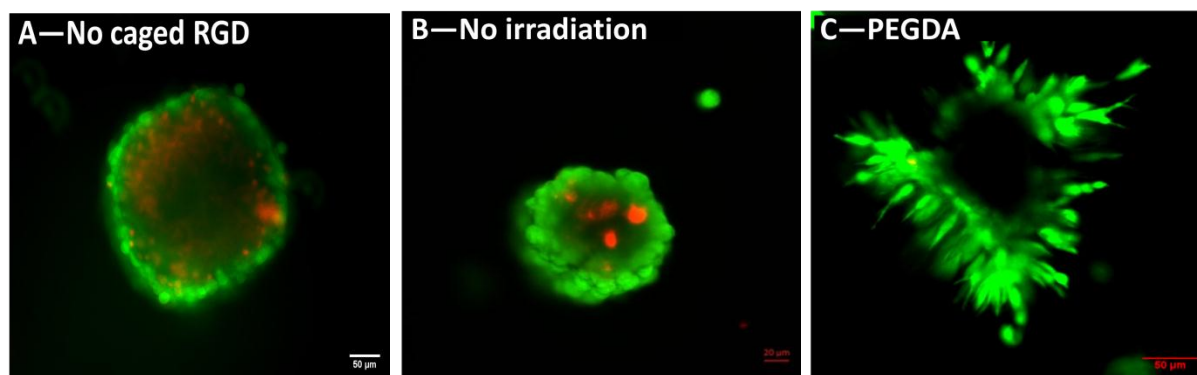


Scheme 3. Proof-of-principle scenarios for the application of PEGDA-DTT optical waveguides. Top part: Setup used to deliver light to a targeted destination by waveguides through tissue. 3D culture of a fibroblast spheroid within a polymeric matrix modified with photoactivatable cell adhesive ligands. After exposure fibroblasts sense the light-activated cell adhesive ligand and migrate out of the spheroid.

Application of printed optical fiber to remotely control cell migration in a hydrogel

These experiments were done in cooperation with Dr. Yijun Zheng. The purpose of this study was to test if the degradable PEG-DTT waveguides connected to a 4.5 mW laser could be used to trigger adhesion and migration of living cells encapsulated in a photoactivatable hydrogel by activating a cell adhesive ligand upon light exposure.^[27-28] For this purpose L929 fibroblast spheroids were encapsulated in a dextran hydrogel functionalized with a photo-activatable cell

adhesive peptide, cyclo[RGD(DMNPB)fC] (**Figure A4** in Appendix). This peptide had been used in previous studies in the group to mediate cell attachment to biomaterials ^[27b, 28a, 29]. Printed PEGDA and PEGDA-DTT waveguides were used to guide light to irradiate the cell-hydrogel construct through 5 cm of porcine muscle (**Scheme 3**). A laser (405 nm, 4.5 mW) was focused on the proximal end of the fiber, and the light intensity at the distal end was measured to be in the range of 5 - 50 mW cm⁻² (**Table A1** in Appendix). This intensity was expected to be sufficient to activate the peptide. After irradiation (15 min), the hydrogels were cultured for a further 2 days and imaged by confocal microscopy. Encapsulated fibroblasts migrated out of the spheroid into the surrounding region (**Figure 6C-6F**) in irradiated cyclo([RGD(DMNPB)fC]) functionalized hydrogels, but they remained confined in the spheroids in the absence of light (**Figure 6B**) or in irradiated gels that had not been modified with the adhesive peptide (**Figure 6A**). These results demonstrate that the intensity of the light delivered by the degradable waveguides was sufficient to trigger DMNPB photocleavage across 5 cm tissue. The possibility to remotely control cell behavior in implanted cells or biomaterials opens application possibilities for this approach in a clinical context, i.e. cell therapies and optogenetic based therapies.



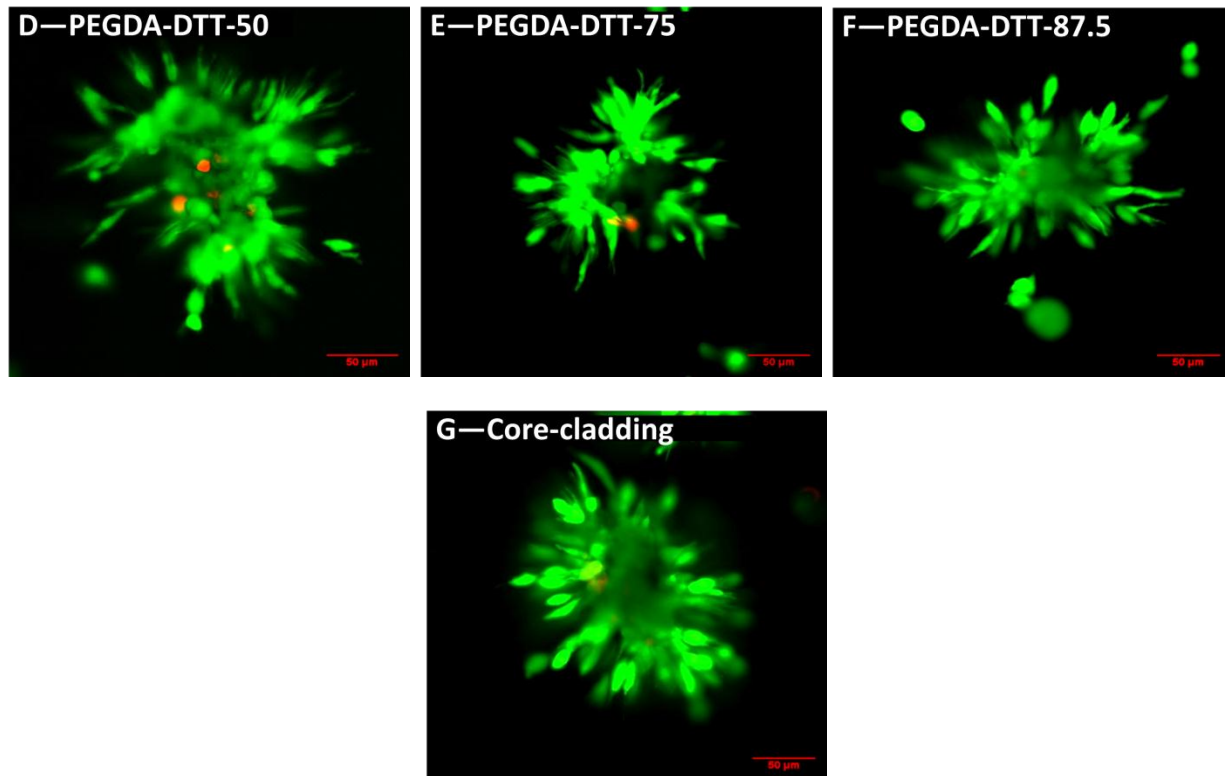


Figure 6. Confocal microscopy images of L929 spheroids encapsulated in dextran hydrogels: (A) Cells spheroid in hydrogel that was not functionalized with cyclo[RGD(DMNPB)fC] and was irradiated for 15min by light (405nm) guided in PEGDA waveguide through 5cm tissue; (B) Cells spheroid in a hydrogel that was functionalized with cyclo[RGD(DMNPB)fC] but not irradiated by light; (C-G) Cells spheroids in hydrogels that were functionalized with cyclo[RGD(DMNPB)fC] and irradiated by light (405nm) guided in 70 wt% PEGDA (C), PEGDA-DTT-50 (D), PEGDA-DTT-75 (E), PEGDA-DTT-87.5 (F) and Core-cladding (PEGDA-DTT-87.5 as core, acrylated Pluronic F127 as cladding) (G) waveguides through 5 cm tissue.

2.3.7 Core-cladding optical waveguides

Core-cladding designs in optical waveguides improve the light guiding efficiency by enhancing total internal reflection. To test whether core-cladding designs could improve the waveguiding properties of PEGDA-DTT waveguides, a coaxial printing process with Pluronic F127 was developed. Pluronic F127 is a polymer

approved by the U.S. Food and Drug Administration (FDA) for pharmaceutical applications,^[15] and forms thermoreversible gels in aqueous solution.^[16] By introducing terminal acrylate groups into the Pluronic F127 chains, covalently crosslinked hydrogels can also be obtained by photopolymerization. The RI of 50 wt/v% Pluronic hydrogel is lower than that of 80 wt% PEGDA-DTT-87.5 hydrogel (**Figure A5A** in Appendix). These properties make Pluronic F127 a convenient complement to PEGDA-DTT-87.5 in a core-cladding optical waveguide design.

80 wt% PEGDA-DTT-87.5 was coextruded with 50 w/v% acrylated Pluronic F127 (Pluronic-DA) as cladding material (**Figure 7A**). Core-cladding fibers with core diameters ranging from 340 to 640 μm and fixed cladding diameter (1.02 mm) were successfully printed using a coaxial printing needle (**Figure 3A**: right) by varying the printing pressure of the core and the cladding material (**Figure A5C** and **A5D** in Appendix). At room temperature, 50 wt/v% of Pluronic-DA behaves like a paste that exhibits shear-thinning, which allows it to be easily extruded and provide a support for the liquid PEGDA-DTT-87.5 solution during the printing of the core-cladding structure. By extending the silicone tube attached to the tip of the coaxial needle (**Figure 3A**), the extruded core and cladding can be simultaneously crosslinked, which fixes the core/cladding structure. From the printed core/cladding fibers, a smooth interface between core and cladding was observed (**Figure 7A**). We assume that the two materials are covalently bound to each other by cross-polymerization of the acrylate groups present at the interface of the core and cladding.

The light guiding properties of core-cladding waveguides with 80 wt% PEGDA-DTT-87.5 core and 50 wt/v% Pluronic-DA cladding were explored and compared with the single PEGDA-DTT-87.5 (65 wt%, to give the same overall water content as in the core/cladding fibers) waveguide design. Core-cladding waveguides with optical loss of $<0.2 \text{ dB cm}^{-1}$ at 405 nm in air were obtained (**Figure 7B**), significantly better than the optical loss of single fibers (around 0.4 dB cm^{-1}).

These correspond to longer propagation distances both in air and in tissue (**Figure 7C** and **A5B** in Appendix). The improved light guiding properties can be attributed to (i) the consistent RI difference between core and cladding (**Figure A5A** in Appendix) aiding total internal reflection to better confine light propagation to the core, and (ii) the presence of cladding avoiding direct contact and a rough interface between the core and tissue. Finally, core-cladding waveguides were also tested in their ability to trigger cell migration within a photoactivatable hydrogel after passing through 5 cm muscle tissue. The core-cladding fibers successfully activated cell migration (**Figure 6G**).

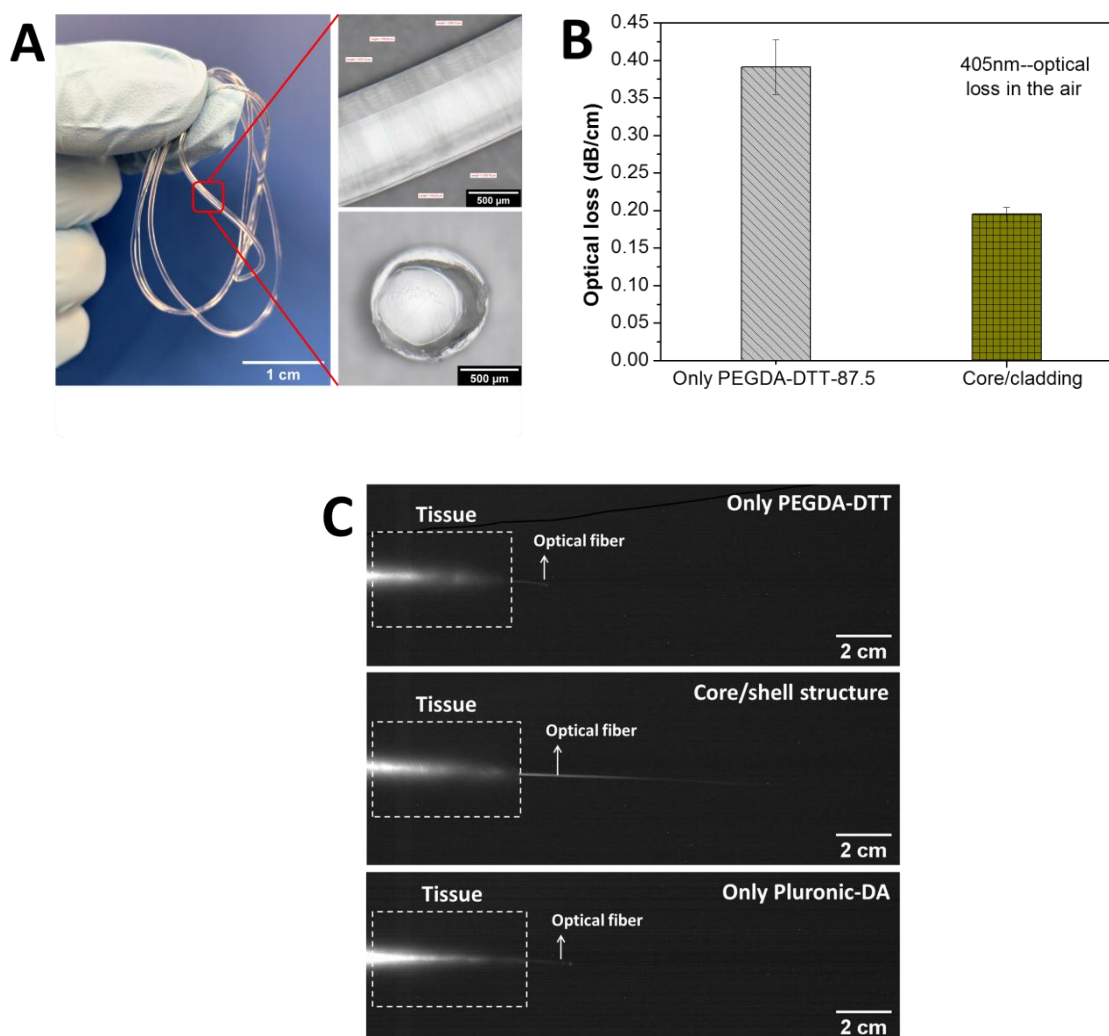


Figure 7. (A) Images of printed core/cladding fibers (80 wt% of PEGDA-DTT-87.5 for core, 50 wt/v% of Pluronic-DA for cladding). Left: printed core/cladding fibers, right: magnified images of core/cladding fiber and the cross-section of the fiber.

(B) Optical loss of single fiber and core/cladding fibers at 405 nm; (C) Image of 405 nm light beam propagating through a single and core/cladding waveguide in tissue.

2.4 Conclusive remarks

PEGDA can be converted into a degradable hydrogel by previous incorporation of DTT units. PEGDA-DTT monomers can be easily synthesized from commercially available precursors. In spite of the longer molecular weight than PEGDA precursor, PEGDA-DTT of all compositions used in this work were liquid and could be easily dissolved in water at high concentration, which is difficult or even impossible for solid PEGDA at high molecular weight. Through photopolymerization of the terminal acrylate functionalities, PEGDA-DTT solution can be converted to hydrogels. These hydrogels are cytocompatible and can be designed to present customized degradability and mechanical properties. The degradation rate can be accelerated from months to weeks and the mechanical properties can be tuned by two orders of magnitude (i.e. Young's Modulus from 100 kPa to 22 MPa) by simply increasing DTT content in the polymer chain. The adjustable degradability allows degradation kinetics to be tailored to the preferred duration of the therapeutic treatment. The broad range of mechanical properties allows stiffness matching with organs of interest, offering flexibility for customized, light-triggered therapies.

The extended polymer chains and the introduction of hydroxyl groups in the backbone decrease the regularity of polymer, which decreases the crystallinity and then improves the optical properties of hydrogels. DTT bridged PEGDA hydrogels demonstrate lower light absorbance, especially at low concentrations, and lower scattering comparing to pure PEGDA hydrogels, which can strengthen the transparency of hydrogels. Besides, PEGDA-DTT hydrogels exhibit higher

refractive indices with higher content of DTT bridges in the backbone, which improves the ability of confining light in materials. The improved optical properties can be exploited for better waveguiding.

PEGDA-DTT precursors can be processed into optical waveguides by printing. The uncomplicated application of the printing technology can be advantageous, especially when complicated geometries are desired, or when the waveguides include core-shell designs. Printing avoids multi-steps to make core/cladding structure, as it is the case in mold-casting processes. The printing technology provides the possibility to integrate multifunctional (optical, electronic and therapeutic) components into single devices to achieve diagnosis, therapy and monitoring functions simultaneously.

The printed PEGDA-DTT fibers exhibit excellent light guiding properties with measured optical losses in the visible range of 0.1 - 0.4 dB cm⁻¹ in air and 0.25 - 0.7 dB cm⁻¹ in tissue, which is superior to the reported PEGDA based hydrogel waveguides with optical loss of 0.17 to 25 dB cm⁻¹.^[11] With printed PEGDA-DTT waveguides, sufficient light can be delivered through many centimeters of porcine tissue to activate photochemical processes, and control cell adhesion and migration in light-responsive hydrogels. The provided examples demonstrate the practical potential of printed PEGDA-DTT hydrogel waveguides for in vivo control of biological processes and clinical applications.

PEGDA-DTT fibers also showed some limitations in these studies. For example, swelling of PEGDA-DTT in water or body fluids is unavoidable. Upon swelling the polymer concentration in hydrogels is decreased, and this can lead to lower refractive indices and softer mechanical properties. The lower refractive index can result in a decreasing critical angle for total internal reflection, and the softer mechanical properties can cause micro or macro bending along the waveguide, both of which could increase the optical loss.

References

- [1] a) J. Zhu, *Biomaterials* **2010**, *31*, 4639; b) J. H. Lee, H. B. Lee, J. D. Andrade, *Progress in Polymer Science* **1995**, *20*, 1043; c) N. A. Alcantar, E. S. Aydil, J. N. Israelachvili, *Journal of Biomedical Materials Research: An Official Journal of The Society for Biomaterials, The Japanese Society for Biomaterials, and The Australian Society for Biomaterials and the Korean Society for Biomaterials* **2000**, *51*, 343; d) K. Knop, R. Hoogenboom, D. Fischer, U. S. Schubert, *Angewandte Chemie International Edition* **2010**, *49*, 6288.
- [2] N. A. Peppas, K. B. Keys, M. Torres-Lugo, A. M. Lowman, *Journal of Controlled Release* **1999**, *62*, 81.
- [3] a) J. Elisseeff, K. Anseth, D. Sims, W. McIntosh, M. Randolph, R. Langer, *Proceedings of the National Academy of Sciences* **1999**, *96*, 3104; b) M. S. Hahn, M. K. McHale, E. Wang, R. H. Schmedlen, J. L. West, *Annals of biomedical engineering* **2007**, *35*, 190.
- [4] K. B. Keys, F. M. Andreopoulos, N. A. Peppas, *Macromolecules* **1998**, *31*, 8149.
- [5] a) B. D. Polizzotti, B. D. Fairbanks, K. S. Anseth, *Biomacromolecules* **2008**, *9*, 1084; b) M. Malkoch, R. Vestberg, N. Gupta, L. Mespouille, P. Dubois, A. F. Mason, J. L. Hedrick, Q. Liao, C. W. Frank, K. Kingsbury, *Chemical Communications* **2006**, 2774.
- [6] M. Ehrbar, S. C. Rizzi, R. Hlushchuk, V. Djonov, A. H. Zisch, J. A. Hubbell, F. E. Weber, M. P. Lutolf, *Biomaterials* **2007**, *28*, 3856.
- [7] A. Metters, J. Hubbell, *Biomacromolecules* **2005**, *6*, 290.
- [8] a) K. T. Nguyen, J. L. West, *Biomaterials* **2002**, *23*, 4307; b) J. P. Fisher, D. Dean, P. S. Engel, A. G. Mikos, *Annual review of materials research* **2001**, *31*, 171.
- [9] a) A. S. Sawhney, C. P. Pathak, J. A. Hubbell, *Macromolecules* **1993**, *26*, 581; b) J. D. Clapper, J. M. Skeie, R. F. Mullins, C. A. Guymon, *Polymer* **2007**, *48*, 6554; c) Z. Jiang, J. Hao, Y. You, Y. Liu, Z. Wang, X. Deng, *Journal of Biomedical Materials Research Part A: An Official Journal of The Society for Biomaterials, The Japanese Society for Biomaterials, and The Australian Society for Biomaterials and the Korean Society for Biomaterials* **2008**, *87*, 45.
- [10] a) J. Zhang, A. Skardal, G. D. Prestwich, *Biomaterials* **2008**, *29*, 4521; b) G. A. Hudalla, T. S. Eng, W. L. Murphy, *Biomacromolecules* **2008**, *9*, 842.
- [11] S. Shabahang, S. Kim, S. H. Yun, *Advanced Functional Materials* **2018**, *28*, 1706635.

-
- [12] a) M. Choi, J. W. Choi, S. Kim, S. Nizamoglu, S. K. Hahn, S. H. Yun, *Nature photonics* 2013, 7, 987; b) M. Choi, M. Humar, S. Kim, S. H. Yun, *Advanced Materials* 2015, 27, 4081.
- [13] Q. T. Nguyen, Y. Hwang, A. C. Chen, S. Varghese, R. L. Sah, *Biomaterials* 2012, 33, 6682.
- [14] a) J. Guo, X. Liu, N. Jiang, A. K. Yetisen, H. Yuk, C. Yang, A. Khademhosseini, X. Zhao, S. H. Yun, *Advanced Materials* 2016, 28, 10244; b) A. K. Yetisen, N. Jiang, A. Fallahi, Y. Montelongo, G. U. Ruiz-Esparza, A. Tamayol, Y. S. Zhang, I. Mahmood, S. A. Yang, K. S. Kim, *Advanced Materials* 2017, 29, 1606380.
- [15] G. Dumortier, J. L. Grossiord, F. Agnely, J. C. Chaumeil, *Pharmaceutical research* 2006, 23, 2709.
- [16] G. Dumortier, J. Grossiord, M. Zuber, G. Couarraze, J. Chaumeil, *Drug development and industrial pharmacy* 1991, 17, 1255.
- [17] X. Liu, H. Yuk, S. Lin, G. A. Parada, T. C. Tang, E. Tham, C. de la Fuente-Nunez, T. K. Lu, X. Zhao, *Advanced Materials* 2018, 30, 1704821.
- [18] D. B. Kolesky, R. L. Truby, A. S. Gladman, T. A. Busbee, K. A. Homan, J. A. Lewis, *Advanced Materials* 2014, 26, 3124.
- [19] D. J. Lorang, D. Tanaka, C. M. Spadaccini, K. A. Rose, N. J. Cherepy, J. A. Lewis, *Advanced Materials* 2011, 23, 5055.
- [20] a) M.-M. Song, Y.-M. Wang, B. Wang, X.-Y. Liang, Z.-Y. Chang, B.-J. Li, S. Zhang, *ACS Applied Materials & Interfaces* 2018, 10, 15021; b) Y.-n. Sun, G.-r. Gao, G.-l. Du, Y.-j. Cheng, J. Fu, *ACS Macro Letters* 2014, 3, 496.
- [21] P. Van de Wetering, A. T. Metters, R. G. Schoenmakers, J. A. Hubbell, *Journal of Controlled Release* 2005, 102, 619.
- [22] H. Ma, A. Y. Jen, L. R. Dalton, *Advanced Materials* 2002, 14, 1339.
- [23] S. L. Jacques, *Physics in Medicine & Biology* 2013, 58, R37.
- [24] a) A. Mehta, *Pharma XChange* 2011, 13, 12; b) D. A. Skoog, F. J. Holler, S. R. Crouch, *Principles of instrumental analysis*, Cengage learning, 2017.
- [25] L. Ouyang, C. B. Highley, W. Sun, J. A. Burdick, *Advanced Materials* 2017, 29, 1604983.
- [26] a) R. Ramaswami, K. Sivarajan, G. Sasaki, *Optical networks: a practical perspective*, Morgan Kaufmann, 2009; b) B. Potter, *Material Science and Engineering Dept, University of Arizona* 2010, 1.
- [27] a) Y. Zheng, M. K. L. Han, Q. Jiang, B. Li, J. Feng, A. del Campo, *Materials Horizons* 2019; b) A. Farrukh, J. I. Paez, A. del Campo, *Advanced Functional Materials* 2019, 29, 1807734.
- [28] a) M. J. Salierno, A. J. García, A. del Campo, *Advanced Functional Materials* 2013, 23, 5974; b) S. Petersen, J. M. Alonso, A. Specht, P. Duodu, M. Goeldner, A. del Campo, *Angewandte Chemie International Edition* 2008, 47, 3192; c) Y. Ohmuro-Matsuyama, Y. Tatsu, *Angewandte Chemie International Edition* 2008, 47, 7527; d) M. Wirkner, J. M. Alonso, V. Maus,
-

- M. Salierno, T. T. Lee, A. J. García, A. del Campo, *Advanced Materials* **2011**, *23*, 3907; e) M. Wirkner, S. Weis, V. San Miguel, M. Álvarez, R. A. Gropeanu, M. Salierno, A. Sartoris, R. E. Unger, C. J. Kirkpatrick, A. del Campo, *ChemBioChem* **2011**, *12*, 2623.
- [29] T. T. Lee, J. R. García, J. I. Paez, A. Singh, E. A. Phelps, S. Weis, Z. Shafiq, A. Shekaran, A. Del Campo, A. J. García, *Nature materials* **2015**, *14*, 352.

3. Printed waveguides from thermoplastic amorphous Poly(D,L-lactide) and derived copolymers

3.1 Abstract

In this chapter optical waveguides from poly(D,L-lactide) and derived copolymers fabricated by extrusion printing are presented. The printed waveguides have elastomeric properties at body temperature and show softness and flexibility in the range relevant for implantable devices in soft organs. The obtained optical waveguides propagate VIS to NIR light in air and in tissue at penetration depths of tens of centimeters.

3.2 Introduction

Light guiding properties are affected by swelling. A lower polymer concentration in a swollen gel leads to lower refractive index^[1]. This is a limitation of hydrogel-based optical waveguides. If the water content in the waveguide is the same as in surrounding tissue, the difference between the refractive index of the waveguide and the tissue is reduced and the total internal reflection condition cannot be achieved. Thermoplastics typically have higher refractive indices than hydrogels, which make them better light guiding materials in tissue. Besides, thermoplastics with hydrophobic polymeric chains do not uptake water and present stable light guiding property in wet environments.

Poly(lactide) (PLA) is a degradable thermoplastic and approved for medical applications. It is widely used to fabricate porous scaffolds for tissue engineering and regenerative medicine by electrospinning or 3D printing technologies.^[2] PLA is an aliphatic polyester derived from lactic acid^[3], a molecule containing an asymmetric carbon and, therefore, available in two optical isomers: the D (dextroisomer) and L (levoisomer) enantiomers.^[4] Accordingly, PLA has three possible enantiomeric forms: PLLA, PDLA and PDLA.

PLA can be synthesized via three different routes: i) polycondensation of lactic acid leading to low molecular weight PLA; and ii) ring opening polymerization of lactide or iii) azeotropic dehydration condensation reaction, both of which can directly yield high molecular weight PLA.^[4-5] In order to improve the processability of PLA, small amounts of lactide enantiomers with opposite configuration are incorporated into the polymer to adjust the melting point. By changing the ratio of D to L enantiomers, PLA polymers can range from amorphous to semi-crystalline and highly crystalline form.^[4] Crystalline PLA has a melting point around 180 °C and amorphous PLA has a glass transition temperature in the range of 50-75 °C.^[6] The thermal properties of PLA are basically related to the composition (the ratio of two isomers) and the molecular weight.^[7]

At lower temperature than T_g , PLA is a rigid and brittle material with tensile strength of 32 MPa and Young's modulus of 2.3 GPa, and low impact strength and elongation at break (5%).^[7-8] The high stiffness and poor toughness limit its application that require plastic deformation below glass transition temperature.^[9] Therefore, PLA is often plasticized by blending with poly(3-methyl-1,4-dioxan-2-one), polycaprolactone (PCL), citrate esters, poly(butylene succinate) (PBS), poly(ethylene glycol)s (PEGs), etc. to transform its brittleness into ductility.^[7, 10] Besides, copolymerizing with low glass transition temperature polymers, for example PCL, can also decrease the stiffness of PLA.^[11]

The degradation of PLA is caused by the hydrolysis of ester bond and does not need the participation of enzymes for catalysis.^[4] The size and shape of PLA, the composition (ratio between isomers), and the condition of hydrolysis (temperature and pH) codetermine the degradation rate of PLA.^[12] The degradation profile of PLA can be adjusted by copolymerizing with other degradable polymers. For example, the degradability of polylactide-co-glycolides (PLGAs) can be tuned by varying the lactide to glycolide ratios in copolymers.^[13]

Based on the biocompatibility and degradability, PLA has been widely used in medical applications, such as fabricating bone scaffolds for tissue engineering, surgical sutures for wound management, nano-particles for drug delivery, and producing biodegradable screws and fixation pins for orthopedic devices.^[5] PLA has good barrier properties, enabling it to be used for green food packaging.^[7, 14]

Besides, based on the transparency, PLA and its copolymers with poly(glycolic acid), PLGA, have been used as biomaterials for optical waveguides to deliver light into tissue.^[15] For example, comb-shaped planar waveguides of 6 cm length were fabricated by laser cutting casted planars from PLA melts and applied to photochemical tissue bonding.^[15a] In a different study, continuous poly(L-lactic acid) (PLLA) fibers of 220 μm diameter were obtained by thermal drawing, and tested for deep brain fluorescence sensing and optogenetic interrogation in vivo.^[15b] An optical lens-microneedle array from PLA was also prepared by press-molding and used for light-based therapy.^[15c] The reported PLA waveguides displayed moderate attenuation ranges, i.e. 1.5 - 1.64 dB/cm for 473 - 532 nm light. In the reported cases, the waveguides were processed by casting, drawing or press-molding from the melts and the fabricating processes required temperatures higher than 200 °C and the obtained waveguides were stiff (Young's Modulus of ~ 3.5 GPa^[15c]) and brittle.

In this Chapter PLA and copolymers will be used as inks to fabricate waveguides by extrusion printing at low temperature. In order to obtain soft and flexible

waveguides, amorphous Poly(D,L-lactide) (Resomer®), its PLGA copolymers and its copolymer with low molecular weight polycaprolactone (PCL) were selected. The printed fibers were soft and flexible at body temperature, and display excellent light guiding properties. The printed waveguides were tested to propagate light through tissue and activate photochemical reactions in vitro.

3.3 Results and Discussion

PLA, PLGA with D,L-lactide/glycolide ratios 75:25 (PLGA-75) and 50:50 (PLGA-50), and Poly(D,L-lactide-co-caprolactone) with 86 mol% of D,L-lactide (PLA-co-PCL) were selected as thermoplastic inks for printing optical waveguides. PLA, PLGA-75 and PLGA-50 are amorphous and transparent polymers with low molecular weight (**Table 1**) and T_g around body temperature, 38 - 46°C (**Table 1**). Accordingly, these materials behave like elastomers at body temperature. The introduction of PGA in the copolymer composition accelerates the degradation rate, e.g. degradation time of PLGA-50 and PLA are 3 and 6 months respectively. Copolymerization of PLA with PCL decreases the glass transition temperature of the polymers. PLA-co-PCL shows a T_g of 16°C (**Table 1**) and behaves as an elastomeric material at room temperature.

For guiding light into tissue, optical waveguides need high transparency and a refractive index (RI) value higher than the RI of tissue (1.38 - 1.51).^[16] The selected PLA and its random copolymers are amorphous (**Figure 1 D-F**) and do not form segregated structures. **Figure 1A** shows the absorption spectrum of the four different polymers within the 350 to 800 nm spectral range. PLA and PLA-co-PCL exhibited excellent transparency. PLGA copolymers showed significant absorbance at wavelengths below 700 nm. This absorbance has been associated to the brown or beige color of the copolymer^[17] (**Figure 1C**). The selected PLA and its copolymers for this study have RI >1.45 (**Figure 1B**) and, therefore, are appropriate candidates for guiding light through most tissues.

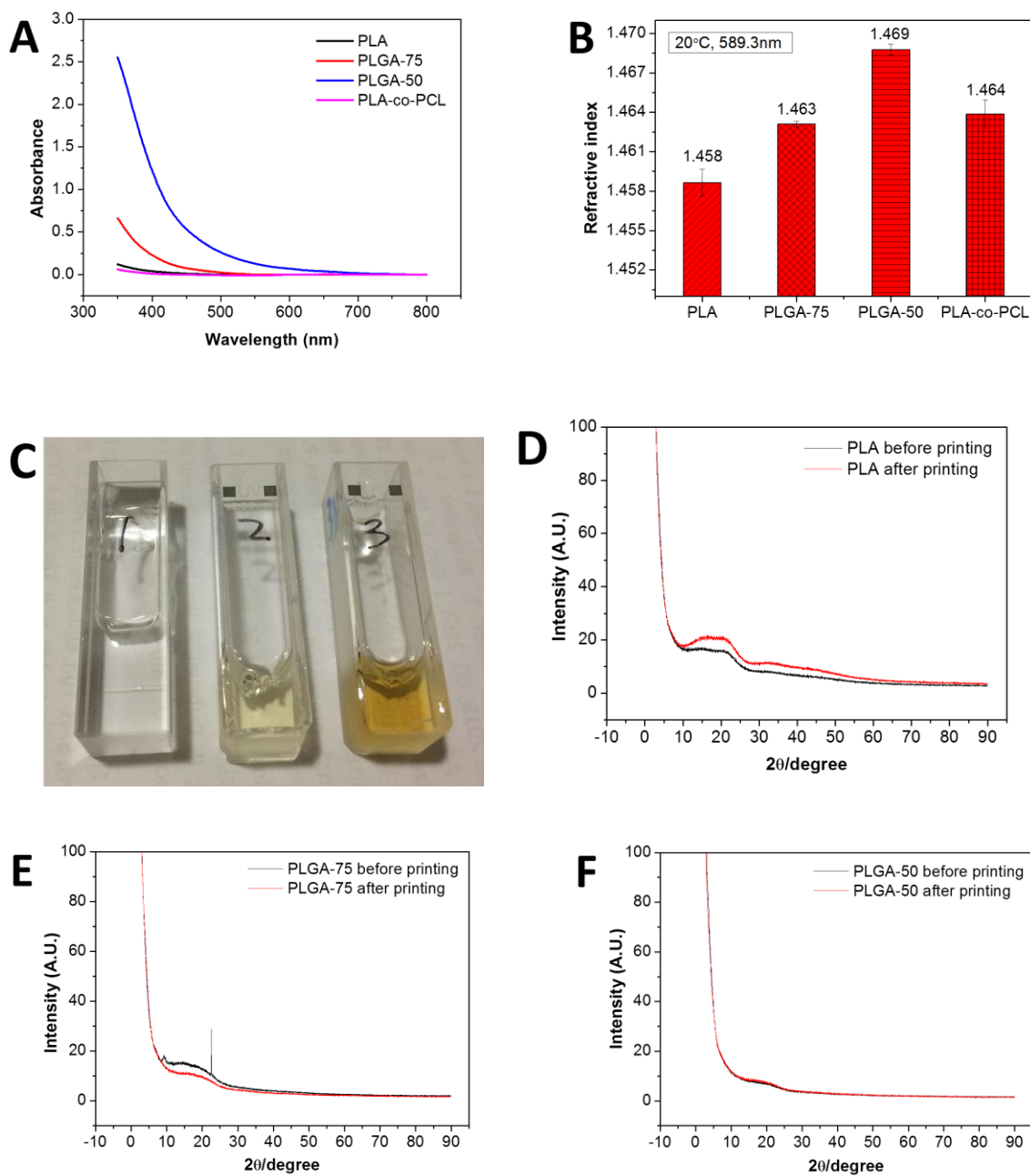


Figure 1. (A) Absorbance spectra of PLA, PLGA-75, PLGA-50 and PLA-co-PCL (B) Refractive index of PLA, PLGA-75, PLGA-50 and PLA-co-PCL measured at 589.3 nm and 20°C. (C) The color of melted PLA (1), PLGA-75 (2) and PLGA-50 (3). (D-F) XRD patterns of the polymers as powders and printed fibers.

Table 1. Physical and chemical properties of selected materials from manufacture and measurement.

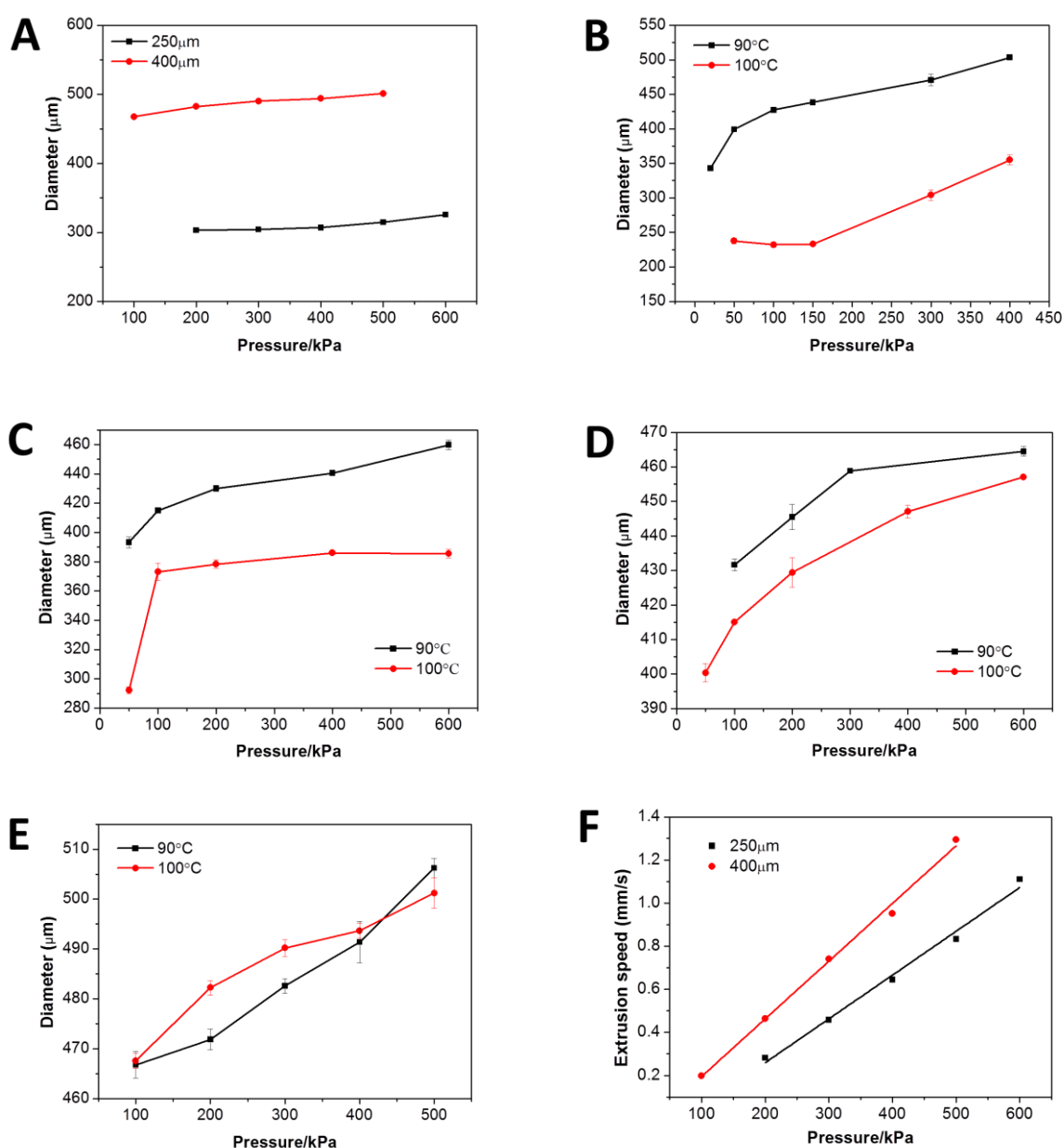
Materials	Tg from manufacture	Measured onset Tg	Measured melting point	Mw from manufacture	Viscosity (0.1 % (w/v) in chloroform(25 °C)) from manufacture	Aggregation morphology	Composition from manufacture
PDLLA	38-42 °C	36°C	93°C	10,000-18,000	0.16-0.24 dL/g	amorphous	/
PLGA-75	42-46 °C	32°C	92°C	4,000-15,000	0.14-0.22 dL/g	amorphous	D,L-lactide:glycolide 75:25
PLGA-50	42-46 °C	38°C	85°C	7,000-17,000	0.16-0.24 dL/g	amorphous	D,L-lactide:glycolide 50:50
PLA-co-PCL	16 °C	16°C	97°C	/	0.7-0.9 dL/g	amorphous	D,L-lactide:caprolactone 85:15

3.3.1 Printing optical waveguides from PLA and copolymers

Fibers of PLA and its copolymers were printed from the melt using a commercially extrusion printer (see experimental information for details in Appendix). We used nozzles with diameter 250 and 400 μm . Fibers were easily obtained at printing temperatures 90 - 100 °C (**Table 1**) and using printing pressure between 20 and 600 kPa. The quality of the printed fibers, i.e. the diameter, shape fidelity along the fiber and the smoothness of the fiber surface, was checked by microscopy imaging for the different printing conditions. Smooth fibers with constant diameter were obtained (**Figure 3A**). The wider nozzle allowed extrusion at lower pressures maintaining constant extrusion temperature (**Figure 2A**), and faster extrusion at constant pressure (**Figure 2F**). Higher extrusion temperatures lead to lower viscosity of melt and thinner waveguides (**Figure 2: B-E**) and allowed faster extrusion at constant pressure (**Figure 2G**). Theoretically, the diameter of the printed waveguides should match the diameter of the nozzle. In reality, due to the Barus effect,^[18] the extruded waveguides were thicker than the inner diameter of the nozzle (**Figure 2: A and B**). Increasing the pressure accentuated this effect. The melt viscosity of the inks increased in the order PLA-co-PCL > PLGAs, PLA (**Table 1**). The higher the viscosity of the ink, the stronger the Barus effect (**Figure 2E**). The final diameter of the extruded fibers was, therefore,

determined by the nozzle size, printing temperature and pressure, and the viscosity of the ink.

At optimized printing conditions, continuous and smooth fibers of >20 cm in length and 300 - 500 μm diameters were obtained (**Figure 3A**). All printed fibers were transparent. Fibers made of PLA, PLGA-75 and PLGA-50 were rigid and brittle at room temperature, while PLA-co-PCL fibers were soft and flexible (**Figure 3A**).



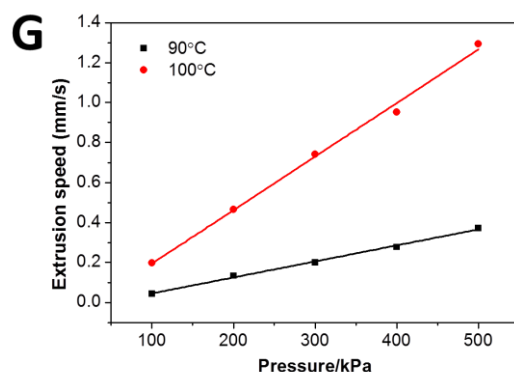


Figure 2. The influence of printing parameters on the diameter of the printed optical waveguides. (A) The diameters of printed PLA-co-PCL waveguides under different pressure with different nozzle sizes at 100 °C; (B-E) The diameter of printed PLA (B), PLGA-75 (C), PLGA-50 (D) and PLA-co-PCL (E) waveguides at different temperature and under different pressure with nozzle size of 400 μm . (F) Extrusion speed of printed PLA-co-PCL fiber at 100°C as function of printing pressures through nozzles of 250 or 400 μm diameter; (G) Extrusion speed of printed PLA-co-PCL fiber as function of printing pressure at printing temperature of 90 or 100°C and a 400 μm nozzle.

3.3.2 Thermal, mechanical and optical properties of the printed waveguides

To examine the flexibility of the printed waveguides at body temperature, PLA, PLGA-75 and PLGA-50 waveguides were immersed in water at 37°C for 5 min (**Figure 3B**). The waveguides, with onset-T_g at 36, 32 and 38°C respectively, became soft and flexible and could be easily twisted in any direction at 37°C.

The polymers in printed fibers were amorphous according to our XRD studies (**Figure 1 D-F**), indicating that the shear forces and cooling program during printing did not lead to the formation of crystalline structures. The absence of crystalline structures is relevant to guarantee the transparency of the printed fibers.

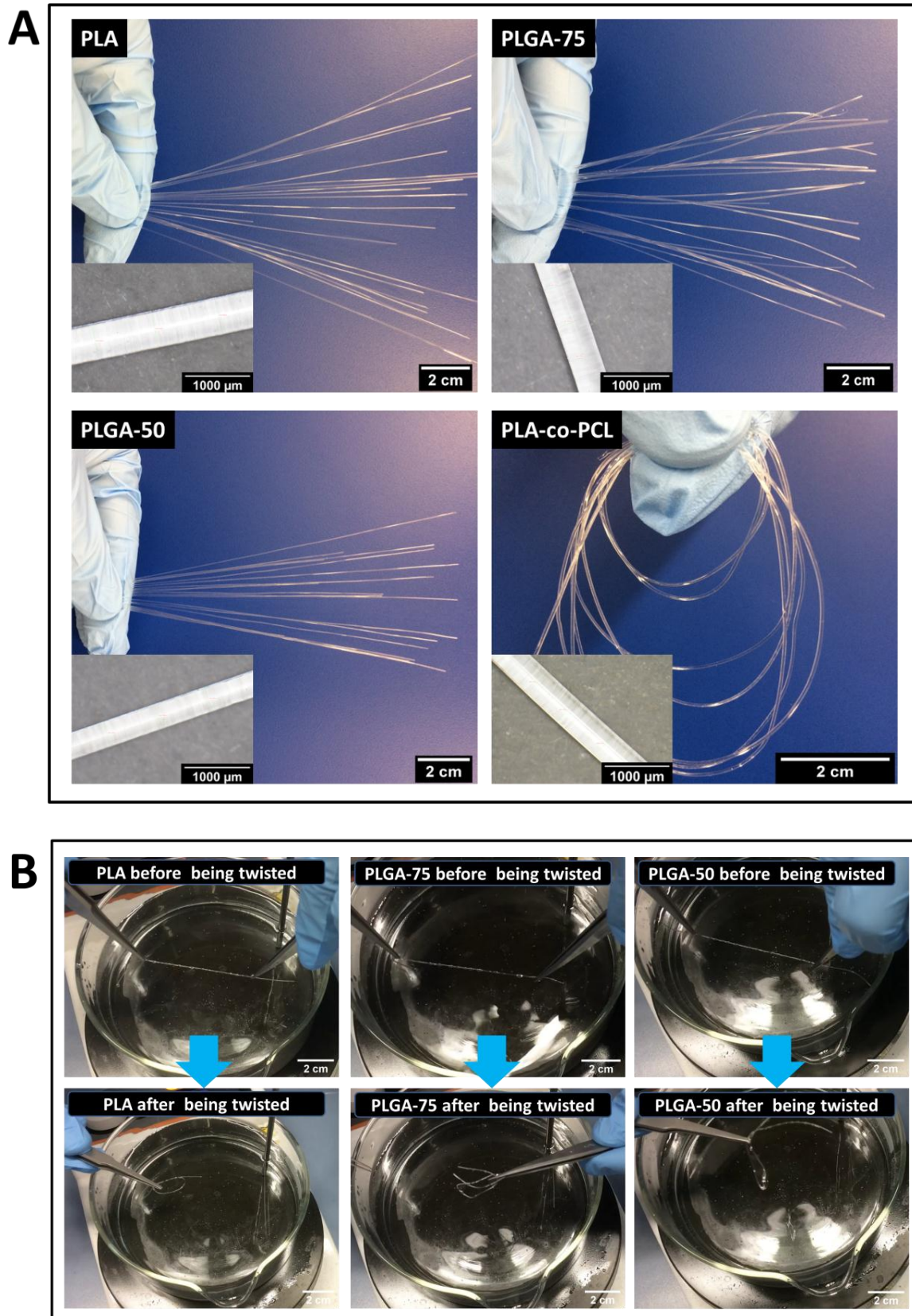


Figure 3. (A) Images of printed optical fibers from PLA and its copolymers. Insets show magnified images of the fibers demonstrating shape fidelity and

smoothness of the fiber surface. (B) Images of PLA, PLGA-75 and PLGA-50 fibers before and after being twisted at 37°C.

In order to characterize the light guiding properties of the printed fibers, a home-made setup was constructed (**Scheme 2** in chapter 2). A laser beam (405, 450, 520, 670, 808 nm) was focused on one end of the waveguide. The propagating light intensity through the fiber was visible by the auto-fluorescence of the material. A camera was used to capture the auto-fluorescence signal. The decay in the auto-fluorescence intensity along the waveguide was evaluated with ImageJ. The fluorescence intensity at the beginning of the fiber (I_0) and at distance L (I_L) was measured. The optical loss was calculated as:^[19]

$$\alpha(\lambda) = (10/L) * \log(I_0/I_L)$$

No auto-fluorescence was excited by illuminating at 670 or 808 nm and, therefore, quantification of the optical loss with this method was not possible for those wavelengths.

Figure 4A displays the values of the optical loss measured for the printed waveguides in air. Optical loss values in ranges of 0.02 - 0.08 dB/cm and 0.1 - 0.3 dB/cm were obtained for PLA and PLA-co-PCL at 405, 450 and 520 nm. In PLGA copolymers the optical loss increased from 0.13 to 0.75 dB/cm and from 0.82 to 3.85 dB/cm at the wavelength of 405 – 520 nm with 25% and 50% of PGA in the copolymer. This is attributed to the high absorbance of the material (**Figure 1A**). Besides, scattering from density fluctuations, compositional inhomogeneity, impurities and surface roughness can also contribute to the optical loss.^[20] Light propagation at wavelengths ≥ 670 nm was better than at shorter wavelengths, according to visual observation (**Figure A6** in Appendix). PLA and PLA-co-PCL fibers propagated light along >50 cm in air.

The optical performance of the fibers was also evaluated in tissue (**Figure 4B**). For this purpose the printed waveguides were sandwiched between two pieces of

porcine muscle. The optical loss of the fibers in tissue was in the range of 0.14 - 0.29 dB/cm, 0.16 - 0.73 dB/cm and 0.22 - 0.44 dB/cm for PLA, PLGA-75 and PLA-co-PCL with wavelength of 405 - 520 nm. The higher optical loss in tissue than in air is a consequence of the higher refractive index of tissue and, possibly, of the rougher interface between tissue and the waveguides. Besides, light absorption by the tissue could also lead to attenuated total reflection. We calculated the penetration depth of light in the tissue (**Figure 4C**), defined by distance at which light intensity decays to $1/e$. The penetration depth of 405nm light in PLA, PLGA-75 and PLA-co-PCL waveguides in tissue is 15, 5 and 10 cm respectively. The penetration depth increased to 32, 28 and 20 cm at wavelength 520 nm. The propagation of light in tissue is visually shown in **Figure 4E**. Note that PLA-co-PCL waveguides were also able to guide light along 90° turns in the fiber (**Figure 4E**). Typical irradiance values for the activation of photochemical or photobiological reactions used to regulate biological processes in vitro are in the range of dozens nW/cm^2 – hundreds mW/cm^2 .^[21] In order to estimate if a 4.5 mW laser coupled to the fibers would be enough to activate such processes, we coupled it to the printed fibers and measured the irradiance delivered by 10 cm optical waveguides sandwiched between two pieces of porcine muscle (8 cm) at wavelengths 405, 450, 520, 670, and 808 nm (**Figure 4D**). Values of 70 - 450 mW/cm^2 for PLA and 30 - 150 mW/cm^2 for PLA-co-PCL were measured in the 405 - 808 nm range. The irradiance values increased with the wavelength in the range of 405 - 520 nm, remained constant in the range of 520 - 700 nm and decreased in the range of 700 - 808 nm. This behavior is consistent with the absorbance of the materials. These results demonstrate sufficient light can be delivered into deep tissue to activate most photochemical or photobiological reactions through our printed fibers.

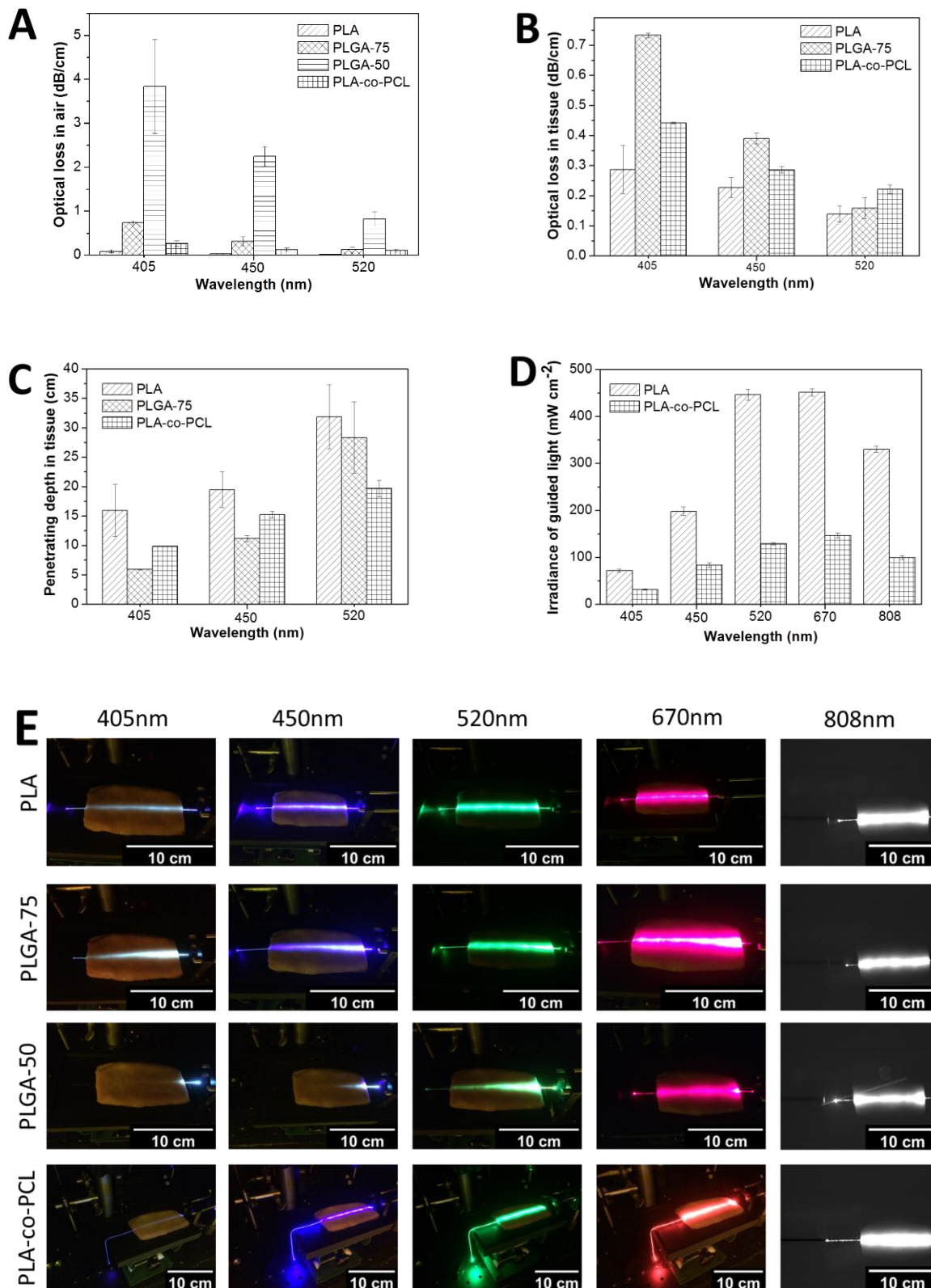


Figure 4. (A) Optical loss of printed waveguides in air; (B) Optical loss of printed waveguides in tissue; (C) Penetration depth of guided light in tissue; (D) The irradiance of light at the distal end of fiber (10 cm) that sandwiched by porcine

muscle (8 cm in length). (E) Images of light propagating through printed waveguides embedded in tissue.

3.3.3 Photostimulation of biological processes across tissue with printed waveguides

We designed the same in vitro experiment as in chapter 2 to demonstrate the suitability of the printed fibers to deliver light through tissue and remotely trigger light-regulated processes in a biological scenario.

These experiments were performed in cooperation with Dr. Yijun Zheng. The 405nm light was delivered to the cell culture by 10 cm printed PLA or PLA-co-PCL waveguides sandwiched by 8 cm of porcine tissue. The 3D cell culture was irradiated for 15 minutes with the waveguide from the top, and then incubated for 2 days. At this irradiation dose cells remained viable according to live-dead assays. **Figure 5** shows the morphology of the spheroids in the irradiated gels and in the non-irradiated controls. Cells remained clustered within the spheroids in the absence of irradiation since the surrounding dextran cell did not present active RGD. In contrast, cells exposed to light through the waveguide migrated out of the spheroids into the surrounding gel. In control experiments using the dextran gel without RGD modification cells did not migrate (results not shown), confirming that the migration was due to the activated RGD ligand by the light delivered by the waveguide. This experiment highlights the suitability of the printed waveguides for delivering light across tissue at sufficient efficiency to activate established photochemical reactions in biological scenarios.

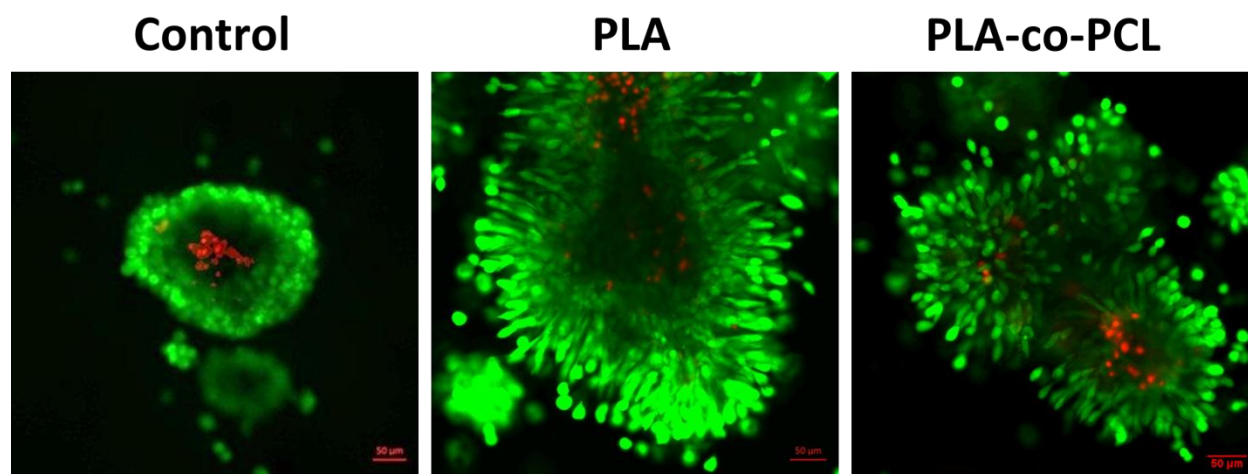


Figure 5. Fluorescence image of L929 fibroblast spheroids embedded in a photoactivatable hydrogel after two days culture. The control gels (left) were not exposed to light. The middle and right images correspond to gels that were exposed to 405 nm light delivered by printed fibers through 8 cm tissue.

3.4 Conclusive remarks

PLA and its copolymers with PGA and PCL are widely used materials to construct porous scaffolds for tissue engineering due to their biocompatibility and degradability.^[22] Being transparent and extrudable materials, they have also been considered for the fabrication of optical waveguides.^[15a, 15b] In this Chapter it is demonstrated that amorphous PLA copolymers are useful inks to print optical waveguides with desired geometries and dimensions. The selected low molecular PLA, PLGA and PLA-co-PCL copolymers demonstrate elastomeric properties at body temperature overcoming the fragility of reported PLA optical waveguides. The elasticity of waveguides at body temperature makes it more compatible with the mechanics of soft tissue and allows the application in moving tissue and organs.

The selected materials were easily fabricated into continuous fibers with printing technology at mild conditions—relatively low pressure (20-60 kPa) and temperature (90-100 °C). The employment of printing technology simplified the

fabrication of fibers, which provides the versatility and the possibility to upscale and manufacture desired sophisticated geometries. The printed PLA and PLA-co-PCL waveguides showed excellent light guiding properties in air and tissue, and can propagate 400 - 808 nm light over long distances in tissue (>10 cm) and also along bent shapes. Fibers showed optical loss in the range of 0.02 - 0.26 dB/cm in air and 0.14 - 0.73 dB/cm in tissue at wavelengths of 405 - 520 nm, which is far better than reported PLA waveguides to date. Note that PLA optical waveguides fabricated by other means have shown attenuation values of 1.5 - 1.64 dB/cm in air for 473 - 532 nm light.^[15a, 15b] The elastomeric properties of these two materials at body temperature and their excellent light guiding properties seem ideal for clinical application scenarios where light has to be delivered into soft organs inside the body, like in optogenetic-based therapies.

However, it must be pointed out that the interactions of polymer chains are weakened in polymers with service temperature above T_g . Water absorption could also occur, which could induce phase separation of the copolymers and decrease the transparency of waveguides. To solve this problem, the fibers could be coated with a super hydrophobic cladding to avoid direct contact between water at the application site.

References

- [1] S. L. Jacques, *Physics in Medicine & Biology* 2013, 58, R37.
- [2] a) B. Seal, T. Otero, A. Panitch, *Materials Science and Engineering: R: Reports* 2001, 34, 147; b) P. S. Poh, M. P. Chhaya, F. M. Wunner, E. M. De-Juan-Pardo, A. F. Schilling, J.-T. Schantz, M. van Griensven, D. W. Hutmacher, *Advanced drug delivery reviews* 2016, 107, 228.
- [3] L.-T. Lim, R. Auras, M. Rubino, *Progress in Polymer Science* 2008, 33, 820.
- [4] D. Garlotta, *Journal of Polymers and the Environment* 2001, 9, 63.
- [5] K. Hamad, M. Kaseem, H. Yang, F. Deri, Y. Ko, *Express Polymer Letters* 2015, 9.

-
- [6] a) J. Ahmed, J.-X. Zhang, Z. Song, S. Varshney, *Journal of Thermal Analysis and Calorimetry* 2009, 95, 957; b) K. Jamshidi, S.-H. Hyon, Y. Ikada, *Polymer* 1988, 29, 2229.
- [7] J. Ahmed, S. K. Varshney, *International Journal of Food Properties* 2011, 14, 37.
- [8] R. A. Auras, S. P. Singh, J. J. Singh, *Packaging Technology and Science: An International Journal* 2005, 18, 207.
- [9] R. Bhardwaj, A. K. Mohanty, *Biomacromolecules* 2007, 8, 2476.
- [10] S. Su, R. Kopitzky, S. Tolga, S. Kabasci, *Polymers* 2019, 11, 1193.
- [11] B. Dhandayuthapani, Y. Yoshida, T. Maekawa, D. S. Kumar, *International journal of polymer science* 2011, 2011.
- [12] D. L. Kaplan, in *Biopolymers from renewable resources*, Springer 1998, p. 1.
- [13] P. In Pyo Park, S. Jonnalagadda, *Journal of Applied Polymer Science* 2006, 100, 1983.
- [14] J. Lunt, *Polymer Degradation and Stability* 1998, 59, 145.
- [15] a) S. Nizamoglu, M. C. Gather, M. Humar, M. Choi, S. Kim, K. S. Kim, S. K. Hahn, G. Scarcelli, M. Randolph, R. W. Redmond, *Nature communications* 2016, 7, 10374; b) R. Fu, W. Luo, R. Nazempour, D. Tan, H. Ding, K. Zhang, L. Yin, J. Guan, X. Sheng, *Advanced Optical Materials* 2018, 6, 1700941; c) M. Kim, J. An, K. S. Kim, M. Choi, M. Humar, S. J. Kwok, T. Dai, S. H. Yun, *Biomedical optics express* 2016, 7, 4220.
- [16] M. Choi, M. Humar, S. Kim, S. H. Yun, *Advanced Materials* 2015, 27, 4081.
- [17] Y. Reyhanoglu, E. Gokturk, *Journal of Saudi Chemical Society* 2019.
- [18] N. Kishi, H. Iizuka, *Journal of Polymer Science Part B: Polymer Letters* 1964, 2, 399.
- [19] a) R. Ramaswami, K. Sivarajan, G. Sasaki, *Optical networks: a practical perspective*, Morgan Kaufmann, 2009; b) B. Potter, *Material Science and Engineering Dept, University of Arizona* 2010, 1.
- [20] a) H. Ma, A. Y. Jen, L. R. Dalton, *Advanced Materials* 2002, 14, 1339; b) S. Shabahang, S. Kim, S. H. Yun, *Advanced Functional Materials* 2018, 28, 1706635.
- [21] a) R. Ohlendorf, R. R. Vidavski, A. Eldar, K. Moffat, A. Möglich, *Journal of molecular biology* 2012, 416, 534; b) A. M. Kloxin, A. M. Kasko, C. N. Salinas, K. S. Anseth, *Science* 2009, 324, 59; c) C. de Gracia Lux, J. Lux, G. Collet, S. He, M. Chan, J. Olejniczak, A. Foucault-Collet, A. Almutairi, *Biomacromolecules* 2015, 16, 3286.
- [22] a) M. S. Lopes, A. Jardini, R. Maciel Filho, *Procedia Engineering* 2012, 42, 1402; b) P. Gentile, V. Chiono, I. Carmagnola, P. V. Hatton, *International journal of molecular sciences* 2014, 15, 3640.
-

4. Printed waveguides from elastomeric materials

4.1 Abstract

In this chapter printable and stretchable optical waveguides are presented. They consist of elastomeric materials, i.e. polydimethylsiloxane (PDMS) and acrylated Pluronic F127 (Pluronic-DA) in core/cladding design, and were fabricated by extrusion-based printing. The optical properties and performance is analyzed.

4.2 Introduction

Polydimethylsiloxane (PDMS) is one member of the family of silicone elastomers. Due to its elasticity, biocompatibility, nontoxicity, blood compatibility, transparency and durability, PDMS finds wide applications in optic/electronic devices, medical equipment and biological research.^[1] The chemical structure of this synthetic polymer has a repetition of silicon and oxygen and methyl groups in its axis.^[1a, 2] The flexible Si-O structure endows PDMS good elasticity and permeability allowing gas diffusion inside, which makes it advantageous for some medical application, such as artificial skin and wound dressing.^[1b, 3] The exposure of methyl groups at the interface minimizes the possible interaction at the interface, which endows it bio-inert properties,^[4] which makes it even more attractive in biomedical application.^[5] However, the high content of methyl groups in repeat units makes PDMS hydrophobic property that could hinder cell attachment, which is the prerequisite for tissue regeneration.^[6] To functionalize

the PDMS surface and improve cell adhesion properties, the polymer is treated with plasma or lasers, or silanized to change surface properties.^[7] Alternatively, coating with proteins that allow cells adhesion, such as collagen, fibronectin and laminin, or conjugating with cell-adhesive peptide on the surface of PDMS have been applied to get long term cell adhesive property.^[8]

PDMS demonstrates better manufacturing ability than conventional materials like glass and silicon.^[1a] The ability to replicate microstructures is widely used for soft lithography and makes PDMS an appropriate material for microfluidics.^[7a, 9] Furthermore, the transparency enables it even more applicable in microfluidics, which allows the in-situ monitoring the fluidic process in the microchannels by optical access.^[7a] The excellent machinability and transparency of PDMS also allow the wide applications in optics, including optical interconnects^[10], blazed gratings^[11], adaptive lenses^[12], solid immersion lenses^[13].

Besides, PDMS presents a low intrinsic loss ($\leq 0.05\text{dB/cm}$ at 850nm ^[14]) and relative high refractive index (≥ 1.40 ^[14-15]). These properties make it an interesting material for optical waveguides.^[14-16] By taking the advantage of the stretchability and transparency, PDMS waveguides have been employed to sense strain^[15b, 16b, 16e] and pressure^[15a, 16a]. For example, PDMS has been fabricated into highly stretchable optical sensors for pressure, strain, and curvature measurement.^[16b] The sensors are made of PDMS elastomer coated with a thin gold reflective layer. The sensors are working by forming micro-cracks within the reflective layer that results in escaping of light and higher optical power losses in light transmission when the sensors are stretched, compressed, or bent. A waveguide made of PDMS was used to deliver light for Scleral cross-linking (SXL).^[16c] SXL was performed on fresh porcine eyes with this waveguide and the sclera cross-linked with the waveguides exhibited stronger mechanical properties compared to that without waveguide. In order to improve the light guiding property and try to avoid light leakage to nontarget, periorbital tissue, a core/cladding waveguide

was developed, which employed polyurethane as core and PDMS as cladding and was further coated with reflective silver layer on the top and side surfaces of the waveguide.^[16d] With the new waveguide, the mechanical properties of crosslinked sclera were further strengthened. By changing the ratio of the base to curing agent, PDMS with different refractive indices can be obtained. With this concept, a stretchable core/cladding optical fiber (ratio of base to curing agent: 5:1 for core, 20:1 for cladding) was fabricated.^[16f] However, in reported PDMS-based waveguides, the optical loss is much higher than the intrinsic loss of PDMS (0.36 dB/cm at 635 nm in a core/cladding fiber^[15c]). In order to enable the light guiding property of PDMS waveguides close to its intrinsic optical property, new designs or new waveguides from PDMS need to be further developed. In addition, all reported PDMS optical waveguides were fabricated by mold-casting^[17], which is not an appropriate method to fabricate complicated structures and to integrate with other component in multifunctional devices. Thus, new manufacturing approaches should be employed to fabricate PDMS based optical waveguides.

In the present work, we describe printable PDMS based core/cladding waveguides. To facilitate and speed-up extrusion of the PDMS fibers and to achieve total internal reflection, core/cladding optical waveguides fabricated by co-extrusion printing of PDMS core and Pluronic-DA cladding materials were printed. As described in section 2.2, physical crosslinked Pluronic-DA hydrogel demonstrates shear-thinning property, which is beneficial to printing processes.^[18] The co-extrusion allows slow curing PDMS to be confined in the core by Pluronic-DA cladding without leakage before being cured. And the in-situ polymerization of Pluronic-DA in silicone tube can keep the fidelity of printed waveguides. The waveguiding properties of the printed stretchable PDMS/Pluronic core/cladding waveguides are described.

4.3 Results and discussion

4.3.1 Synthesis and physicochemical properties of Pluronic-DA

Pluronic-DA was synthesized following a reported method by reaction of the terminal hydroxyl groups of the Pluronic chains with acryloyl chloride (**Scheme A1** in Appendix).^[19] The successful synthesis was confirmed by ¹H NMR (**Figure A7A** and **B** in Appendix), and Pluronic-DA with substitution degree 70% was used for the studies. The transition temperature of Pluronic-DA solutions in water (20-50 wt%) was studied by rheology (**Figure 1A** and **Table A2** in Appendix). Note that this concentration range is well above the critical micellar concentration of Pluronic (2.8×10^{-6} M at 37°C in water)^[20] and, therefore, we expect micelle formation in all samples. The characteristic sigmoidal in G' and G'' vs. T curves confirmed the phase transition^[21] for the 20-50 wt% solutions at temperatures between 5 and 37 °C (**Figure 1A**). At the transition temperature H bonds between water molecules and the hydrophilic Pluronic segments in the chains become destabilized, desolvation of the chains occur and the hydrophobic interactions among the poly(oxypropylene) domains increase, resulting in gel formation.^[21] The transition temperature decreases with increasing polymer concentration and in Pluronic-DA solutions at >30 wt/v% concentration the transition temperatures drop below room temperature. This is the interesting range for processing Pluronic-DA by printing. As physical gel, Pluronic-DA shows shear-thinning properties. The viscosity of Pluronic-DA gels get lowers with increasing shear rate (**Figure 1B**). The shear-thinning property also facilitates extrusion.

The mechanical stability of Pluronic-DA hydrogels before and after photoinitiated crosslinking of the DA groups was analyzed (**Table A2** and **Figure A7C** in Appendix). The resulting Young's Modulus was obtained from the rheology measurements. Pluonic-DA hydrogels were soft, with a Young's Modulus of 43

kPa before DA crosslinking in 50 wt% gels, which increased to 151 kPa after photopolymerization. Pluronic-DA hydrogels showed decreasing swelling ratios with increasing polymer content (**Table A2** in Appendix): from 1082% at 30 wt% to 759% at 50 wt%. Pluronic F127 is a nonionic polymer^[21] and, therefore, its swelling ratio is mainly determined by the crosslinking degree, which is a function of polymer and DA concentration.

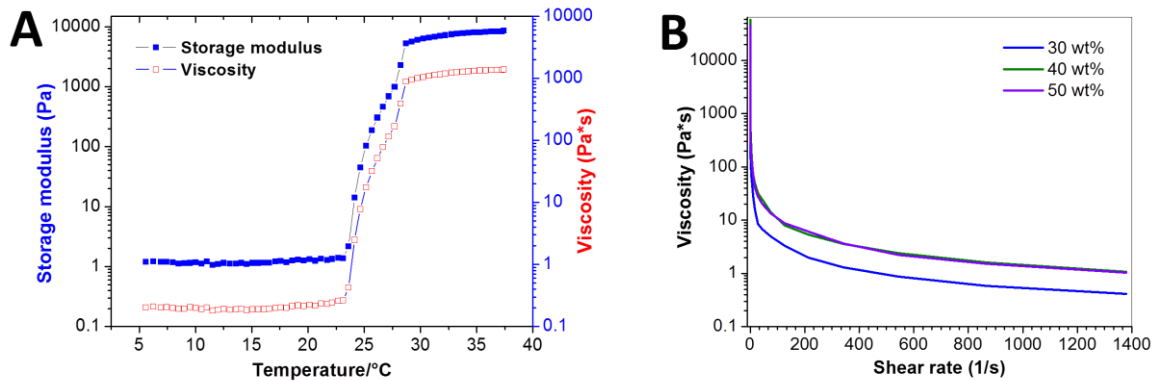


Figure 1. (A) The storage modulus and viscosity of 20 wt/v% Pluronic-DA in a temperature sweep rheology experiment (5 – 37 °C). (B) The viscosity of different concentration of Pluronic-DA at increasing shear rate.

4.3.2 Optical properties of PDMS and Pluronic-DA

Thermal and UV-curable PDMS (T-PDMS and UV-PDMS) were used in our study as core materials for printable core/cladding waveguides. At room temperature, both PDMS are viscous liquids (viscosity 3.5 Pa*s for T-PDMS and 2.7 Pa*s for UV-PDMS; data from manufacturer). The curing time for these polymers is in the range of minutes to hours (48 hours for T-PDMS at room temperature and 20 min*1mW/cm² for UV-PDMS, data from manufacture). Cured PDMS showed high transparency, with a slight increase in absorbance at wavelengths <400 nm (**Figure 2B**).

Due to the existence of evanescent wave in cladding when total internal reflection occurs at the interface between core and cladding,^[22] the absorbance of cladding

materials is also an important factor affecting light guiding properties of waveguides. The absorbance of Pluronic F127 and Pluronic-DA solutions and their physical and covalent hydrogels was measured by UV-Vis spectrometer. For both Pluronic F127 and Pluronic-DA solutions, the temperature induced phase transition didn't change the transparency (**Figure 2A**). However, the absorbance of Pluronic-DA solutions and their physical hydrogels increased sharply in the range of 350-380 nm, which is attributed to the absorbance of acrylate groups. Furthermore, the absorbance of covalently crosslinked Pluronic-DA hydrogels was further increased, which was caused by the formation of hydrophobic network after the polymerization of acrylate groups. The hydrophobic network can induce phase separation in a hydrophilic environment and then cause increasing absorbance. The absorbance of Pluronic-DA hydrogels at different concentrations after photopolymerization was also characterized. All Pluronic-DA hydrogels exhibited good transparency above 450 nm, but strongly absorbed light at shorter wavelengths (**Figure 2B**). No significant differences in absorbance values were observed with the polymer concentration in the hydrogel.

The scattering properties of crosslinked Pluronic-DA hydrogels and cured PDMS were also measured using a home-made setup (**Scheme 1** in chapter 2). A decrease in scattering intensity was observed with increasing polymer concentration in the Pluronic-DA hydrogels (**Figure 2C**). Inhomogeneity and phase separation in the hydrogel can induce light scattering^[23] and this tends to decrease with decreasing water content and increasing molecular weight of the polymer networks.^[23b] For PDMS, the scattering values are relative higher than that of Pluronic-DA hydrogels and T-DPMS demonstrates higher scattering intensity than UV-PDMS (**Figure 2C**). Scattering in elastomers is typically originated by compositional fluctuations or inhomogeneity in the crosslinked network.

The difference of refractive indices (RI) between core and cladding materials is a key parameter for the optical properties of waveguides. For total internal reflection the light guiding material should have a higher RI than the surrounding cladding material. The RI of Pluronic-DA hydrogels was measured between 1.363 and 1.377 for the concentration of 30 - 50 wt/v%, which are lower than that of T-PDMS (1.414) and UV-PDMS (1.410) (**Figure 2D**). The difference of RI is ideal for fabricating step-index optical waveguides with Pluronic-DA cladding and PDMS core.

Considering the close optical properties among different concentrations of Pluronic-DA hydrogels (**Figure 2B, 2C and 2D**), and the stronger mechanical properties and lower swelling ratios with higher concentrations (**Table A2** in Appendix), 50 wt/v% of Pluronic-DA hydrogel was selected as cladding material for fabricating core/cladding waveguides in later study.

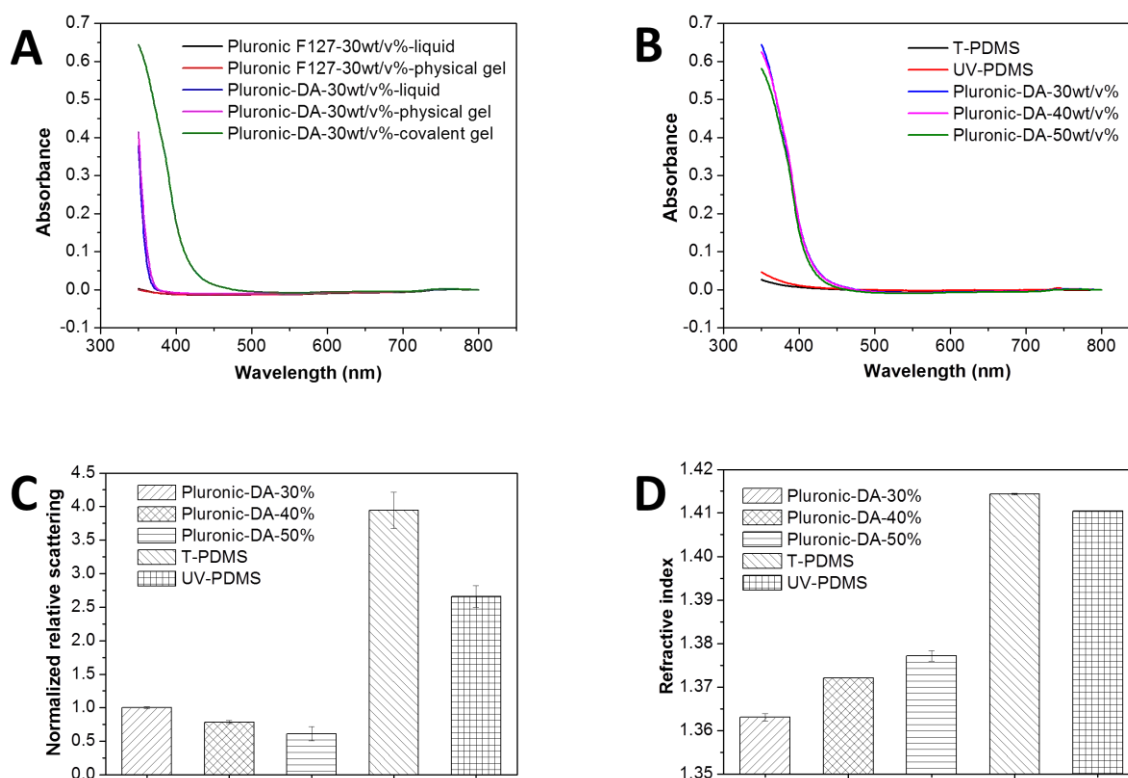


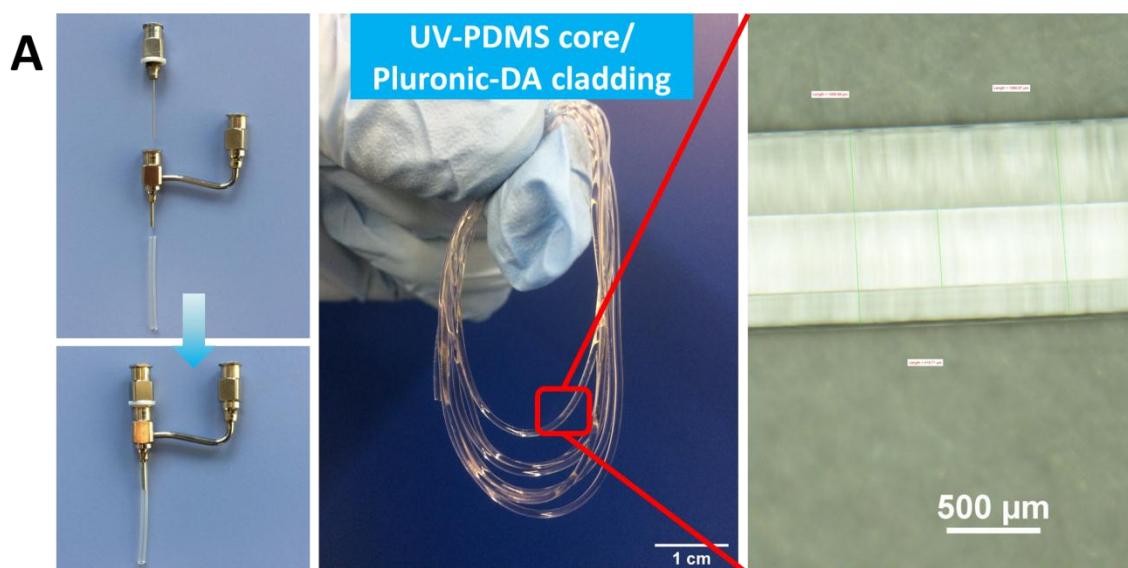
Figure 2. (A) Absorbance spectra of Pluronic F127 and Pluronic-DA solutions and their physical and covalent hydrogels. (B) Absorbance spectra of cured PDMS and

covalently crosslinked Pluronic-DA hydrogels at different concentrations. (C) Relative scattering intensity of cured PDMS and covalently crosslinked Pluronic-DA hydrogels at different concentrations. (D) Refractive index of cured PDMS and covalently crosslinked Pluronic-DA hydrogels at different concentrations.

4.3.3 Printing optical waveguides

A commercial printer equipped with an extrusion head coupled to a coaxial extrusion needle (**Figure 3A**: left) were used for printing the core/cladding fibers. A silicone tube extension was connected to the needle and a LED lamp was focused to the tube for in-situ photocrosslinking the materials inside the tube.^[24] 50 wt/v% Pluronic-DA solution, with a transition temperature of 6.2-9.6 °C, was used as ink for the cladding, and also as supporting material to allow confining the PDMS in the core. The printing process was done with surrounding temperature at 18 °C. At this temperature 50 wt/v% Pluronic-DA is a physical crosslinked gel, and it can be easily extruded based on shear-thinning property. Pluronic and PDMS are not miscible and the liquid PDMS remained within the Pluronic-DA cladding without leakage. In order to stabilize the PDMS/Pluronic-DA fiber, UV exposure passing through the silicone tube connected to the needle was performed. UV exposure initiates the radical polymerization of the Pluronic-DA cladding. When UV-PDMS was used for the core, the illumination step also initiated crosslinking of the PDMS resin, and most probably covalent linking at the interface between the two polymers via acrylate groups. An additional post-printing exposure step was needed for fully crosslinking the UV-PDMS core. In the case of T-PDMS the UV exposure step can only induce crosslinking and curing on the cladding Pluronic-DA layer and the T-PDMS core remained liquid after printing. A post-printing step with additional UV exposure and heating at 37°C for 48 hours was performed.

By adjusting the printing conditions, fibers > 50 cm in length with 1.02 mm outer diameter and 100-500 μm core diameters were continuously printed (**Figure 3A**: middle). The printed fibers are flexible, and demonstrate smooth surface and high transparency. From the microscopy image of printed fiber (**Figure 3A**: right), the core/cladding structure can be easily observed and the clear interface between core and cladding proves the low miscibility of these two materials. The inner size of the silicone tube, the printing pressure on the core and cladding inks, and the UV intensity determined the diameter of the printed waveguides. The inner size of the silicone tube decided the outer diameter of printed fibers because the cladding layer was covalently crosslinked by in-situ photopolymerization of Pluronic-DA solution. The diameter of the core was determined collaboratively by pressure on the core and cladding and the intensity of UV source. The core size increased with the pressure applied to the core solution, and decreased with increasing pressure applied to the cladding solution and with the intensity of the UV source applied to the silicone tube (**Figure 3B, 3C and 3D**).



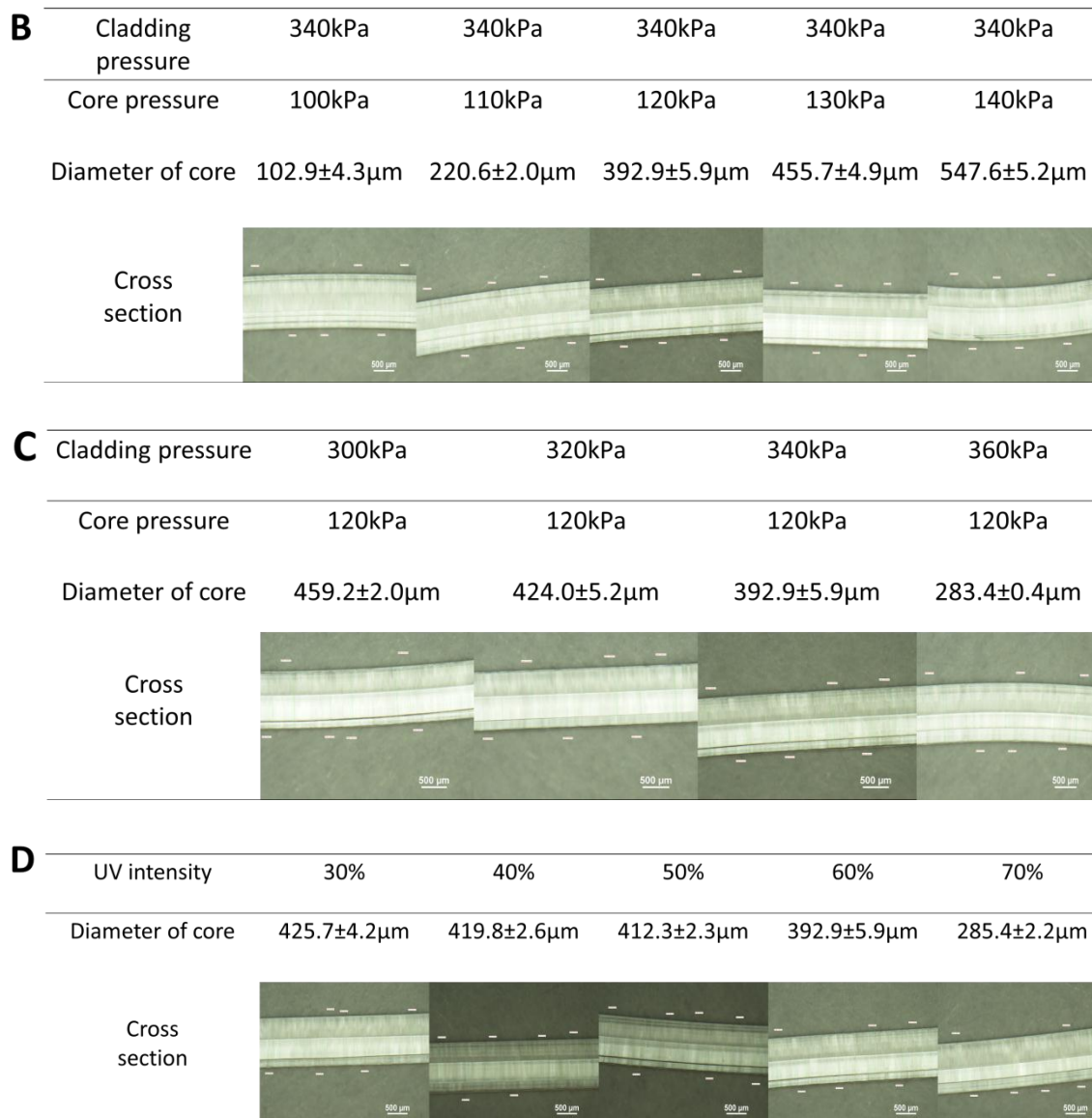


Figure 3. (A) left: Image of the coaxial needle used to print the fibers, and its extension with the silicone tube, middle: Printed flexible optical waveguides, right: Microcopy picture of printed fiber showing the clear core/cladding structure. (B) The effect of printing pressure on the UV-PDMS ink on the diameter of the core. (C) The effect of printing pressure on the Pluronic-DA ink on the diameter of the core (with UV-PDMS core). (D) The effect of UV exposure intensity on the core diameter.

4.3.4 Optical and mechanical properties of the optical waveguides

A home-made setup was used to quantify the optical loss of the printed waveguides (**Scheme 2** in chapter 2). The optical loss, $\alpha(\lambda)$, is defined by: $\alpha(\lambda)=(10/L)*\log(I_0/I_L)$, where L is the distance between two positions in the fiber with unit of cm, I_0 stands for the intensity of the light at any initial position and I_L stands for the intensity of the light after it propagates the distance L. The auto-fluorescence was used as a measure of the light intensity through the waveguide. The optical loss of UV-PDMS and T-PDMS based waveguides in air varied between 1.1 and $<0.1 \text{ dBcm}^{-1}$ in the range of 405-520 nm and was lower at longer wavelengths (**Figure 4B** and **Figure A8** in Appendix). Waveguides with UV-PDMS cores exhibit much lower optical loss than that in T-PDMS based waveguides (**Figure 4B**), which might be due to a smoother interface between the core and the cladding where the covalent crosslinking of the two polymers by the acrylate groups may occur.

In tissue, the light guiding properties of UV-PDMS core waveguides did not vary significantly (**Figure 4C** and **4E**), indicating that total internal reflection is achieved at the core/cladding interface, and the change in the external medium does not affect too much on light propagation through the core. With these parameters, the values of the penetration depth of light in UV-PDMS based core/cladding waveguides, defined as the distance at which the intensity of light decreases to $1/e$, range from 13 to 36 cm with light of wavelengths between 405 and 520 nm (**Figure 4D**). Due to that longer wavelength cannot activate the auto-fluorescence, the propagation of longer wavelengths (670 and 808 nm) was checked visually (**Figure 4E**). Longer wavelengths can propagate in printed waveguides between tissues for a longer distance. These numbers demonstrate the suitability of the printed waveguides to deliver light deep into tissues, even at short wavelengths (i.e. 405nm).

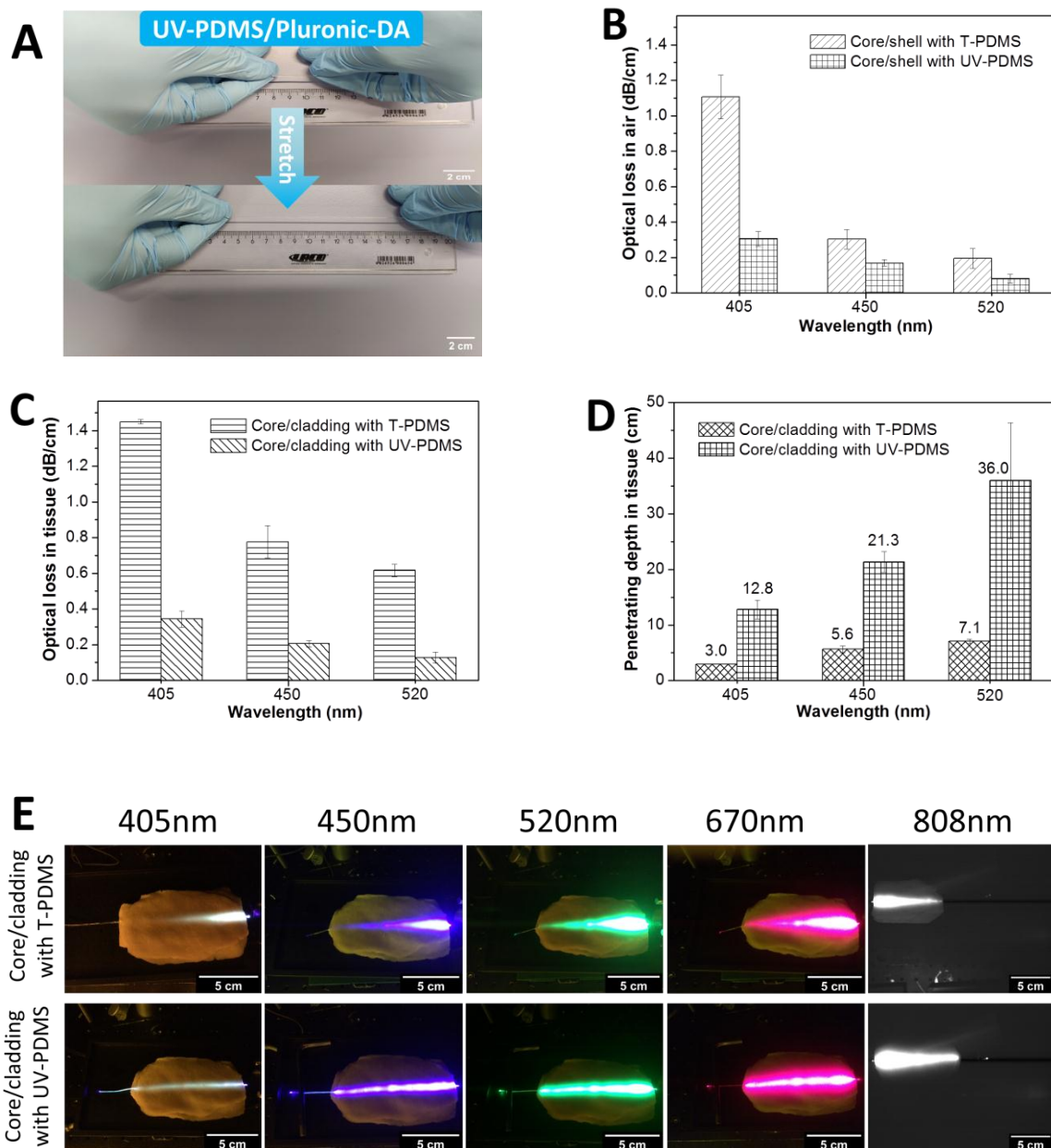


Figure 4. (A) Stretching of printed waveguides (core: UV-PDMS, cladding: 50 wt/v% Pluronic-DA). (B) Optical loss of T- or UV-PDMS/Pluronic-DA (50 wt/v%) core/cladding waveguides in air. (C) Optical loss of T- or UV-PDMS/Pluronic core/cladding waveguides in tissue. (D) Penetration depth of light guided by a UV-PDMS/Pluronic-DA (50 wt/v%) core/cladding waveguide. (E) Images of lightened T- or UV-PDMS/Pluronic core/cladding waveguides sandwiched between two pieces of 10 cm tissue, scale bar: 5cm.

The stretchability of the printed waveguides was checked manually. The printed waveguides (with UV-PDMS core) were stretched to 4 times of their original length (**Figure 4A**). The elastomeric nature of the PDMS and Pluronic-DA make this possible. The covalent crosslinkings in the Pluronic cladding, along with the physical interactions in the micellar structure, provide elasticity and toughness to the material.^[21]

4.3.5 Photoactivation of biological processes in vitro with printed waveguides

The ability of UV-PDMS/Pluronic-DA (50 wt/v%) to deliver light through tissue at sufficient intensity to activate photochemical reactions was tested in the same scenario as in chapter 2. A 10 cm long core/cladding waveguide was sandwiched between two 8 cm long pieces of porcine muscle tissue. A laser beam (405 nm) was focused at the proximal end of the waveguide, and light propagated through the waveguide to the distal end after passing through the tissue (**Figure 5A**). The light at the distal end of fiber was used to illuminate a 3D cell cultures, and to trigger cellular responses based on photoactivation of biological active molecules contained in the culture.

This experiment was performed in collaboration with Dr Yijun Zheng. The 3D culture was irradiated at 405 nm for 30 minutes delivered by the core/cladding waveguide (**Figure 5A**), and then cultured for two days to allow cells detecting the adhesive ligands and migration. Exposed cell cultures through the waveguide showed migration of the fibroblasts outside of the spheroids and penetrate the surrounding hydrogel, while in the non-exposed cultures fibroblasts remained confined in the spheroids (**Figure 5B**). These results clearly indicate that the delivered light by the waveguides was sufficient to photo-cleave DMNPB groups across 8 cm tissue and remotely control the behavior of embedded cells.

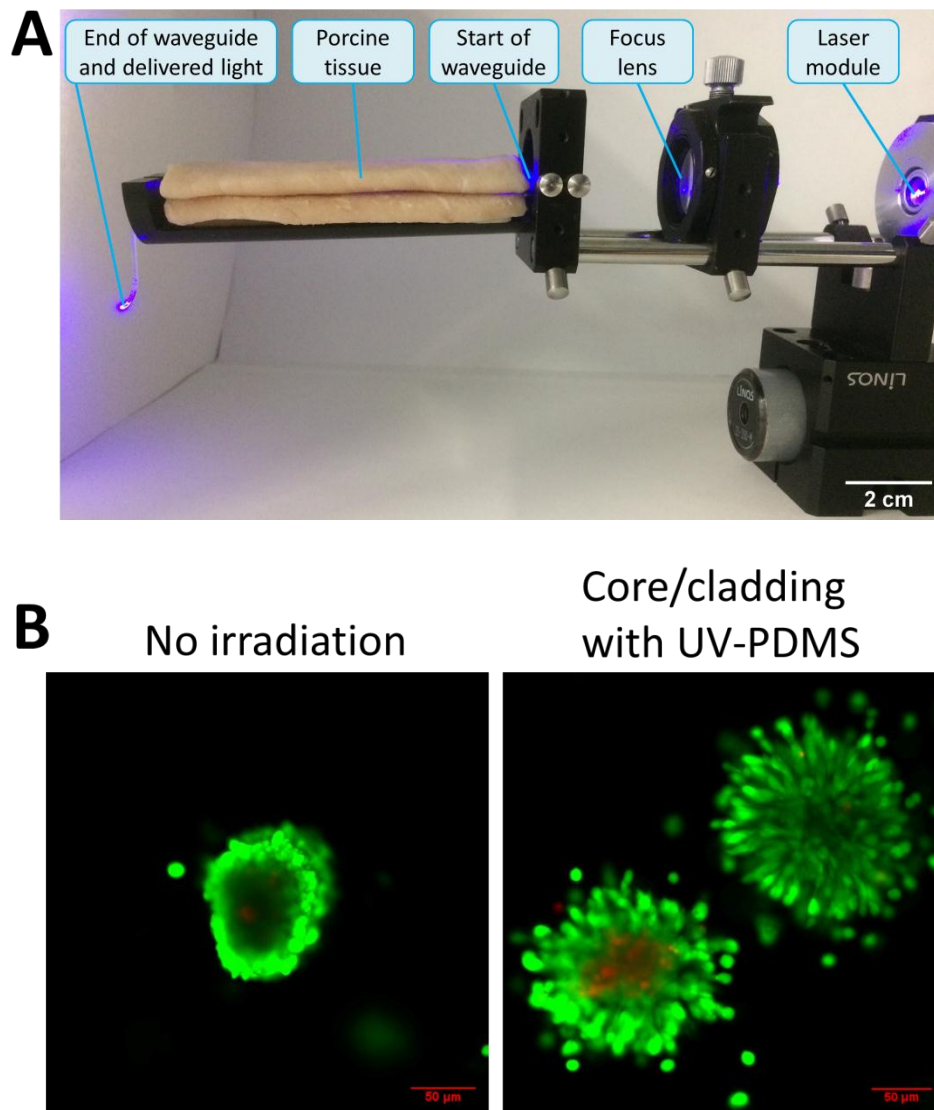


Figure 5. (A) Experimental design for illumination of 3D culture with printed waveguides after passing through the tissue. (B) Live/dead staining of fibroblast spheroids inside Dex-MA hydrogel modified with the photoactivatable cell adhesive peptide cyclo[RGD(DMNPB)fC] after two days culture. The cell culture on the left was not illuminated; the gel on the right was illuminated for 30 min at 405 nm using a UV-PDMS/Pluronic waveguide to activate the RGD units that support invasion of the gel by the fibroblasts.

4.4 Conclusion

PDMS has been widely applied in optic/electronic devices, medical equipment and biological research based on its elasticity, biocompatibility, nontoxicity and durability. Besides, the high transparency allows it to be used to fabricate optical waveguides. In this chapter, PDMS was used as core material to develop core/cladding waveguides with Pluronic-DA as cladding. The waveguides were fabricated through extrusion based printing by taking the advantage of the shear-thinning property of semi-solid Pluronic-DA physical hydrogels. The slowly curing process of PDMS makes it difficult to directly fabricate waveguides through printing technology, which can be overcome by using supporting materials. In present work, reversible Pluronic-DA hydrogel was employed as both supporting material preventing leakage of liquid PDMS during printing and cladding layer after being photocrosslinked to achieve total internal reflection. Comparing to reported mold-casting methods to fabricate PDMS waveguides, the present co-extrusion printing avoids the multisteps in the process and allows easy tuning the dimension of waveguides by simply changing the pressure of core and cladding. Furthermore, the employment of reversible Pluronic or Pluronic-DA as supporting material provides an effective approach to directly print low viscos or slow curing materials no matter for fabricating single material fiber or multimaterials based complicated devices.

The elasticity of PDMS and the toughness of covalently crosslinked Pluronic-DA hydrogel endow printed waveguides good stretchability that allows it to be stretched to 4 times of its original length, which allows the application in wearable or implantable devices for moving tissue or organs. Most importantly, the printed waveguides, especially UV-PDMS based waveguides exhibit excellent light guiding properties no matter in air or in tissue. The optical loss of UV-PDMS based waveguides was measured to be the lowest value in reported PDMS based

waveguides to date.^[23b] The further application of UV-PDMS based core/cladding waveguides in delivering near-UV light (405 nm) to remotely trigger cells migration demonstrates the efficacy of delivered light across tissue (≥ 8 cm). The presented work opens the door to easily integrating of optical components from medically approved polymers into possible medical devices by printing technologies. In the future with more developed printing technologies, fabricating complicated and multifunctional medical devices will be possible.

It is noteworthy that the hydrogel based cladding can absorb water from surrounding tissue when implanted, which can cause swelling in cladding layer. The different swelling ratios in core and cladding can induce bending structures along the fiber and causing higher optical loss. To avoid this, choosing proper concentration of Pluronic-DA or pre-implantation in the tissue to equilibrate water content of waveguides could be effective options.

References

- [1] a) A. Victor, J. Ribeiro, F. F. Araújo, *Journal of Mechanical Engineering and Biomechanics* 2019, 4, 1; b) A. Subramaniam, S. Sethuraman, in *Natural and synthetic biomedical polymers*, Elsevier 2014, p. 301.
- [2] J. Kuncova-Kallio, P. J. Kallio, presented at 2006 International Conference of the IEEE Engineering in Medicine and Biology Society 2006.
- [3] T. J. Keane, S. F. Badylak, presented at Seminars in Pediatric Surgery 2014.
- [4] M. Owen, *Chimie nouvelle* 2004, 27.
- [5] H. Chen, M. A. Brook, H. Sheardown, *Biomaterials* 2004, 25, 2273.
- [6] E. Zamir, M. Katz, Y. Posen, N. Erez, K. M. Yamada, B.-Z. Katz, S. Lin, D. C. Lin, A. Bershadsky, Z. Kam, *Nature cell biology* 2000, 2, 191.
- [7] a) K. Raj M, S. Chakraborty, *Journal of Applied Polymer Science* 48958; b) X. Q. Brown, K. Ookawa, J. Y. Wong, *Biomaterials* 2005, 26, 3123; c) C. Chen, J. Wang, Z. Chen, *Langmuir* 2004, 20, 10186.
- [8] a) L. Wang, B. Sun, K. S. Ziemer, G. A. Barabino, R. L. Carrier, *Journal of Biomedical Materials Research Part A: An Official Journal of The Society for Biomaterials, The Japanese Society for Biomaterials, and The Australian Society for Biomaterials and the Korean Society for Biomaterials* 2010, 93, 1260; b) B. Li, J. Chen, J. H. C. Wang, *Journal of Biomedical Materials Research Part A* 2006, 79, 989.

-
- [9] a) V. Lien, Y. Berdichevsky, Y.-H. Lo, *IEEE Photonics Technology Letters* 2004, 16, 1525; b) D. Psaltis, S. R. Quake, C. Yang, *Nature* 2006, 442, 381.
- [10] S. Kopetz, D. Cai, E. Rabe, A. Neyer, *AEU-International Journal of Electronics and Communications* 2007, 61, 163.
- [11] Y. Xia, E. Kim, X.-M. Zhao, J. A. Rogers, M. Prentiss, G. M. Whitesides, *Science* 1996, 273, 347.
- [12] a) L. Pang, U. Levy, K. Campbell, A. Groisman, Y. Fainman, *Optics express* 2005, 13, 9003; b) D.-Y. Zhang, N. Justis, Y.-H. Lo, *Applied Physics Letters* 2004, 84, 4194.
- [13] Y. Gambin, O. Legrand, S. R. Quake, *Applied Physics Letters* 2006, 88, 174102.
- [14] J. Missinne, S. Kalathimekkad, B. Van Hoe, E. Bosman, J. Vanfleteren, G. Van Steenberge, *Optics express* 2014, 22, 4168.
- [15] a) J. Missinne, G. Van Steenberge, B. Van Hoe, K. Van Coillie, T. Van Gijsegem, P. Dubruel, J. Vanfleteren, P. Van Daele, presented at Photonics Packaging, Integration, and Interconnects IX 2009; b) C. K. Harnett, H. Zhao, R. F. Shepherd, *Advanced Materials Technologies* 2017, 2, 1700087; c) A. Ersen, M. Sahin, *Journal of biomedical optics* 2017, 22, 055005.
- [16] a) M. Ramuz, B. C. K. Tee, J. B. H. Tok, Z. Bao, *Advanced Materials* 2012, 24, 3223; b) C. To, T. L. Hellebrekers, Y.-L. Park, presented at 2015 IEEE/RSJ International Conference on Intelligent Robots and Systems (IROS) 2015; c) S. J. Kwok, M. Kim, H. H. Lin, T. G. Seiler, E. Beck, P. Shao, I. E. Kochevar, T. Seiler, S.-H. Yun, *Investigative ophthalmology & visual science* 2017, 58, 2596; d) S. J. Kwok, S. Forward, C. M. Wertheimer, A. C. Liapis, H. H. Lin, M. Kim, T. G. Seiler, R. Birngruber, I. E. Kochevar, T. Seiler, *Investigative ophthalmology & visual science* 2019, 60, 2563; e) J. Guo, M. Niu, C. Yang, *Optica* 2017, 4, 1285; f) J. Guo, B. Zhou, C. Yang, Q. Dai, L. Kong, *Advanced Functional Materials* 2019, 1902898; g) M. Kolle, A. Lethbridge, M. Kreysing, J. J. Baumberg, J. Aizenberg, P. Vukusic, *Advanced Materials* 2013, 25, 2239; h) I. Martincek, D. Pudis, P. Gaso, *IEEE Photonics Technology Letters* 2013, 25, 2066; i) A. Samusjew, M. Kratzer, A. Moser, C. Teichert, K. Krawczyk, T. Griesser, *ACS Applied Materials & Interfaces* 2017, 9, 4941.
- [17] Z. Cai, W. Qiu, G. Shao, W. Wang, *Sensors and Actuators A: Physical* 2013, 204, 44.
- [18] X. Liu, H. Yuk, S. Lin, G. A. Parada, T. C. Tang, E. Tham, C. de la Fuente-Nunez, T. K. Lu, X. Zhao, *Advanced Materials* 2018, 30, 1704821.
- [19] M. R. Kim, T. G. Park, *Journal of Controlled Release* 2002, 80, 69.
- [20] J. Suksiriworapong, T. Rungvimolsin, A. Atitaya, V. B. Junyaprasert, D. Chantasart, *Aaps PharmScitech* 2014, 15, 52.
-

- [21] J. J. Escobar-Chávez, M. López-Cervantes, A. Naik, Y. Kalia, D. Quintanar-Guerrero, A. Ganem-Quintanar, *Journal of Pharmacy & Pharmaceutical Sciences* **2006**, *9*, 339.
- [22] F. De Fornel, *Evanescent waves: from Newtonian optics to atomic optics*, Springer Science & Business Media, **2001**.
- [23] a) Y.-H. Wu, H. B. Park, T. Kai, B. D. Freeman, D. S. Kalika, *Journal of Membrane Science* **2010**, *347*, 197; b) S. Shabahang, S. Kim, S. H. Yun, *Advanced Functional Materials* **2018**, *28*, 1706635; c) R. J. Williams, B. A. Rozenberg, J.-P. Pascault, in *Polymer analysis polymer physics*, Springer **1997**, p. 95.
- [24] L. Ouyang, C. B. Highley, W. Sun, J. A. Burdick, *Advanced Materials* **2017**, *29*, 1604983.

5. Conclusion and Outlook

In this PhD thesis, soft optical waveguides made from different biocompatible materials were designed and fabricated via extrusion based printing. Hydrogels (PEGDA), thermoplastics (PLA and copolymers) and or elastomeric (PDMS) materials were used for this purpose. Single-fiber and core-cladding designs were printed as continuous fibers under mild processing conditions. The printed waveguides are based on medically approved materials and exhibit stiffnesses comparable to nature tissues. Therefore, good cyto- and tissue compatibility is expected for their potential application inside the body. In proof-of-concept experiments, the obtained optical waveguides demonstrated light guidance through 5-8 cm of porcine muscle to activate exemplary photochemical reactions used in biomaterials for cell encapsulation.

The major conclusions of this work are the following:

- 1) PEGDA can be easily modified with DTT to generate PEGDA-DTT precursors which can be continuously processed into soft optical fibers by extrusion printing using an in-situ photocuring step. This fabrication process is more straightforward and scalable than photocuring inside transparent molds currently used in literature. The hydrogel fibers are cytocompatible and present adjustable degradability and mechanical properties.
- 2) The introduction of DTT units in the PEG backbone increases the molecular weight and decreases the structural order of the hydrogel precursors, which in turn decreases light scattering in resulting hydrogels. The obtained PEGDA-DTT hydrogels also demonstrate higher refractive indices than that of pure PEGDA hydrogels, which can enhance light confinement. The

improved optical properties endow these printed waveguides much more competitive light guiding properties than those reported for pure PEGDA waveguides obtained by mold casting. The successful activation of photochemical processes proves that the printed waveguides can deliver sufficient light through tissue to realize remote control by light.

- 3) Hydrogel-based PEGDA-DTT waveguides undergo unavoidable swelling when surrounded by soft tissue. This reduces the polymer concentration and lowers the mechanical properties (e.g. Young's modulus), both of which can result in higher optical loss. Choosing proper concentration of polymer, proper ratio of DTT to PEGDA for specific tissue and purpose is very important to overcome this limitation.
- 4) Amorphous PLA copolymers are appropriate materials for processing into fibers by extrusion printing at low temperature, giving soft fibers at body temperature. These materials are commercially available medical polymers (Resomer®). Among the selected thermoplastics, PLA and PLA-co-PCL copolymer are the most appropriate materials for light guiding, demonstrating lowest optical loss in visible range versus previously reported thermoplastic waveguides. The flexibility of these waveguides at body temperature enables light guiding along curved paths without breaking, which could allow their application in high movement in vivo scenarios.
- 5) The low T_g of selected PLA and copolymers is beneficial for flexibility, but also brings the disadvantage of printed waveguides turning opaque when surrounded by high humidity and temperature (> T_g). The weak interaction between polymer chains allows water absorption and the formation of water-rich phases. To solve this, highly hydrophobic cladding (e.g. PDMS) could be considered to avoid direct contact between water and the core material.

- 6) Stretchable UV-PDMS/Pluronic-DA core/cladding fibers can be fabricated via coaxial extrusion-based printing. Physical crosslinking of the Pluronic-DA cladding temporarily maintains the shape of the extruded liquid PDMS core, and then photopolymerization stabilizes both the printed materials and their interface. The elasticity of PDMS and toughness of Pluronic-DA hydrogel allow stretchability of the printed fibers up to 4 times their original length. The printed UV-PDMS/Pluronic-DA waveguides exhibit better light guiding properties comparing to reported PDMS waveguides in both air and tissue.
- 7) The hydrogel cladding absorbs water from surrounding tissue which can cause micro- and/or macro-bending along UV-PDMS/Pluronic-DA fibers, increasing optical losses. A pretreatment of the fabricated fibers to equilibrate the water content to that of the surrounding tissue before implantation could perhaps alleviate this issue.
- 8) 3D printing is a simple, scalable, and versatile technique for producing flexible optical waveguides more conveniently than current literature reports. The excellent optical and mechanical performance of the obtained waveguides exemplify how medically approved biomaterials can be rationally selected to produce cost-effective and flexible optical components for light delivery in medical contexts.

6. Appendix

This section includes the materials, experimental methods and some supporting results for chapter 2, 3 and 4.

6.1 Appendix of Chapter 2

6.1.1 Materials and Methods

Synthesis of PEGDA-DTT

The method of preparing PEGDA-DTTs was adapted from previous report^[1] with some modification (**Figure 1A** in chapter 2). Briefly, a certain amount of DTT (Sigma Aldrich) was dissolved in Milli-Q water (100 mL) in a flask, which was followed by adding PEGDA ($M_n=700$, Sigma Aldrich) (16mmol) inside. After being fully dissolved, triethylamine (Sigma Aldrich) (100 μ L) was drop-wise added into the solution to catalyze the reaction. The mixture was stirred with a magnetic apparatus for 3 hours at room temperature to make sure DTT was fully consumed. After reaction, the solution was filtered and PEGDA-DTTs were obtained by freeze drying the filtrate.

Characterization of the reaction between DTT and PEGDA

A reaction between DTT and PEGDA was set at a feed molar ratio of 0.9375:1 to check the amount of free thiol. 50 μ l of mix solution was taken at time points: 0, 1, 5, 10, 20, 30, 40, 50 and 60 min. The amount of free thiol groups in solution with time was determined by using Fluorometric Thiol Assay Kit (Sigma Aldrich). The proprietary thiol detecting reagent can generate a fluorescent adduct upon reacting with free thiol. The fluorescence intensity for each sample was measured

by fluorescence spectrophotometer (UB Uwe Binniger Analytik) with 490nm for excitation and 520nm for emission and related to free thiol concentration through a standard curve relating fluorescence intensity to known thiol concentrations.

The remaining acrylate groups of final product were characterized by $^1\text{H-NMR}$. The integral of the signal corresponding to the PEG backbone (3.75–3.50 ppm) was set to 52H (corresponding to M_n of 700Da) and the integral of acrylate groups (6.50– 5.90 ppm) was accordingly obtained. The amount of remaining acrylate groups can be obtained by comparing the integral of the acrylate groups in PEGDA-DTT with that of the PEGDA precursor.

The product was further characterized by checking the number-averaged molecular weight by Gel permeation chromatography (GPC).

Synthesis of Pluronic-DA

Pluronic-DA was synthesized by following previous method.^[2] Pluronic F127 (Sigma Aldrich) (20 g) and of triethylamine (0.55mL) were dissolved in dry dichloromethane (200 mL). Then acryloyl chloride (Sigma Aldrich) (250 μL) was drop-wise added inside. The mixture was stirred on the ice for 12h and then in air (room temperature) for 12h. After reaction, the mixture was filtered and condensed to around 30 ml by rotary evaporation (37°C, 200mbar, BÜCHI Labortechnik AG). The crude product was purified by precipitation in diethylether (500 mL) and dried under vacuum for 2 days. The product was confirmed by $^1\text{H-NMR}$.

Characterization of PEGDA-DTT hydrogel

Light absorption

PEGDA-DTT hydrogels were prepared in standard 1-cm-wide poly(methyl methacrylate) disposable cuvettes by photo-polymerization. The hydrogel precursor contained a specified concentration of PEGDA-DTT (between 5 wt% and 70 wt%) in water and 0.1 wt/v% of Irgacure 2959 (Sigma Aldrich) as initiator. The precursors were injected into the cuvettes and irradiated by a 1mW 365nm UV

lamp (LTF-Labortechnik) for 15min. Light absorbance was measured by using a UV-Vis spectrophotometer (Agilent Technologies).

Refractive index

Hydrogel samples for refractive index measurement were prepared in a Teflon mold with diameter of 5mm and depth of 2mm. The hydrogel precursor contains a certain concentration of PEGDA-DTT and 0.1% wt/v of Irgacure 2959 as initiator. 40 μ l of precursor was injected in the mold and covered by a coverslip. The samples were illuminated by a 1mW 365nm UV lamp for 15min. The refractive indices of hydrogels were measured on a refractometer (Anton Paar).

Relative scattering

Samples were prepared in a cuvette, in the same way as for light absorption measurements. The scattering was measured by a home-made setup as shown in **scheme 1** in chapter 2. A 520nm laser beam was focused to pass through the hydrogel (CrystaLaser). A camera (Thorlabs) was set in the vertical direction to take picture of the scattered light. The laser power (500mW) and exposure time (5ms) of the camera were fixed for all gels. The intensity of scattering light in the picture was quantified by free software ImageJ and normalized by the scattering of PEGDA to get the relative scattering for PEGDA-DTT hydrogels with the different DTT ratios.

Swelling ratio

PEGDA-DTT hydrogels with different ratio of DTT to PEGDA were fabricated by UV-induced photo-polymerization (Irgacure 2959: 0.2 wt/v%) at the same concentration (70wt%) in Teflon mold (diameter: 5mm) covered by glass slides. The fabricated hydrogels were immersed in water for 24h and weighed to obtain swollen mass of hydrogels (W_s). Then the same networks were freeze dried to get dry mass (W_d). Swelling ratio was calculated through equation S1, in which SR stands for swelling ratio, W_s for the weight of swollen hydrogel, W_d for the weight of dry polymer.

$$SR\% = \frac{W_s - W_d}{W_d} \times 100 \quad (\text{equation S1})$$

For the swelling ratios of printed waveguides in tissue, the printed fibers were measured to get hydrogel mass (W_1), and then sandwiched between two pieces of porcine muscle for 1h. The swollen hydrogels were measured to get W_2 . The swelling ratios (SRs%) of printed waveguides were calculated by following the equation S2.

$$SRs\% = \frac{W_2 - W_1}{W_1} \times 100 \quad (\text{equation S2})$$

Degradation of PEGDA-DTT hydrogel

Degradation of PEGDA-DTT hydrogels prepared by UV-induced photopolymerization (Irgacure 2959: 0.2wt/v%) at the same concentration (70 wt%) containing various amounts of DTT bridges was characterized by weighting the dry mass of hydrogels after incubation in aqueous buffer (PBS). Dry mass of hydrogels after 0, 7, 14, 28, 35, 42, 49 and 56 days of incubation in PBS at 37°C were measured. Before weighting, samples were incubated in Milli-Q water to remove buffer salts and dried in a vacuum oven at 50°C for 24h.

Mechanical testing of PEGDA-DTT hydrogel

Compressive tests were performed to examine the mechanical properties of PEGDA-DTT hydrogels. The hydrogel samples at the same concentration (70 wt%) containing various amounts of DTT bridges were prepared by UV-induced photopolymerization (Irgacure 2959: 0.2 wt/v%) in Teflon molds with depth of 1.5mm. The sizes of samples were measured with a vernier caliper. The compressive tests were performed on a Dynamic Mechanical Analyzer (TA Instruments) equipped with a 225N load cell. The compression speed was set at 0.01mm s⁻¹. The applied force to the surface of the hydrogel and compressed distance were recorded, based on which the mechanical properties of the hydrogels were calculated.

Viscosity of hydrogel precursors

The viscosity of hydrogel precursors at the same concentration (50 wt%) containing various amounts of DTT bridges were measured by flow sweep on a rheometer (TA Instruments) equipped with a 20mm plate. The shear rate ranges from 2.5 s^{-1} to 100 s^{-1} .

Printing optical waveguides

The optical waveguides were fabricated on a 3D-Bioscaffolder (GESIM). The method was adapted from a reported protocol.^[3] Briefly, the prepared ink was loaded into a UV blocked syringe and mounted onto the printhead. In order to realize in-situ crosslinking, the needle used for printing was extended by inserting a certain length of light permeable silicone tubing (HELIX MEDICAL EUROPE GMBH) over the needle tip (**Figure 4A**: right, in chapter 2). The UV lamp was adjusted to illuminate the photo-permeable tubing with the desired intensity. The printing parameters, such as pressure, UV intensity, the diameter and length of silicone tubing were adjusted to get the printing windows for different inks, which contain various amounts of DTT bridges, different concentration of PEGDA-DTT or initiator. To make sure all the PEGDA-DTT monomers are reacted, additional light irradiation (365nm, 1mW, 10min) was performed on the printed fibers. After additional irradiation, the printed fibers were stored in a sealed petri dish with a wet tissue inside to control the humidity.

For the printing of core/cladding structure, a coaxial needle (**Figure 4A**: right in chapter 2. core: 21G, cladding: 17G, Leonardo) was adopted, which was extended by a silicone tubing with diameter of 1.08mm and length of 3cm. Core/cladding filaments were produced by providing pressure for both channels. It's worth noting that the order of switching on and off the pressure of channels is very important. To start printing core/cladding structure, the pressure of core should be first switched on followed by switching on the pressure of cladding. To stop printing, the pressure for core should be switched off after the pressure of cladding was stopped.

Light guiding properties of printed waveguides

The optical loss was measured with a home-made setup (shown in **scheme 2** in chapter 2). A laser (Thorlabs) was focused on one end of printed fiber. The light propagated in the fiber and activated the auto-fluorescence of the material. A camera with a filter (550nm) was set in the vertical direction to take the picture of auto-fluorescence. With the picture, the intensity of auto-fluorescence at beginning (I_0) and end (I_L) positions can be obtained by ImageJ. The optical loss of printed fibers can be calculated with equation 2. For optical loss in tissue, the fiber was sandwiched by two pieces of porcine muscle for 10min to allow the water in fibers to reach equilibrium. The intensity of auto-fluorescence of fiber before and after propagating in tissue was measured to calculate optical loss in tissue.

The determination of the intensity of delivered light in tissue

For 405 nm light, the fiber (7 cm) was sandwiched between two pieces of porcine muscle (5 cm) for 10min to allow the water in fibers to reach equilibrium. And then the laser beam (405 nm, 5 mW, Thorlabs) was focused on one end of the fiber as the incident light. At the other end, a power meter (Coherent Labmaster with LM-2 sensor) was used to detect the power of light. The intensity of delivered light at the end of fiber was calculated by dividing the power of light by the area of fiber cross-section. For 450 nm light, the fiber length was 10 cm, the tissue was 8 cm in length and the laser was 450 nm (5 mW, Thorlabs). Results are in **Table A1**.

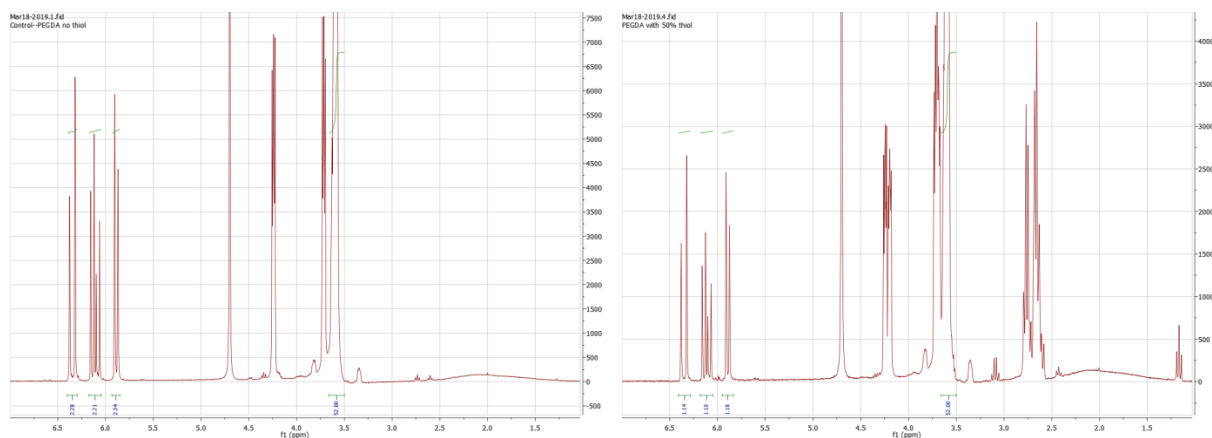
Cell migration assay

3D cultured cells spheroids were used to check the efficacy of guided light in printed waveguides through porcine muscle (**Scheme 3** in chapter 2). Fibroblast spheroids were encapsulated in DexMA hydrogel functionalized with cyclo[RGD(DMNPB)fC] (synthesized by colleague Qiyang Jiang by following

reported protocol^[4]). The encapsulation of fibroblast spheroids was done by colleague Yijun Zheng by following reported protocol.^[5]

Photoactivation of fibroblast migration with printed optical waveguides: A printed fiber (length: 7cm) was sandwiched between two pieces of porcine muscle (5cm in length) for 10min to allow the water in fibers to reach equilibrium. Then a laser (405nm, 5mW, ThorLabs) was focused on one end of the fiber. At the other end the hydrogel DexMA hydrogel containing the spheroids was placed for exposure. The delivered light is expected to photoactivate the cell adhesive peptide cyclo[RGD(DMNPB)fC] and mediate migration of the fibroblasts through the gel. Hydrogels were exposed for 15 minutes. Then cell medium was changed once and spheroids were kept in culture under the protection from light. After two days, live and dead assay was performed to visualize the cell viability and spheroid morphology.

6.1.2 Supporting results



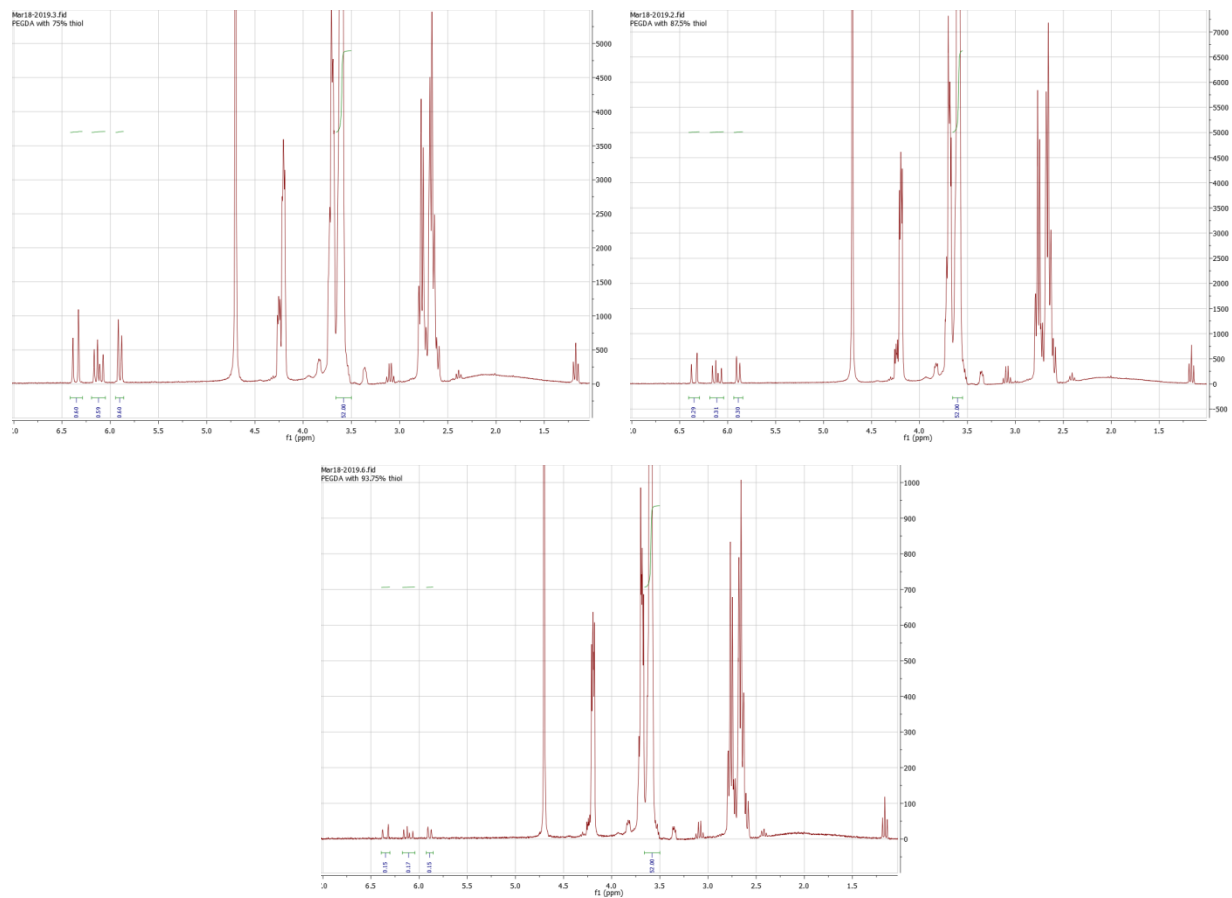


Figure A1. ^1H NMR of PEGDA-DTT with different feed ratios of DTT to PEGDA.

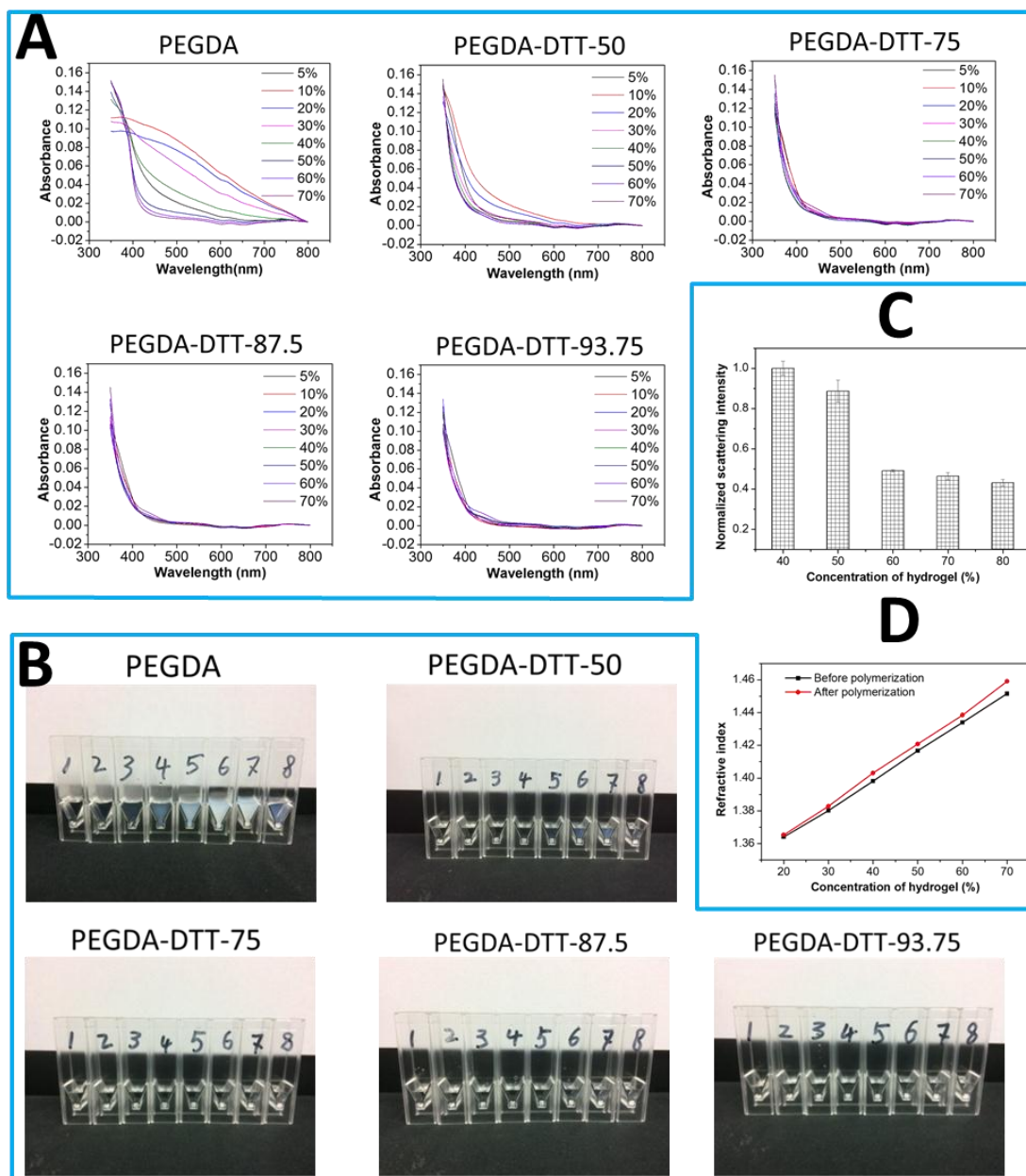


Figure A2. (A) Absorbance of PEGDA-DTT hydrogels at different concentrations; (B) Images of PEGDA-DTT hydrogels in (A). Numbers 1 to 8 stand for the polymer concentration in the hydrogels: 1-70wt%, 2-60wt%, 3-50wt%, 4-40wt%, 5-30wt%, 6-20wt%, 7-10wt%, 8-5wt%; (C) The relative scattering of PEGDA-DTT-87.5 hydrogels at different concentration; (D) The refractive index of PEGDA-DTT-93.75 hydrogels at different concentrations before and after polymerization.

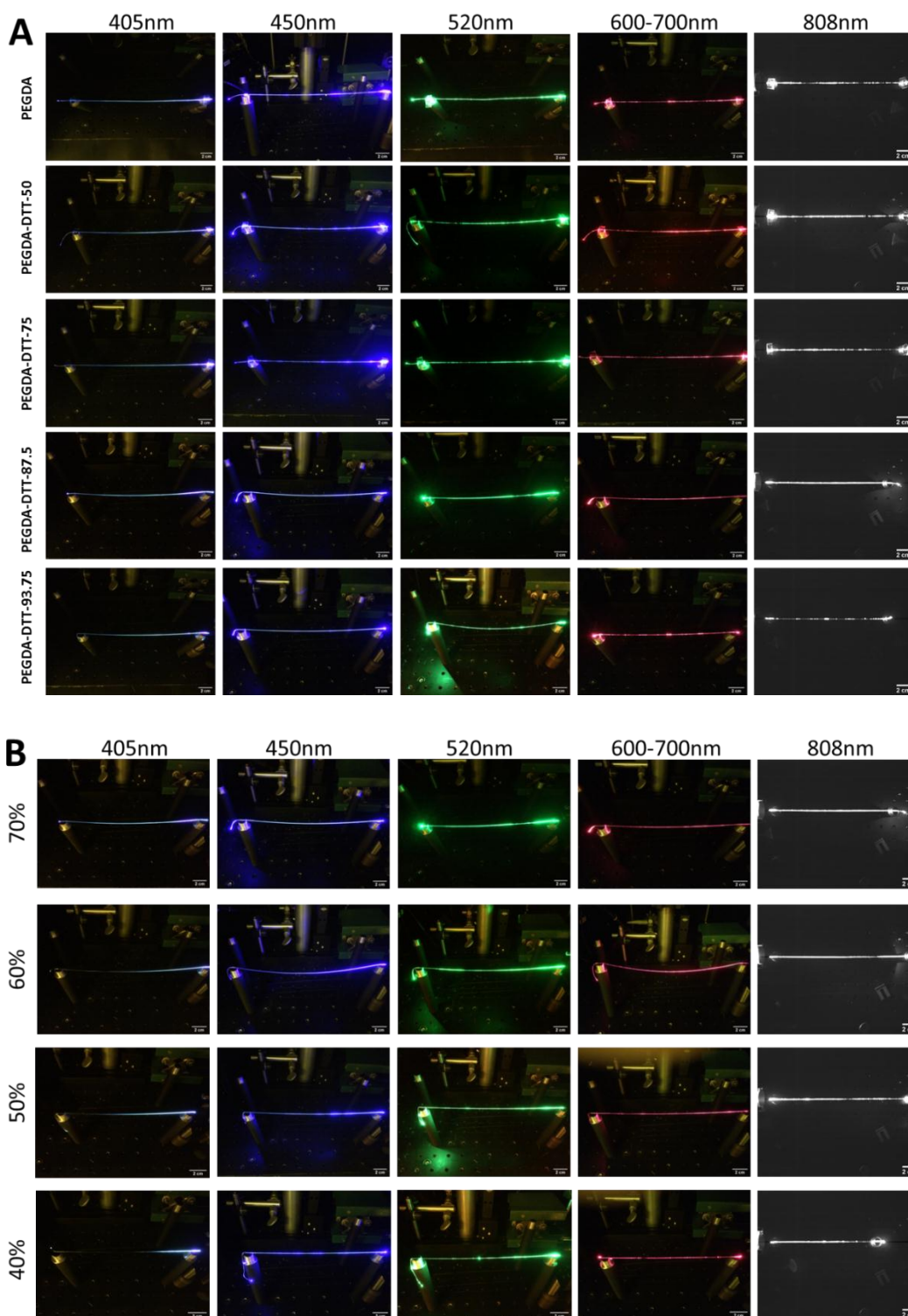


Figure A3. (A) Images of light guided through printed PEGDA-DTT waveguides in air; (B) Images of light guided through printed PEGDA-DTT-87.5 waveguides at different concentration in air.

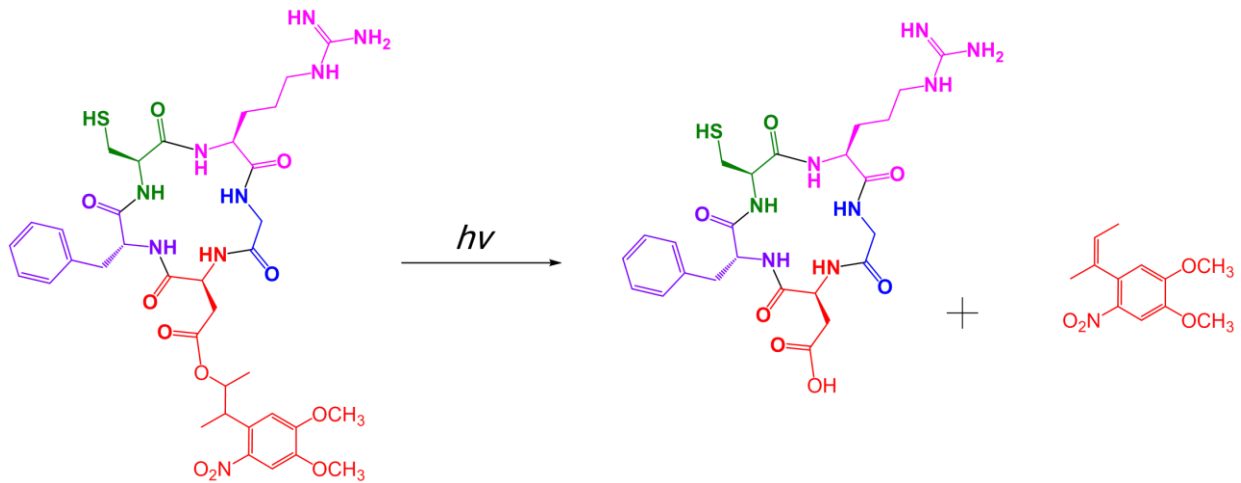
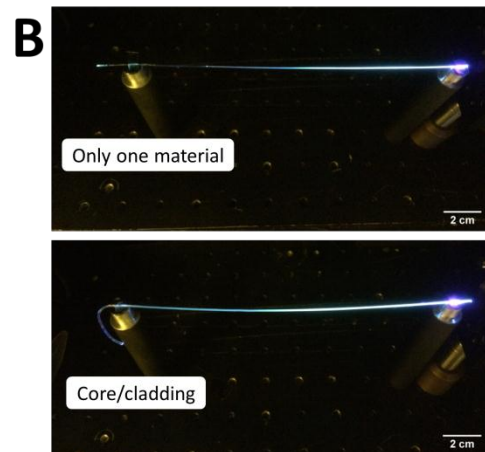
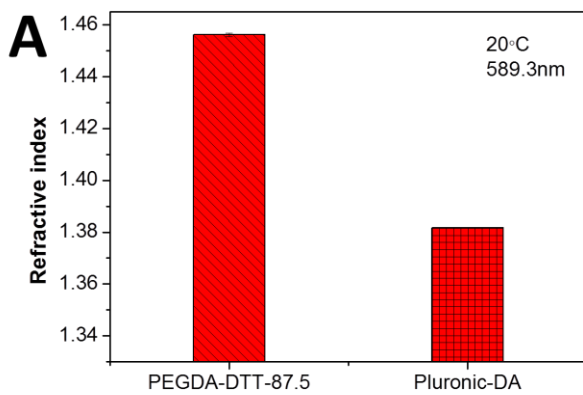


Figure A4. Chemical structure of the cyclo[RGD(DMNPB)fC] and the photolysis product after exposure.



C

Cladding pressure	500kPa	500kPa	500kPa	500kPa	500kPa
Core pressure	160kPa	170kPa	180kPa	190kPa	200kPa
Diameter of core	440.5±6.5μm	465.2±2.4μm	522.5±2.5μm	552.7±7.3μm	634.8±4.7μm
Cross section					

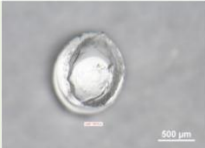
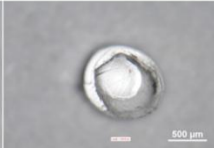
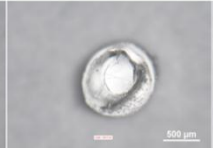
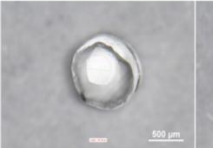
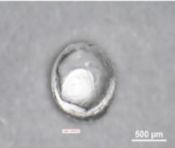
D	Cladding pressure	500kPa	510kPa	520kPa	530kPa	540kPa
	Core pressure	170kPa	170kPa	170kPa	170kPa	170kPa
	Diameter of core	465.2±2.4µm	436.8±1.1µm	390.4±3.3µm	357.1±4.1µm	339.9±3.3µm
	Cross section					

Figure A5. (A) Refractive index of 80% PEGDA-DTT-87.5 and 50 wt/v% Pluronic-DA; (B) Image of 405 nm light beam propagating through a single fiber and core/cladding waveguides in air; (C) and (D) The effect of increasing printing pressure applied to core (C) and cladding (D) solution during the printing of core/cladding waveguides.

Table A1. The intensity of delivered light at the end point of fiber sandwiched between tissues.

	PEGDA-700	PEGDA-DTT-50	PEGDA-DTT-75	PEGDA-DTT-87.5
405 nm (mW cm ⁻²) ^{a)}	32.1±3.1	42.7±3.1	48.9±4.8	9.8±1.2
450 nm (mW cm ⁻²) ^{b)}	/	192.2±7.3	/	/

a) 7 cm of fiber was sandwiched between two pieces of 5 cm porcine muscle, and the laser power is 5 mW. b) 10 cm of fiber was sandwiched between two pieces of 8 cm porcine muscle, and the laser power is 5 mW.

6.2 Appendix of Chapter 3

6.2.1 Materials and Methods

Materials

Poly(D,L-lactide) (Resomer[®] R 202 S, Mw 10,000-18,000), Poly(D,L-lactide-co-glycolide) (Resomer[®] RG 752 S, lactide:glycolide 75:25, Mw 4,000-15,000),

Poly(D,L-Lactide-co-Glycolide) (Resomer® RG 502, lactide:glycolide 50:50, Mw 7,000-17,000), Poly(D,L-lactide-co-caprolactone) (DL-lactide 86 mol %, lactide:caprolactone 85:15) were purchased from Sigma Aldrich (Germany) and used as received.

Physicochemical characterization of polymers

Absorption spectra of the polymers in the range of 350-800 nm were measured with a UV-Vis spectrophotometer (Agilent Technologies). 1cm*1cm quartz cuvettes (Hellma Analytics) were filled with 1g of polymer powder and melted in oven at 130°C under vacuum for 12 hours for the measurement.

For the measurements of the refractive index, the polymers were molded in Teflon molds with diameter of 5mm and depth of 2mm and covered by a glass slide. The refractive indices were measured on a refractometer (Anton Paar) at 20°C with 589.3nm light.

The thermal properties of the polymers were measured by Differential Scanning Calorimetry (Mettler Toledo). A heating rate from -10°C to 140°C at 10 °C min⁻¹ heating rate was used.

XRD measurements were carried out with a D8 ADVANCE (Bruker AXS). Polymer powders and printed fibers were characterized.

Printing process

A 3D-Bioscaffolder (GESIM) printer was used for printing the thermoplastic polymers via melting extrusion method. Before printing, 1g of polymer powder was loaded into 10ml stainless steel cartridge (GESIM) connected to the stainless steel dispensing nozzles (diameter 250 µm or 400 µm, GESIM) and melted in oven at 130°C under vacuum for 24 hours. This process helps to remove air bubbles from the polymer melt. After that, the filled cartridges were mounted on the printing head and connected to the pneumatic system. A heater (GESIM) controlled the temperature of the polymer melt in the printing head. Printing temperatures of 90-100 °C and printing pressures of 20-600 kPa were used.

The printed waveguides were imaged by a SMZ1270 (Nikon) optical microscope to measure the diameter of the fibers and check homogeneity. For the calculation of the extrusion speed, the length of the printed fibers within a given time and printing conditions were measured.

To check the flexibility of printed fibers at biological temperature macroscopically, PLA, PLGA-50 and PLGA-75 fibers were immersed in water at 37°C for 5 min, and then twisted using tweezers.

Measurement of light guiding properties of printed optical waveguides

The optical loss was measured with a home-made setup shown in **scheme 2** in chapter 2. A laser was focused on one end of printed fiber. The light propagated in the fiber and activated the auto-fluorescence of the material. A camera was set in the vertical direction to take the picture of auto-fluorescence. In order to eliminate the disturbance from scattered light, a 550 nm long pass filter was placed between the waveguide and the camera so that only fluorescence could be detected. With the picture, the intensity of auto-fluorescence at beginning (I_0) and end (I_L) positions can be obtained by ImageJ and used to calculate the optical loss by the equation

$$\alpha(\lambda) = (10/L) * \log(I_0/I_L)$$

For the measurements of the optical loss in tissue, the fiber was sandwiched between two pieces of porcine tissue. The intensity of auto-fluorescence of fiber before and after passing through the tissue was measured to calculate the optical loss.

Quantification of light intensity delivered by the printed optical waveguides

A printed fiber (10 cm) was sandwiched between two pieces of porcine muscle (8 cm). A laser beam (405, 450, 520, 670, 808 nm, 4.5 mW, Thorlabs) was focused on the proximal end of the fiber. A power meter (Coherent Labmaster with LM-2 sensor) at the distal end was used to quantify the intensity of the delivered light.

The irradiance was calculated by dividing the power (mW) by the area of the crosssection of the fiber.

Photoactivation of cellular processes with printed optical waveguides

The same 3D cells spheroid system as chapter 2 was used to check the possibility of applying printed waveguides to deliver light through porcine muscle to photoactivate cellular processes. A printed fiber (length: 10 cm) was sandwiched between two pieces of porcine (8 cm in length). A laser (405nm, 4.5mW, ThorLabs) was focused on the proximal end of the fiber. The light was delivered at the distal end to the top of the DexMA hydrogel in the well for 15min. Then cell medium was changed after irradiation and spheroids were kept in culture under the protection from light for 2 days. A live and dead assay was performed to visualize the cell viability and spheroid morphology.

6.2.2 Supporting results

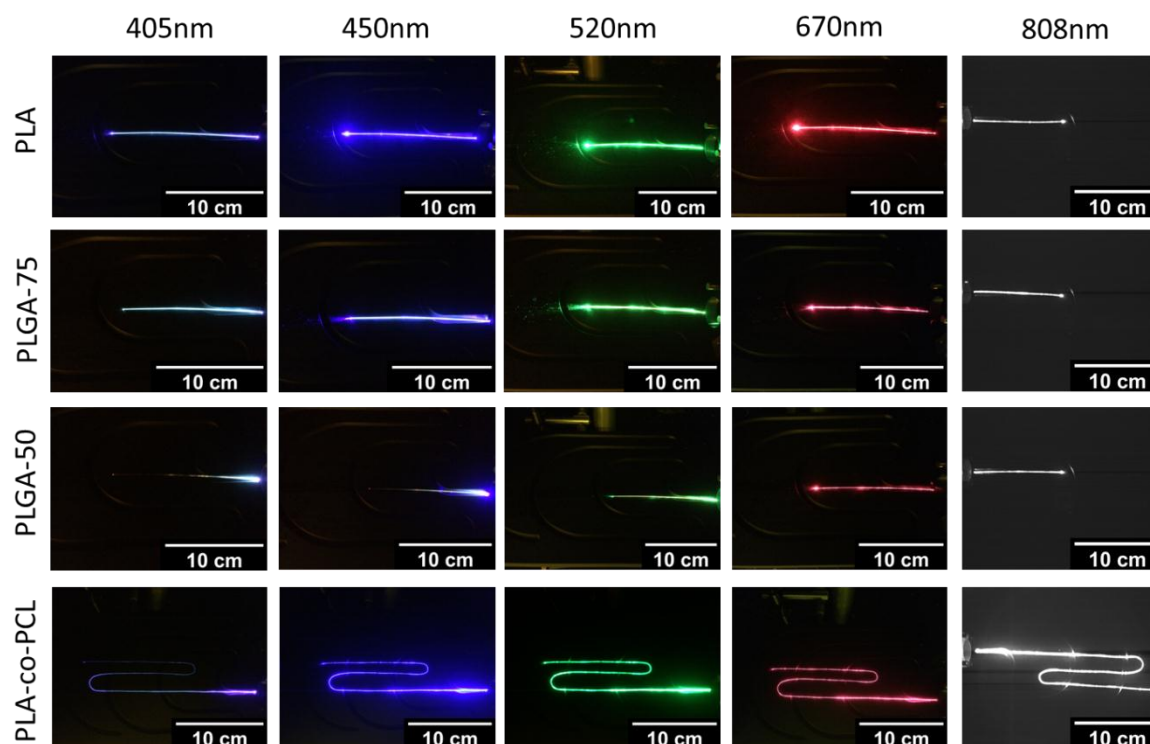


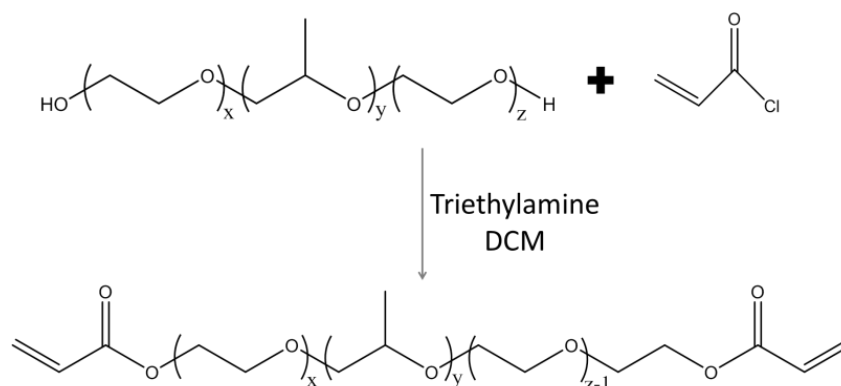
Figure A6. Images showing light propagating through printed optical waveguides in air.

6.3 Appendix of Chapter 4

6.3.1 Experimental information

Synthesis of Pluronic-DA

Pluronic-DA was synthesized following a reported protocol (**Scheme A1**).^[2] 20g of dry Pluronic F127 (Sigma Aldrich) and 0.55ml of triethylamine (Sigma Aldrich) were dissolved in 200ml of dry dichloromethane (Sigma Aldrich) in 500ml round-bottom flask. Then 250 μ l of acryloyl chloride (Sigma Aldrich) was added dropwise, after which the flask was sealed to avoid the moisture. The mixture was stirred on the ice for 12h and then in air (room temperature) for 12h. After reaction, the mixture was filtered and condensed to around 30ml by rotary evaporation (37°C, 200mbar, BÜCHI Labortechnik AG). The crude product was purified by precipitation in 500ml of diethylether and dried under vacuum for 2 days. The chemical structure of Pluronic-DA and the extent of acrylation were determined by ¹H-NMR (**Figure A7A** and **A7B**). The new peaks at 5.98-6.52 ppm confirmed the substitution of acryloyl groups. The extent of acrylation was determined by comparing the integral of acrylic protons at each end of Pluronic-DA (5.98-6.52 ppm) to the three protons of methyl group of propylene oxide unit (1.05-1.28 ppm) in the polymer chain. The measured degree of substitution was about 70%.



Scheme A1. The reaction between Pluronic F127 and acryloyl chloride to form Pluronic-DA.

Characterization methods

The characterization of the sol-gel transition temperature of Pluronic-DA solutions at different concentrations (20 wt/v%-50 wt/v%) was performed by rheology (DHIII rheometer, TA Instruments) in a temperature-sweep experiment using a parallel plate geometry with 20mm stainless steel plates. The temperature range was from 5 to 37 °C and the heating rate was 5 °C /min. Measurements were performed at 0.5% strain and 1 Hz frequency. The shear thinning behavior of the Pluronic-DA hydrogels at room temperature was characterized within the range of shear rates from 0.01/s to 1000/s. For this experiment the Pluronic-DA solutions were loaded between the two parallel plates and kept at room temperature for 10min to allow the hydrogel to form, after which the flow sweep measurement was started.

The elastic shear modulus of physically and covalently crosslinked Pluronic-DA hydrogels at different concentration (30 wt/v%-50 wt/v%) was measured by rheometry in a time sweep experiment at room temperature using the parallel plate geometry with 20mm stainless steel plates. A 0.5% strain and 1 Hz frequency were used for the measurements. During the first 5 min of the experiments the measurements were performed without light exposure, followed by other 5 min measurements during which the hydrogel was illuminated at 365 nm (10 mW/cm^2) to trigger photoinitiated crosslinking. Irgacure 2959 was added as initiator at 0.2%. The Young's Modulus was calculated from the storage modulus (G') and Poisson ratio (ν for hydrogels = 0.45–0.5, in present work 0.5 was adopted) by following equation:^[7]

$$E = 2 G (1 + \nu)$$

The swelling ratio Pluronic-DA hydrogels with different polymer concentrations were calculated by

$$SR\% = \frac{W_s - W_d}{W_d} \times 100$$

where SR is the swelling ratio, W_s is the weight of the swollen hydrogel, W_d is the weight of the dry polymer. The samples were obtained by photopolymerization of Pluronic-DA solution containing Irgacure 2959 (0.3 wt/v%) as initiator in a Teflon mold with 5 mm diameter. The hydrogels were then immersed in water for 24h and weighed to obtain swollen mass of hydrogels (W_s). Then the hydrogels were freeze dried and the dry mass was weighted (W_d).

Characterization of optical properties of Pluronic-DA hydrogels

The transparency of Pluronic-DA hydrogels were characterized by measuring the light absorbance in the spectral range from 350nm to 800nm. The samples were prepared in standard 1-cm-wide poly(methyl methacrylate) disposable cuvettes by photo-polymerization. The hydrogel precursor contained a given concentration of Pluronic-DA and 0.3 wt/v% of Irgacure 2959 as initiator. The precursors were pipetted into the cuvettes and irradiated at 365 nm ($1\text{mW}/\text{cm}^2$) using a UV lamp (LTF-Labortechnik) for 15min. Light absorbance was measured with a conventional UV-Vis spectrophotometer (Cary 4000, Agilent Technologies).

The relative scattering of the Pluronic-DA hydrogels was measured using a home-made setup as shown in **scheme 1** in chapter 2. Hydrogel samples were prepared in the same way as for absorbance measurements. A 520 nm laser (CrystaLaser) was focused and crossed the hydrogel horizontally. A camera (Thorlabs) was placed at 90° and images of the scattered light were taken. The laser power (500mW) and exposure time (5ms) of the camera were fixed. The intensity of the scattered light from the images was quantified using the free software ImageJ. The average scattering intensity of Pluronic-DA-30% hydrogels was set as reference and the scattering of the other hydrogels was normalized by this value. The refractive indices of Pluronic-DA hydrogels were measured with a refractometer (Anton Paar) at 20°C and at 589.3 nm. Hydrogel samples were

prepared in a Teflon mold with diameter of 5mm and depth of 2mm. The hydrogel precursors contained Pluronic-DA at defined concentrations and 0.3% wt/v of Irgacure 2959 as initiator. 40 μ l of precursor solution was injected in the mold and covered by a coverslip. The samples were illuminated at 365 nm (1mW/cm²) for 15min in order to photoinitiate crosslinking of the DA functions.

Printing of optical waveguides

A 3D-Bioscaffolder (GESIM, Dresden) 3D printer was used for printing.^[3] The cooled 50 wt/v% Pluronic-DA inks including 0.3 wt% Irgacure 2959 as initiator were loaded into UV blocked syringes (Fluid dispensing system, Nordson) and kept on ice until all bubbles disappeared, and then kept at room temperature to allow formation of the physical crosslinked hydrogels. After that, the syringe was mounted onto the printhead and connected to the pneumatic tube. The printing coaxial needle (Coaxial Spinneret Needle, inner needle: 22G, outer needle: 17G, LEONARDINO) was extended with a transparent silicone tube (1.02mm, MONO-LUMEN TUBING, FREUDENBERG MEDICAL) to allow photopolymerization of the printed thread (**Figure 3A** in chapter 4). The UV lamp (Series 1500, OmniCure) was adjusted to focus on the silicone tube with a defined intensity.

For printing the core/cladding structure, thermocurable polydimethylsiloxane (T-PDMS: Dow Corning®184 Silicone Elastomer) and UV-curable PDMS (UV-PDMS: Shin-Etsu, KER-4690) were used as core, and 50 wt/v% of Pluronic-DA was used as cladding. For the preparation of T-PDMS precursor, the prepolymer and cross-linking agent were mixed at weight ratio of 10:1. For UV-PDMS, two parts were mixed at weight ratio of 1:1. The bubbles in prepared mixtures were removed under vacuum for 30 min. The mixture was loaded into the UV blocked syringe and connected to pneumatic tube. Core/cladding filaments were produced by providing pressure for both channels. It's worth noting that the order of switching on and off the pressure of channels is very important for successful printing of the core/cladding structures. To start printing core/cladding structure, the pressure of

core should be applied first, followed by applying the pressure on the cladding. To stop printing, the pressure to the core should be stopped after stopping pressure on the cladding. After printing, the core/cladding waveguides with T-PDMS were irradiated by 365nm UV light ($1\text{mW}/\text{cm}^2$) for 20 min to get fully crosslinked cladding layer, and then stored in sealed box with wet tissue paper and kept in oven at $37\text{ }^\circ\text{C}$ for 48 hours. The waveguides with UV-PDMS were further irradiated by 365nm UV light ($1\text{mW}/\text{cm}^2$) for 20 min to get fully crosslinked core and cladding. The post-treated waveguides were stored in sealed box with wet tissue paper to keep the humidity.

The effect of printing parameters, such as pressure, UV intensity on the diameter of core was studied. 2.5cm length of silicone tube, 0.3wt% initiator concentration and 50 wt/v% of Pluronic-DA were fixed in all the experiments. For the study of the effect of pressure, the UV intensity was set at 60%. For the study of the effect of UV intensity, the pressure for core and cladding were set at 120 and 340 kPa.

Characterization of printed waveguides

The optical loss was measured with a home-made setup (shown in **scheme 2** in chapter 2). A laser was focused on one end of printed fiber. The light propagated along the fiber and activated the auto-fluorescence of the material. A camera with a filter (550nm) was set in vertical direction to take the picture of auto-fluorescence. With the picture, the intensity of auto-fluorescence along the fiber can be obtained by ImageJ. The optical loss of printed fibers can be calculated with equation:

$$\alpha(\lambda) = (10/L) * \log(I_0/I_L)$$

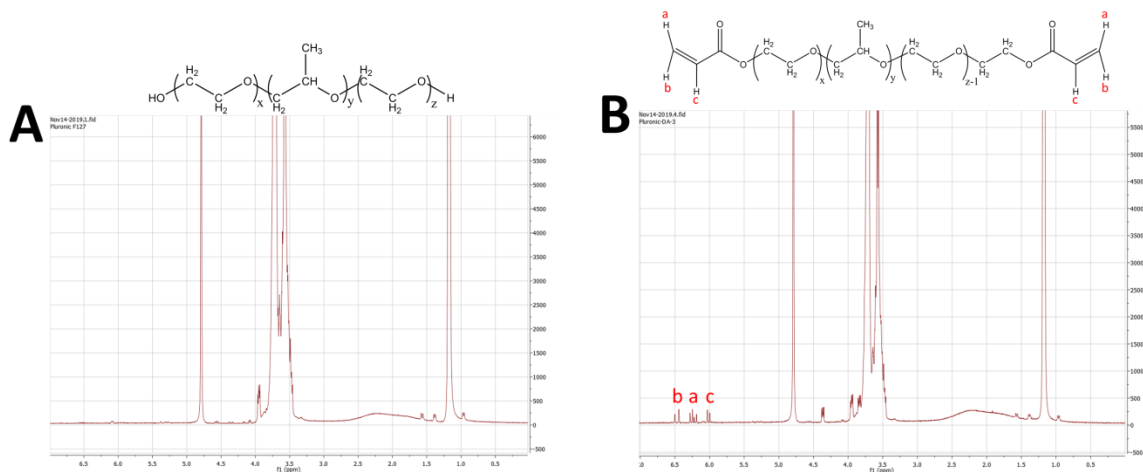
where L is the distance between two positions in the fiber with unit of cm, I_0 stands for the intensity of the auto-fluorescence at any initial position and I_L stands for the intensity of auto-fluorescence after light propagates the distance L.

For measuring the optical loss in tissue, the fiber was sandwiched by two pieces of porcine muscle tissue. The intensity of auto-fluorescence of fiber before and after propagating in tissue was measured to calculate optical loss in tissue.

Application of printed optical fiber in controlling cells migration

The same 3D cells spheroid system as chapter 2 was used to check the possibility of applying printed waveguides to deliver light through porcine muscle to photoactivate cellular processes. As shown in **Figure 5A** in chapter 4, a printed fiber (length: 10cm) was sandwiched between two pieces of pig muscle tissue (8cm in length, 2mm in thickness). A laser (405nm, 5mW, ThorLabs) was focused on one end of the fiber. The light was delivered to the top of cells spheroids containing DexMA hydrogel by propagating in the fiber through the tissue. The delivered light will photolyze Cyclo[RGD(DMNPB)fC] to activate the cells in the spheroids. The activation finished after 30 min irradiation by delivered light. Then cell medium was changed once and spheroids were kept in culture under the protection from light. After two days, live and dead assay was performed to visualize the cell viability and spheroid morphology.

6.3.2 Supporting results



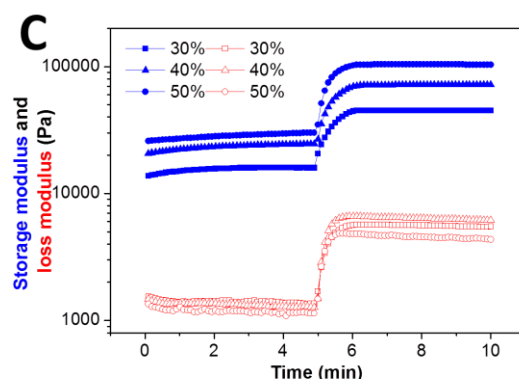


Figure A7. (A) ^1H NMR of Pluronic F127. (B) ^1H NMR of Pluronic-DA. (C) The storage and loss modulus of Pluronic-DA solutions at different polymer concentrations before (0-5min) and after (5-10min) photoinitiated covalent crosslinking.

Table A2. The transition temperature of different concentrations of Pluronic-DA solutions, Young's Modulus of different concentration of Pluronic-DA gels before and after photocrosslinking, and the swelling ratio in water of different concentrations of Pluronic-DA hydrogels.

Concentration of Pluronic-DA	20%	30%	40%	50%
Transition temperature	23.6-28.7 °C	15.5-19.9 °C	12-14.6 °C	6.2-9.6 °C
Young's Modulus before Photocrosslink (kPa)	/	25.6±1.5	37.3±2.9	42.7±1.9
Young's Modulus after Photocrosslink (kPa)	/	70.8±4.9	125.8±5.8	151.4±4.1
Swelling ratio	/	1082%	970%	759%

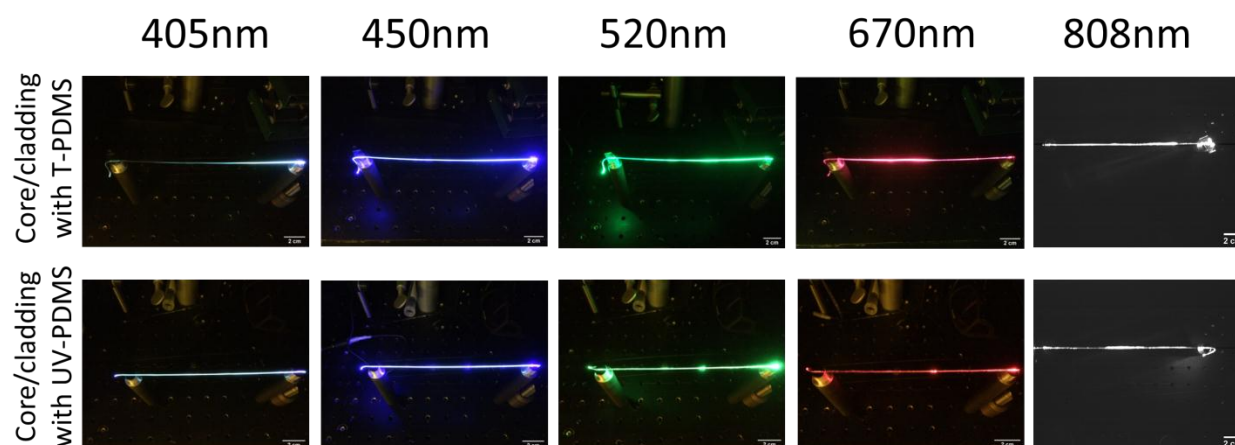


Figure A8. Images of light guided by printed waveguides in air, scale bar: 2 cm.

References

- [1] G. A. Hudalla, T. S. Eng, W. L. Murphy, *Biomacromolecules* 2008, 9, 842.
- [2] M. R. Kim, T. G. Park, *Journal of Controlled Release* 2002, 80, 69.
- [3] L. Ouyang, C. B. Highley, W. Sun, J. A. Burdick, *Advanced Materials* 2017, 29, 1604983.
- [4] T. T. Lee, J. R. García, J. I. Paez, A. Singh, E. A. Phelps, S. Weis, Z. Shafiq, A. Shekaran, A. Del Campo, A. J. García, *Nature materials* 2015, 14, 352.
- [5] Y. Zheng, M. K. L. Han, Q. Jiang, B. Li, J. Feng, A. del Campo, *Materials Horizons* 2020.
- [6] a) S. Sankaran, A. del Campo, *Advanced Biosystems* 2019, 3, 1800312; b) S. Sankaran, J. Becker, C. Wittmann, A. del Campo, *Small* 2019, 15, 1804717.
- [7] S. R. Caliori, J. A. Burdick, *Nature methods* 2016, 13, 405.

Publication list

- (1) **Jun Feng**, Yijun Zheng, Shardul Bhusari, Samuel Pearson, Aránzazu del Campo. "Printed degradable optical waveguides for guiding light into tissue" (submitted to *Advanced Functional Materials*)
- (2) **Jun Feng**, Qiyang Jiang, Peter Rogin, Peter W. de Oliveira, Aránzazu del Campo. "Printed soft optical waveguides of PLA copolymers for guiding light into tissue" (submitted to *ACS Applied Materials & Interfaces*)
- (3) **Jun Feng**, Shardul Bhusari, Aránzazu Del Campo. "Printed stretchable optical waveguides to deliver light into deep tissue." (*Paper in preparation*)
- (4) **Jun Feng**, Xuan-Anh Ton, Qiyang Jiang, Julieta I. Paez, Samuel Pearson, Aránzazu del Campo. "Bioinspired progress in dental gluing: substituted catechols compatible with acrylate polymerization." (*Paper in preparation*)
- (5) Han, Lu, Yijun Zheng, Hao Luo, **Jun Feng**, Roxanne Engstler, Lulu Xue, Guangyin Jing, Xu Deng, Aránzazu del Campo, and Jiayi Cui. "Macroscopic self-evolution of dynamic hydrogels to create hollow interiors." *Angewandte Chemie International Edition* (2019).
- (6) Włodarczyk-Biegun, Małgorzata Katarzyna, Julieta I. Irene Paez, Maria Villiou, **Jun Feng**, and Aranzazu Del Campo. "Printability study of metal ion crosslinked PEG-catechol based inks." *Biofabrication* (2020).
- (7) Zheng, Yijun, Mitchell Kim Liong Han, Qiyang Jiang, Bin Li, **Jun Feng**, and Aránzazu del Campo. "4D hydrogel for dynamic cell culture with orthogonal, wavelength-dependent mechanical and biochemical cues." *Materials Horizons* (2019).
- (8) **Feng, Jun**, Xuan-Anh Ton, Shifang Zhao, Julieta I. Paez, and Aránzazu del Campo. "Mechanically reinforced catechol-containing hydrogels with improved tissue gluing performance." *Biomimetics* 2, no. 4 (2017): 23.

Curriculum Vitae

Jun Feng

Date of Birth: 25th November 1987

Place of Birth: Sichuan, China

10.2015-present **PhD study** at INM- Leibniz Institute for New Materials,
Saarbrücken, Germany

Title of Thesis: Printed Soft Optical Waveguides for Delivering
Light into Deep Tissue

Supervisor: Prof. Aránzazu del Campo

09.2012-06.2015 **M.Sc.** in Materials Science, Wuhan University of Technology,
Wuhan, China

Title of Thesis: Orderly Proton Conductor based on
Polyelectrolyte Brushes

Supervisor: Prof. Haining Zhang

09.2007-06.2011 **B.Sc.** in Polymer Materials and Engineering, Wuhan University
of Technology, Wuhan, China